Journal of The Electrochemical Society, **162** (14) F1-F36 (2015)
0013-4651/2015/162(14)/F1/36/$33.00 © The Electrochemical Society

Review—Recent Progress in Electrocatalysts for Oxygen Reduction Suitable for Alkaline Anion Exchange Membrane Fuel Cells

Qinggang He[a,z] and Elton J. Cairns[b,c,*]

[a]*College of Chemical and Biological Engineering, Zhejiang University, Hangzhou, Zhejiang 310027, People's Republic of China*
[b]*Chemical and Biomolecular Engineering Department, University of California, Berkeley, California 94720, USA*
[c]*Lawrence Berkeley National Laboratory, Berkeley, California 94720, USA*

Alkaline fuel cell technology has been reinvigorated since the recent rapid development and deployment of anion exchange membranes. Without the "acid-stability" requirement in low pH environments such as that of proton exchange membrane fuel cells, a much wider range of materials including noble metals, non-noble transition metals, and even metal-free electrocatalysts for the oxygen reduction reaction (ORR) in alkaline media have been developed due to both thermodynamic and kinetic reasons. As compared to the rapidly increasing number of reports on the development of novel catalyst materials, the understanding of the reaction mechanisms of the various ORR electrocatalysts is quite insufficient, and the application and investigation in real alkaline anion exchange membrane fuel cells (AAEMFCs) is even scarcer. By reviewing the compositions, preparation methods, physiochemical properties and ORR performance of different categories of cathodic electrocatalysts that have emerged in the past few years, some common and intrinsic properties and factors that account for the superior activity of these materials may be extracted and summarized, which may further help to identify the reasons for the kinetic facility of the ORR in alkaline media. Some practical issues of utilization of the promising novel replacement materials for the state-of-the-art Pt-based cathodic electrocatalysts in AAEMFCs are pointed out. In addition to the progress on the development of novel materials with outstanding ORR activity, many and varied compositions and morphologies in one, two and three dimensions, scalable preparation technologies, low cost, and other unique properties, some feedback on the performance and especially the problems of their use as cathodes in AAEMFCs is urgently needed. Such feedback should provide guidelines for the design and manufacture of next-generation electrocatalysts and accelerate the application of AAEMFCs.

Manuscript submitted August 5, 2015; revised manuscript received September 21, 2015. Published 00 0, 2015.

Although the alkaline fuel cell (AFC) was the first to be put into practical use in the history of fuel cells, it has been largely ignored by the electrochemical research community for decades due to technical problems[1–3] and some other economic factors. A renaissance of AFC technology was catalyzed by the replacement of the conventional liquid electrolyte by the alkaline anion exchange membrane.[4–6] Some long standing limitations such as electrolyte leakage and high purity fuels with low CO_2 concentrations were overcome by the usage of a solid state electrolyte. The development of alkaline anion exchange membrane fuel cells (AAEMFCs) is further motivated by the intrinsic advantages over their acidic analog proton exchange membrane fuel cells (PEMFCs). The merits of an AAEMFC as shown in Figure 1 include the following: (i) The electrode kinetics of the cathodic reduction reaction is more facile in a high pH environment; (ii) Many non-noble-metal materials that are unstable in the PEMFC acidic environment can be used as electrode components; (iii) Hydroxide anion and electroosmotically driven water molecules generally migrate from the cathode to the anode, suppressing the crossover of anodic fuels in the opposite direction; (iv) Even with the exposure to air or in the case of direct methanol fuel cells where CO_2 is inevitably produced, the metal carbonate/bicarbonate formation and precipitation problems no longer exist since anion exchange membranes are free of metal ions.[7] Although for the current AAEMFC technology there still remain a number of major issues such as the low conductivity of the membranes[6] and unsatisfactory performance of membrane electrode assemblies,[8,9] the successful application can be foreseen with scientific and engineering improvement and continuous industrial and policy support.

Among many factors controlling the AAEMFCs' performance, electrocatalysis plays a central role in electrochemical reactions. There are two distinct electrochemical processes for the reactants at the two electrodes (i.e. electrooxidation on the anode and electroreduction on the cathode). The oxygen reduction reaction (ORR) is notorious for suffering from sluggish kinetics[10–12] that may be affected by electrolyte pH,[13] the nature of the counter cation of the hydroxides,[14] temperature,[15] etc. From Figure 2 the reaction scheme of the ORR in alkaline media is similar to that in the acidic environment. Instead of H_2O_2 and H_2O formation when protons are abundant, the ORR in alkaline media generates peroxide anion in the series pathway and hydroxide anion as the final product. However, the ORR is generally more facile in alkaline media for both thermodynamic and kinetic reasons.[12,16–18] It has been commonly concluded that the rate-controlling-step is the first electron transfer to the adsorbed $O_{2,ad}$ (inner sphere reaction) or formation of the superoxide radical anion $O_2^{\bullet-}$ (outer sphere reaction) during ORR in both acidic and alkaline media,[12,19–22] although there is a controversial viewpoint that dissociative chemisorption of molecular O_2 on the electrode surface

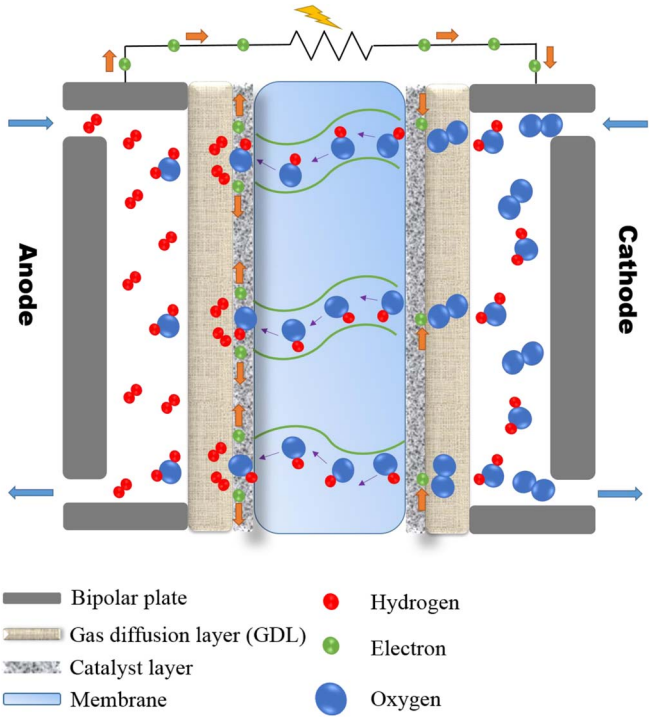

Figure 1. A schematic illustration of an H_2/O_2 alkaline anion exchange membrane fuel cell (AAEMFC).

*Electrochemical Society Active Member.
[z]E-mail: qghe@zju.edu.cn

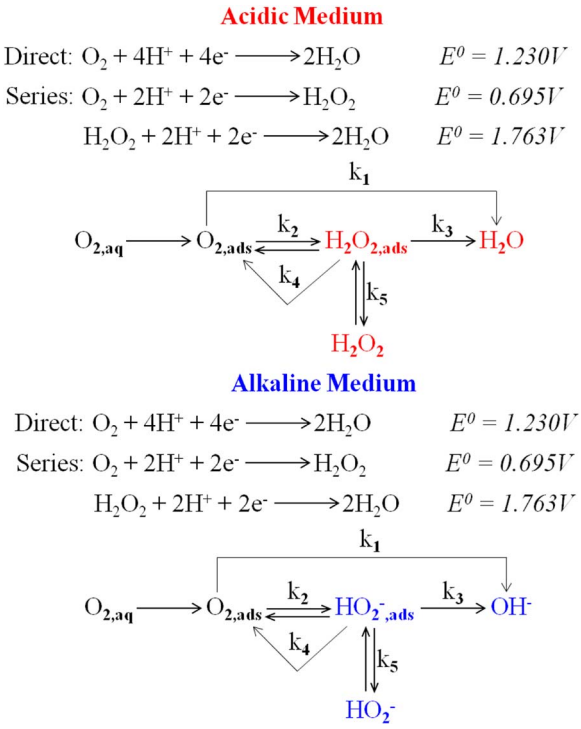

Figure 2. Reaction pathways for ORR in acidic and alkaline media (redrawn from Ref. 371).

determines the ORR rate according to Yeager.[23–25] Figure 3a shows the first electron transfer reactions and overall reduction reactions of oxygen molecules in acidic and alkaline media. For the reaction 1a (& 1b), it typically happens on some specific electrode surface on which an exothermic process of O_2 adsorption is involved. For those electrode materials without strongly chemisorbed O_2 such as ideal graphite, the reaction 1a′ (& 1b′) accompanied with an outer sphere electron transfer process is dominant. Because there is no proton (or hydroxide ion) involved, both reaction 1a (& 1b) and reaction 1a′ (& 1b′) are pH independent. However, the overpotential of the ORR is actually correlated with the difference of equilibrium potential between the first electron transfer reaction and the overall reaction (see Figure 3a). Because protons (or hydroxide ions) are involved in both the $2e^-$ transfer reaction (2a & 2b, or 2a′ & 2b′) and the $4e^-$ transfer reaction (3a & 3b, or 3a′ & 3b′), the overpotential of ORR is still pH dependent considering the overall process. To clearly show the influence of pH on the facility of the ORR, Blizanac et al.[18] contributed detailed theoretical calculations and constructed a modified form of the Pourbaix diagram (Figure 3b) with the overpotential of the ORR instead of the equilibrium potential as the y axis.

From Figure 3b, some very important information can be obtained. (i) Without strong adsorption of O_2 on the electrode (see line 3), the overpotential values to form H_2O_2 and HO_2^- are much less than those to form H_2O (~40% less at pH = 1 and ~70% less at pH = 13). That means it is always more energetically favorable to go through the peroxide intermediate species during ORR. In other words, a $2e^- + 2e^-$ serial four-electron pathway is preferred on those electrodes without specific adsorption ability for O_2 (outer sphere reaction). However, in the case of line 3′ with an inner sphere reaction, a cross-section can be noticed at ~ pH = 12 for line 3′ and line 2. This indicates that a direct 4-electron transfer pathway can be realized on some specific electrodes (e.g. Pt) but only in alkaline media. (ii) For simplicity, considering the reaction 1 (line 3) only as the initial step of ORR (instead of both line 3 and line 3′), the minimum overpotential to form H_2O designated by the difference between line 3 and line 1 decreases significantly from pH = 1 (~1.5 V) to pH = 13(~0.8 V). When the incomplete reduction reaction to form H_2O_2 is considered, the minimum overpotential between line 3 and line 2 is only ~0.3 V at pH = 13. The dramatic decrease of the intrinsic overpotential of ORR that is evaluated by the above difference of standard potential from a low pH to a high pH environment was presumed as the primary thermodynamic reason for a feasible ORR process on a large number of electrode materials.[18,26] Nevertheless, in fact, a smaller overpotential does not necessarily indicate "surface-independency" of the rate-determining step of ORR in alkaline media.

This question was better explained by Nagappan et al.[12] with consideration of the double layer structure and outer-sphere electron transfer mechanisms (see Figure 3c). In the schematic illustration of the double-layer structure during ORR in alkaline media (Figure 3c), Nagappan et al. show a "universal" scenario with both chemisorbed O_2 at the inner Helmholtz plane (IHP) and water solvated O_2 packed at the outer Helmholtz plane (OHP). The inset (a) in Figure 3c depicts a common inner-sphere electron transfer mechanism applicable for both acidic and alkaline media. More interestingly, the inset (b) shows an outer-sphere reaction that is unique to alkaline media. The uniqueness is actually coming from the interaction between the H atom in OH_{ads} and the O atom in the solvent water molecule via an H bond. Such "H bond" interaction appears less likely in acidic media because the electrode will be mainly covered with anions (e.g. ClO_4^-, SO_4^{2-}) from the supporting electrolyte. Though much lower than the chemisorption energy associated with O_{2ads}, the hydrogen bond energies (<35 kJ mol^{-1}) are just enough to overcome the minimum overpotential between line 3 and line 2 in high pH environment as shown in Figure 3b. As a direct consequence, an outer-sphere electron transfer to form the superoxide species can be promoted in alkaline media regardless of the underlying electrode surface. As an important conclusion, the promotion by the interaction between the $O_2 \cdot (H_2O)_n$ cluster and the surface hydroxyl species was assigned as the fundamental reason for the so-called "nonspecificity" of the rate-determining step of the ORR in alkaline media, which creates the possibility to use a broad range of conducting materials as ORR electrodes.

However, the above conclusion was built on some presumptions, that for example the first reaction step involving the redox couple of $O_{2,ad}$/ $O_{2,ad}^-$ is a surface-independent outer-sphere electron transfer process.[27] Under real conditions in which more complex multistep and multielectron processes and different types of adsorbed intermediates and surface modified electrodes are considered, a better understanding of the generally more facile ORR in alkaline media has to be made from the point of view of kinetics. It is only reasonable to compare the kinetics of the ORR at extreme pH conditions (traversing from 0 to 14) on the same electrode surface because many factors (Eq. 1[18]) such as the order of activity of active sites and coverage of spectator species vary with different electrodes.

$$i = nFkc_{O_2}(1 - y\Theta_{ad})^x \exp\left(\frac{-\beta FE}{RT}\right) \exp\left(\frac{-\gamma r\Theta_{ad}}{RT}\right) \quad [1]$$

First of all, for the benchmark catalyst material of Pt for ORR, the kinetics is even inhibited to some extent in alkaline media.[11,28,29] From the work pioneered by Conway[30] and others, the surface of a polycrystalline Pt electrode is covered by oxide species with an onset potential of ca. 0.75 V (vs. RHE), either due to water activation in acid or OH^- anion adsorption in alkaline media. However, as long as the strong Pt-O_2 interaction is not fully blocked typically below 1.15 V (vs. RHE),[31] the energy barrier of the first electron transfer for the redox couple of $O_{2,ad}/O_{2,ad}^-$ can still be easily overcome due to the strong interaction between Pt and molecular O_2 in both inner- and outer-sphere manners. Consequently, some catalytically active sites for molecular O_2 may be blocked by the overwhelming OH^- species in high pH environment, and a 25 mV overpotential and nearly one order of magnitude lower exchange current density were obtained when switching from a 0.1 M $HClO_4$ solution to a 0.1 M NaOH solution.[11] In contrast, on a Ru electrode the ORR kinetics in alkaline media becomes much faster than the acidic media.[11] The very oxophilic surface of Ru grants its superior ability for water activation. As such it has been a good assistant to remove poisoning adsorbed species (e.g. CO) on adjacent

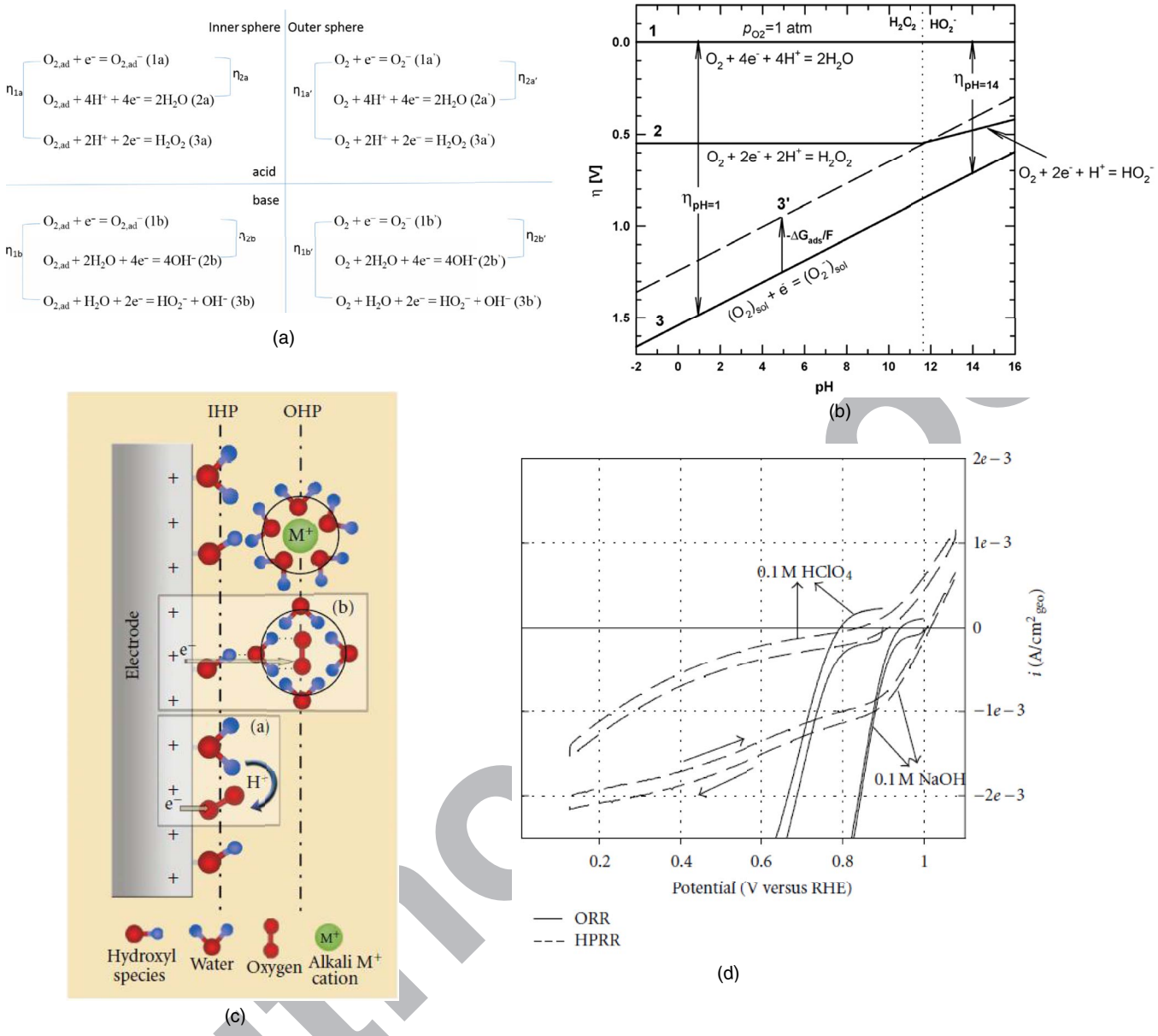

Figure 3. (a) The first electron transfer and overall oxygen reduction reactions in acidic and alkaline media considering two electron-transfer mechanisms of the inner-sphere reaction and the outer-sphere reaction. (b) Modified form of Pourbaix diagram. All potentials are expressed relative to the equilibrium potential for reaction $O_2 + 4H^+ + 4e^- = 2H_2O$. Line 1: pH dependence of equilibrium potential for reaction $O_2 + 4H^+ + 4e^- = 2H_2O$ ($p_{O_2} = 1$ atm); line 2: pH dependence of equilibrium potential for reaction $O_2 + 2H+ + 2e^- = H_2O_2$ ($\log(p_{O_2} / (H_2O_2)) = 0$, $\log(p_{O_2}/(HO_2^-)) = 0$); line 3: pH dependence of equilibrium potential for reaction (3) ($\log(p_{O_2} /(O_2^-)) = 0$); line 3: pH dependence of equilibrium potential for reaction $O_2 + e^- = O_2^-$ proceeding as a inner sphere reaction (ΔG_{ads} is adsorption free energy of $O_{2,ad}^-$; in this case, as illustration, ΔG_{ads} is ca. −30 kJ/mol). Reprinted with permission from Ref. 18 Copyright 2007 Elsevier. (c) Schematic illustration of the double-layer structure during ORR in alkaline media. Insets (a, b) illustrate the inner- and outer-sphere electron transfer processes. Reprinted with permission from Ref. 12 Copyright 2012 Hindawi Publishing Corporation. (d) ORR and H_2O_2 Reduction Reaction (HPRR) on a FeTPP/C catalyst (pyrolyzed at 800°C) in acidic and alkaline electrolytes. All measurements were performed at 900 rpm rotation rate and 20 mV/s scan rate. Reprinted with permission from Ref. 12 Copyright 2012 Hindawi Publishing Corporation.

alloyed Pt sites during anodic electrooxidation of methanol through a bifunctional mechanism.[32] However, the surface oxides may block efficient O_2 adsorption, resulting in large overpotentials.

Thanks to the nonspecificity of the underlying electrode for the first electron transfer in alkaline media,[11] the ORR can still proceed at relatively high potentials on Ru that may be covered with oxide species already. This "nonspecificity" is originated from the interaction between the solvation shell of the $O_2 \cdot (H_2O)_n$ cluster and the excessive OH^- species on the electrode surface through a H bond.[11] In general, it is the easier outer-sphere electron transfer process in alkaline medial that compensates the weak interaction between the electrode and the O_2 molecules. This compensation effect also works on the non-noble-metal electrodes such as pyrolyzed metal macrocycle compounds and recently reported N or S doped two dimensional carbon materials.[33–35] For instance, a 200 mV positive shift of the half wave potential for ORR has been seen on Fe or Co based metal-N composite electrodes when they are transferred from acidic to alkaline media.[36,37] The above mentioned "nonspecificity" and promotion of outer-sphere electron transfer are certainly beneficial for ORR to "occur" in alkaline media. However, on the other hand, it may be considered as a disadvantage for "complete" oxygen reduction since peroxide species are the main products of the outer-sphere reaction mechanisms, given the fact that the 2-electron + 2-electron series pathway is more likely according to direct evidence from rotating

ring disk electrode (RRDE) studies.[11,38,39] As such, a more important reason for the faster kinetics in alkaline media is the better stabilization of the peroxide intermediate and faster following reduction. It has been known that the predominant ORR intermediate species stay as the HO_2^- anion at pH>12,[40] which is different from the neutral molecule of H_2O_2 at pH<12. Under the real fuel cell operating conditions where the potential on the cathode is typically much higher than the potential of zero charge (pzc) value, the positive charge on the electrode may provide an electrostatic attraction force toward the negatively charged HO_2^- and the possibility of further reduction to OH^- on the catalytically active sites. From Figure 3d, it can be seen that a more positive onset potential and higher current density for the hydrogen peroxide reduction reaction were obtained on a FeTPP/C catalyst in 0.1 M NaOH than that in 0.1 M $HClO_4$, indicating that peroxide reduction is more kinetically favored in alkaline media. In summary, from the point of view of kinetics, the fundamental reason for more facile ORR in alkaline media than acidic media is the stabilization effect of the peroxide intermediate of HO_2^- due to its negative charge as opposed to the neutrality of H_2O_2 in the case of acid solutions.

The thermodynamic and kinetic facility of the ORR stemming from the electrode surface independency of the first electron transfer and the stabilization effect on the peroxide intermediate in alkaline media, has opened the gate for usage of a large variety of electrodes including non-noble metal materials. On the other hand, the general "nonspecificity" of the ORR in alkaline media does not mean that any conductive material can be employed as a cathode electrocatalyst in AAEMFCs. Some prerequisites and common requirements (adsorption of O_2, metals that have multiple valence states, easy desorption of products and electronic conductivity, etc.) have to be met to exhibit good enough catalytic activity for the ORR. One aim of this review is to decipher the intrinsic properties of different types of catalysts including modified Pt group metals, non-Pt-group metals (alloys), non-noble-metal oxides with or without being imbedded in macrocycles, and nanocarbon materials, etc. that have appeared during the past three years.

This review may serve as the basis for designing the next generation of novel electrocatalysts with benefits gained from new materials for further improvement of the ORR kinetics. Aside from the fundamental standpoint, technologically speaking, the cornerstone and success of any newly developed catalyst for replacement of the state-of-the-art Pt/C is to pass the critical judgement with employment in a real alkaline fuel cell, in which the thickness of the electrode, volumetric current density, durability, gas diffusion, membrane-electrode interface, water management and so many other factors may play roles individually or in combination. As such, the second aim of this review to summarize the recent progress in terms of the practical applications of replacement candidates for Pt/C and point out the deficiencies and urgent needs of electrocatalysis research for acceleration of AAEMFCs technologies.

Fundamental Contributions from Recent Innovations of Material Development

Modification of traditional Pt based electrocatalysts.— Until now Pt/C is still most commonly used and referenced for evaluation of novel materials for ORR, indicating its unassailable role as the mainstay of electrocatalysts in AFCs. The somewhat inhibited catalytic activity due to strong adsorption of abundant OH^- species in alkaline media and the aspect of small molecule alcohol tolerance during ORR maintain it as an interesting topic for modifications on Pt based electrodes by alloying, changing its structure on the nanoscale, etc. Indeed, in acidic media, it has been a routine strategy to improve the catalytic activity of Pt for ORR by increasing the Pt d-band vacancies,[41] the sacrificial effect,[42] modification of the nanostructure[43–45] and other factors via alloying with 3d transition metals (e.g. Fe, Co, Ni). However, the number of reports about alloyed Pt electrocatalysts for ORR in alkaline media is much less, partially because these 3-d transition metals usually remain as oxide or hydroxide forms with low conductivity

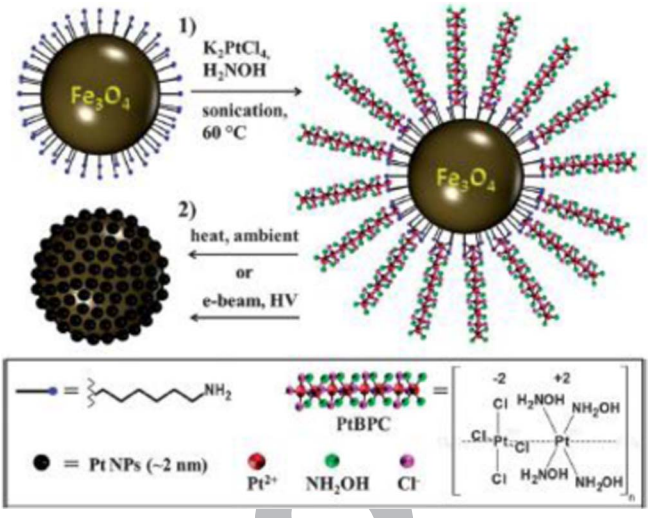

Figure 4. Synthesis and proposed general structure of platinous backbone-polymerized complexes–magnetite hybrid nanostructure (PtBPC–MHN) and platinum–magnetite hybrid nanostructure (Pt–MHN). Reprinted with permission from Ref. 56 Copyright 2013 Royal Society of Chemistry.

and stability at pH = 14.[46] Therefore, the pertinent work was more focused on alloying Pt with other noble metals. Nanoporous PtPd alloys with various ratios of Pt were fabricated using a "one-step" method by dealloying PtPdAl precursors.[47] The superior activity of the PtPd alloyed catalyst was ascribed to both shrinking of the Pt lattice and stronger binding energies for OOH (beneficial for the first electron transfer) but lower adsorption of OH (less blockage and inhibition by oxide species) on PtPd alloys.[48,49] Alloying Pt with In, Au, Ru and Ag, and ORR testing were also demonstrated with a combination of good activity and other gains such as tolerance for CO and alcohols and long term stability.[50–54] Actually bimetallic Pt-3d transition metal catalysts do not disappear from the scene completely, providing the possibility of fabrication of unique structures.[55–57] For example, as shown in Figure 4, Fe_3O_4 nanoparticles with epitaxial growth of Pt show improved specific activity for ORR due to electron transfer between the Fe_3O_4 core and the Pt shell, in which the underlying Fe_3O_4 was fully protected from corrosion by the unique core-shell structure.[56] Apart from the above-mentioned electronic effect, the ORR kinetics on Pt can be improved by changing the crystal structure in the microscopic range. Devivaraprasad et al.[58] correlated ORR activity with the crystal structure of Pt nanoparticles, and established the order of Pt-tetrahedral ({111}-facet dominant) > Pt-polycrystalline ≈ Pt-cubic({100}-facet dominant) > Pt-cuboctahedral ({100}-facet dominant), which agrees with the single crystal studies in 0.1M KOH or NaOH with the order of {111}>{110}>{100}.[28,59] In contrast, changing the morphology macroscopically only showed a marginal effect on improvement of ORR activity of Pt.[60,61] Neither does the replacement of the porous carbon support (e.g. Vulcan Carbon) with graphene[51,60] or carbon xerogels[62] exhibit noticeable kinetics benefits since the nanoparticle dispersion and strong metal-support interaction are well established on regular porous carbon, except that the stability of the catalysts can be significantly improved by depositing Pt on some new types of supports such as ITO,[63] carbides[64,65] and nitrides.[66,67] It is worthwhile to mention a big advantage of the modification of Pt with the above methodologies to reduce the sensitivity to the crossover of anode fuels.[51,52,68] Besides the studies focused on materials, new inputs about the fundamental mechanisms of ORR in alkaline media are highlighted and summarized in Table I. Although a progressive understanding of ORR mechanisms on Pt-based electrocatalysts was put forward, some important aspects are still puzzling and additional investigation is needed from the following perspectives: 1 The interactional effects of blockage of active sites for O_2 adsorption and the facilitating of electron transfer due to OH adsorption; (2) details of the effect of ion adsorption on ORR kinetics; (3) details of the

Table I. Recent discoveries about fundamental mechanisms of ORR on Pt based electrocatalysts in alkaline media.

Material	Study tool/method	Main scope	New inputs for mechanisms of ORR	Ref
Pt/C	RRDE, Electrogenerated chemiluminescence	The influence of KOH concentration, oxygen partial pressure and temperature	• Solubility, diffusion coefficient, and limiting current all drop as the concentration of KOH increases. • The averaged electron transfer number change from 3.81 (in 0.5M KOH) to 1.87 (in 8M KOH), indicating more HO_2^- formation. • ORR intermediate species (HO_2^-) can be detected by a fluorescent probe. • "Salting-effect" makes O_2 pressure influence become weak in high concentration KOH. • Temperature shows dual effects by mediating strong OH^- adsorption and decreasing O_2 solubility.	383
Pt/C	RDE, SEM	The effect of temperature (over 100 °C) and pressure on ORR kinetics	• The transfer coefficient (α) of O_2 is constant in the Langmuir region (large current density), but is temperature dependent in the Temkin region (low current density). • Diffusion coefficient (D_O) of O_2 is independent on pressure. • Connection between O_2 concentration (C_O^*) and pressure and temperature was established. • ECSA of the Pt electrode increases largely at high temperatures.	384
PtCu/C	RRDE	The effect of OH_{ads} coverage on Pt based electrodes	• The rate determine step of ORR is the same at extreme pH conditions. • Basic kinetics current of ORR is inversely proportional to OH_{ads} coverage. • Lower rate of increase of OH_{ads} coverage can be achieved on PtCu than Pt. • At certain high potential (ca. $0.83 < E < 0.90$ V), a universal rate of $d\theta/dE$ was found on any Pt based catalysts.	385
Polycrystalline Pt nanoparticles	RRDE, TEM	The effect of the shape of Pt nanoparticles	• The order of ORR activity is Pt-TD > Pt-PC ≈ Pt-NC > Pt-CO (TD: tetrahedral, PC: polycrystalline, NC: cubic; CO: cuboctahedral). • The order of peroxide formation is Pt-CO > Pt-PC > Pt-TD > Pt-NC.	58
Pt single crystals	Hanging meniscus rotating disk electrode	The effect of surface structure of Pt single crystals on ORR kinetics	• Pt(111) is the most active surface for ORR in alkaline media. • Introduction of step density (defects) on single crystal's (except (100)) surface diminish the ORR activity due to large OH adsorption energy on steps. • OH adsorption strength depends on the surface structure of Pt instead of pH. • Lower activity for ORR on Pt(100) is due to stronger OH adsorption. • The surface sites covered by OH also participate in electron transfer.	59
Polycrystalline Pt	Cyclic and hydrodynamic RDE-LSV	The effect of anion-exchange cationic functionalities on Pt activity for ORR	• Inhibition of ORR specific activity follows the order: blank KOH < KOH-KCl < KOH-TMA <KOH-BOTMHA < KOH-BTMA < KOH-BAABCO < KOH-BMI.	379

ORR pathway, intermediates, and mechanisms in highly concentrated basic solutions (close to the real conditions of AAEMFCs cathode); (4) reasons for the very slow kinetics of oxygen reduction.

Non-Pt noble metal electrocatalysts.—Pd and Ag based electrocatalysts.— The high cost and scarcity of Pt have always been the major impediments for commercialization of fuel cells. Fortunately the more facile ORR process creates the possibility of replacing Pt with less expensive and more abundant "noble-metals". Pd or Ag based catalyst materials indeed have exhibited very promising ORR performance comparable to that of Pt/C.[69–71] Among the major efforts for further improvement of ORR kinetics on Pd or Ag based electrocatalysts, some progress has been realized in recent years. One general and reasonable strategy is to make and disperse nanoparticles on functionalized carbon support for increasing the surface area of metal particles and accelerating electron transfer and other processes. Given enough consideration on the shape and size effects,[72–79] Jeon et al.[80,81] deposited Pd and Ag nanoparticles on linker grafted graphene support and achieved remarkable electrocatalytic activity. Figures 5a and 5b show the unique role of the linkers to facilitate intermolecular charge-transfer and dispersion and stability of metal nanoparticles.

In addition to sphere-shaped nanoparticles, some recent advances on preparing metallic Pd and Ag nanocrystals with special shapes and excellent ORR activity can be found. Various shaped Pd and Ag nanoparticles such as Pd nanocubes,[82] Pd cubes and octahedra,[83] hollow Pd nanoshells,[75] Pd icosahedra,[84] Ag nanodecahedra

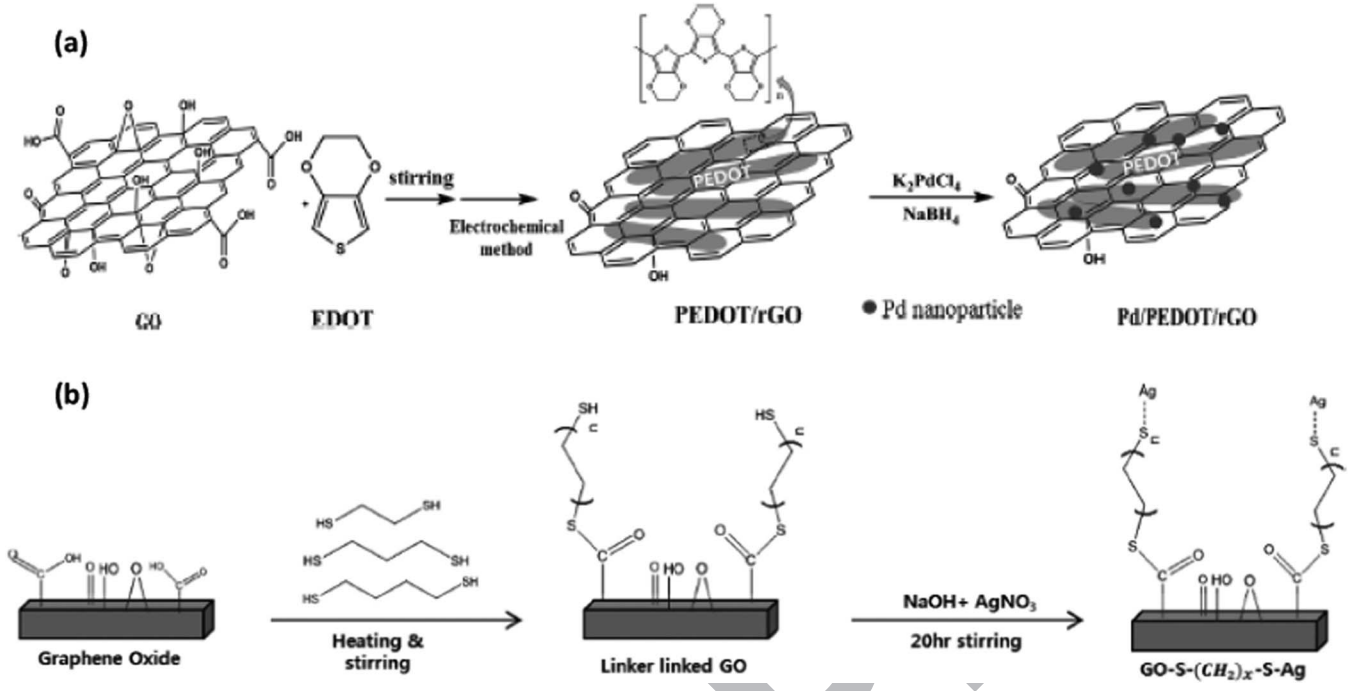

Figure 5. Schematic diagram of synthesis of linkages Grafted Graphene supported palladium (a) (Reprinted with permission from Ref. 80 Copyright 2015 Elsevier.), and silver (b) nanoparticles Reprinted with permission from Ref. 81 Copyright 2015 The Electrochemical Society.

and nanocubes,[77] Ag nanoclusters,[85] worm like and angular Ag nanoparticles,[76] all seem to be able to catalyze ORR in rather facile ways, and further exploration is needed for better understanding of the shape effects. Besides, it is a little counterintuitive to develop noble metal oxides as ORR electrocatalysts since they were expected to block effective O_2 adsorption as in the case of PtO_x. Surprisingly, PdO/C synthesized by heat treatment of Pd/C in air at 250°C showed almost identical catalytic activity to that of Pd/C, and a PdO/C-4h sample synthesized by the reaction of $PdCl_2$ with a Mn_3O_4/C substrate showed superior activity and kinetics as compared to Pd/C.[86] Higher specific activity but a smaller number of electrons transferred were also found on Ag particles with oxide surfaces.[76] Although the ORR mechanism of outer-sphere electron transfer and more efficient interaction between $O_{2,ads}$ and extra OH^- species at the double layer interface is still a hypothesis, it can be certainly inferred that ORR processes are different on the above materials and highlight it as a very interesting topic for further investigation.

Similar to the surface modification of Pt by alloying with other metals, a number of novel Pd and Ag based alloy electrocatalysts including core-shell structured materials have been tested for ORR in alkaline media and reported in recent years. Some typical examples that can be used as references for further alloyed catalyst development are listed in Table II. Generally, some more inert elements for ORR such as Au have been added to improve the stability of the catalysts as it functionalizes in acidic media.[87] It can be noticed that the choice of alloying elements have been broadened very much because 3d transition metals (e.g. Cu, Fe, Ni, Co) can be widely employed and even enhanced stability of the catalysts can be obtained.[88,89] Since high temperature heat treatment is not always necessary for synthesis of the above alloy catalysts, the enhanced activity may be attributed to stronger synergistic and better ensemble or miscibility effects with Pd or Ag although no detailed studies on this hypothesis are available yet.

Different from forming alloys or core-shell structures with other metals, some metal oxides were also added into Pd or Ag based catalysts and helped to improve the overall ORR performance. Slanac et al.[90] synthesized Ag-MnO_x/C composites with a new electroless co-deposition method. From the STEM imaging and EDS elemental mapping in Figure 6i Ag nanoparticles are interconnected with MnO_x nanodomains, providing a ligand effect and an ensemble effect on ORR activity of the composite catalyst approaching that of Pt in Figure 6ii. From others' reports, Pd or Ag-MnO_x/CoO_x composites were prepared using a solvothermal method,[91] immersion-calcination

Table II. Novel Pd and Ag based alloy electrocatalysts for ORR in alkaline media.

Catalyst	Preparation method	Kinetics parameter	Highlights	Ref.
with Au $Au_{10}Pd_{40}Co_{50}$/C-core-shell, $Au_{10}Pd_{40}Co_{50}$/C-intermetallic	For the core-shell structure, Co/C was formed by reduction of $CoCl_2$, which is followed by coating of Au and Pd. The core-shell catalyst subjects a structure change to intermetallic with heat treatment.	Mass activity at 0.9 V, Intermetallic: 0.13 (A/mg), Core-shell: 0.09 vs. $Pt_{3.5nm}$/C: 0.14	• Structurally ordered $Au_{10}Pd_{40}Co_{50}$ catalysts that exhibit comparable activity to conventional platinum catalysts • Core-shell structure changed to intermetallic ordered structure with high temperature treatment • Au atoms help to significantly improve the stability of the catalysts	386
Pd–Au nanochain networks / reduced graphene oxide (rGO)	Wet-chemical co-reduction method with the assistance of caffeine	Mass activity at −0.1V (vs. Ag/AgCl), ~ 14 mA/mg	• Better electrochemical performance than commercial Pd-black and Pd–C toward ORR	387

Table II. (*Continued.*)

Catalyst	Preparation method	Kinetics parameter	Highlights	Ref.
AuPd Nanochain/carbon black	Two-step galvanic replace-ment reaction	Half wave potential ($E_{1/2}$) (vs. SCE), $Au_{0.8}Pd_{0.2}NN_S$/C: −0.097 V Pt/C: 0.02 V	• ORR activity of $Au_{0.8}Pd_{0.2}NN_S$/C surpasses Pt/C	388
Au@Pd core–shell nanothorns	Wet-chemical sequential reduction method with the assistance of L-ascorbic acid	Mass activity at 0.9 V, ∼ 16 mA/mg	• Higher ORR activity and stability than both of commercial Pd black and Pt black • Thorn like morphology and synergistic effects between the Au core and the Pd shell	389
Au@Ag electrodes	Under potential deposition (UPD) of Pb on Au followed by surface replacement of Ag	Kinetics current, half an order of magnitude improvement vs. Ag	• Surface oxygen affinity of Ag is improved by electronic interaction with Au sublayer	390
With Cu				
PdCu/rGO	Homogeneous hydrothermal reduction	Mass activity at −0.26 V (vs. SCE), 38.4 mA/mg	• Improved electrocatalytic performance and high methanol-tolerance ability	391
PdCu/graphene	"Dispersing-mixing vaporizing solvent" method	Mass activity at −0.25 V (vs. SCE), G-Cu_3Pd: 45.4 mA/mg_{NCPs}	• G-Cu_3Pd NCPs exhibit the highest electrocatalytic activity compared with other G-Cu_xPd_y • The durability of G-Cu_3Pd NCPs is superior to commercial Pt/C catalysts	88
Ag/octopus-tentacle-like Cu nanowire	Epitaxial growth of Ag nanocrystals on Cu nanowire	–	• Efficient approach for synthesizing metal heterostructures with large lattice misfit (>5%)	89
With Fe				
FeCo@Fe@Pd	Microwave-induced top-down nanostructuring and decoration	Exchange current density (j_o) = 1.26* 10^{-2} mA cm^{-2})	• High tolerance to methanol	392, 393
FeAgPc/C	Pyrolysis of iron(II) and silver(II) phthalocyanines (MPc)	$E_{1/2}$ = 0.931 V	• Effective interaction between Fe and Ag and unique nanostructure were formed during heat treatment	394
With Ni				
Palladium-nickel (PdNi) hollow nanoparticles	Galvanic replacement method	Mass activity at −0.1 V (vs. Ag/AgCl), 588.97 $mA/g_{(Pd)}$	• Superior ORR performance was achieved as compared to commercial Pt/C or Pd/C	375
With Co				
AgCo/Ti	Electrodeposition of Co particles on the dendrite-Ag/Ti electrode and further modified by Polyani-line (PANI)	–	• ORR activity: PANI-Ag_xCo_y/Ti > Ag_xCo_y/Ti > PANI-Ag/Ti > Ag/Ti • Methanol or ethanol tolerant	101
AgCo	Incipient-wetness followed by rapid heating reduction	Specific Activity at 0.85 V, ∼1.5 mA $/cm^2$ $_{(Ag)}$	• Subsurface Co-ligand effects as the primary source of enhanced activity	395
With Sn				
Ag_4Sn/C	A solution phase reduction method	Mass activity at 0.75 V, 15.68 mA /mg, Specific activity at 0.75 V, 1.05 mA $/cm^2$ $_{(geo)}$	• High methanol tolerance and good long-term stability	396
With Mo				
AgMo hybrid	A hydrothermal method	Mass Activity at −0.1 V (vs. Hg/HgO), AgMo-22: 0.67 mA /mg	• Better stability than Pt/C	397
PdAg alloy				
AgPd alloys with different ratios	Wet-chemical co-reduction	Mass activity at −0.05 V (vs. NHE), Ag_9Pd: 3778 $mA/mg_{(Pd)}$, Ag_4Pd: 3518, Ag_2Pd: 2057, $AgPd_2$: 2011, Pd: 799	• The activity of more active Pd was enhanced by less active Ag by tuning the heteroatomic interactions	398
Ternary alloy				
Pd_2NiAg	Solid−liquid phase chemicalroute	$E_{1/2}$ = −0.131 V (vs. Ag/AgCl)	• Increased availability of surface Ni sites and the features of twinned structural defects • Improved catalytic activity	399
Comparison study				
MPd_3 (M = Fe, Cu, Ag, Au, Cr, Mo, W) nanocrystals/graphene	Electrostatic assembly and hydrogen reduction	–	• G-$FePd_3$ NCPs exhibit the highest catalytic activity	400

*ORR kinetics parameters were obtained at room T, 1 atmosphere. Potentials were referred to the reversible hydrogen electrode (RHE) unless they are addressed otherwise.

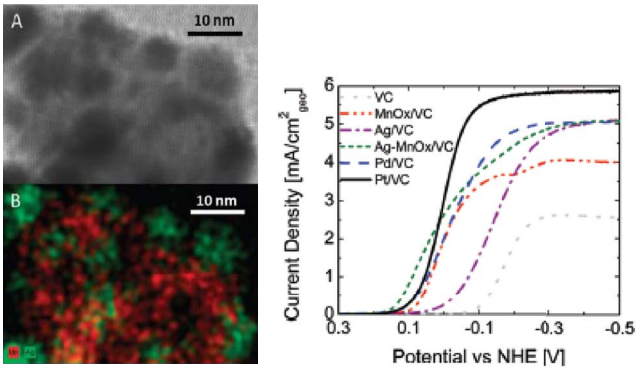

Figure 6. (i) STEM imaging and EDS elemental mapping of 20% Ag - 35% MnO_x on Vulcan carbon XC72 (VC) The (A) bright field image shows darker regions (silver) surrounded by lighter regions (MnOx and carbon). In (B) STEM-EDS mapping shows that the darker regions from the bright field images correspond to silver (green) nanoparticles, whereas the regions between the Ag are covered with MnOx (red). Carbon mapping is not shown here as the signal would show up everywhere due to both Ag and MnOx being supported on carbon. (Reprinted with permission from Ref. 90) Copyright 2012 American Chemical Society. (ii) RDE polarization curves (cathodic scans) for plain VC, VC loaded with MnO_x, and $AgMnO_x$ with respect to commercial standards of Pt/VC and Pd/VC. Reprinted with permission from Ref. 90 Copyright 2012 American Chemical Society.

method,[92] a carbon reduction-calcination method,[93] or a hydrothermal-wet reduction method,[94] from which promising ORR performance was achieved individually probably due to the presence of a metal-oxides interface.[90]

From the aforementioned reports on Pd and Ag based catalysts, commercial porous carbon black supported Pt, Pd and Ag were typically employed for comparison and evaluation of ORR performance of various types of catalyst materials. However, it has been known that the carbon black support may interfere with the ORR by promoting the $2e^-$ outer-sphere electron transfer and incomplete reduction of O_2. Moreover, carbon may suffer from being used as nanoparticles due to severe corrosion and oxidation under the real fuel cell operating conditions, resulting in general degradation of the performance of supported catalysts. Many research groups endeavored to disperse Pd and Ag particles on other support materials to improve the long term stability. For instance, Lu et al.[95] developed a new class of Pd tetrahedron−tungsten oxide nanosheet hybrids with an organopalladium complex precursor and in situ-synthesized $W_{18}O_{49}$ nanosheets. From Figure 7, the binding energy of Pd 3d and the binding energy of W 4f for $Pd/W_{18}O_{49}$ move in opposite directions. This indicates that partial electrons may transfer from Pd to W due to the strong interaction. A Similar phenomenon was found on a CuFe/C bimetallic catalyst with soft X-ray absorption measurement.[96] The lowering of electron density on Pd may significantly help to enhance the dissociative adsorption of O_2 and the following 4-electron reduction.[95,97–99] In addition to the Pd-WO_x hybrids with both enhanced activity and stability, some robust metals like Ti (or TiO_x)[100,101] and Ni foam,[102] some 2-dimental carbon materials like carbon nanotubes (CNT)[103,104] and graphene,[105–107] and other carbon supports like B doped C,[108] carbon nitride,[109] carbon nanofibers[110] were also used to support Pd or Ag nanoparicles and nanoalloys.

Other non-Pt noble metal electrocatalysts.—Other than Pd and Ag, the number of reports of other non-Pt noble metal electrocatalysts is rather limited. Among the research efforts on Au,[111–113] Ru,[114,115] Ir[116] and other precious metal catalysts for ORR in alkaline media, the main motivations seem to be devoted to the understanding of ORR mechanisms on a broad scope or assist in the study of other materials such as supports and mediators, rather than using them as replacement for Pt based electrocatalysts. Rodriguez and Koper[117] have made a thorough review on electrocatalysis of gold, in which some basic conclusions were drawn regarding topics such as the pH and crystallographic orientation effects on the kinetics of ORR, the distinct roles of the d band of metal electrodes in extreme pH conditions, the shape sensitivity of Au nanoparticles for ORR, and the influence of the support and the particle size on kinetic currents. Given the fact that the non-Pt precious metals except Pd and Ag can usually catalyze ORR in a $2e^-$ pathway by themselves, it is a little surprising to see that a $AuCu_3$ alloy catalyst can show 1.5 times mass current density of commercial Pt/C for the ORR in 0.1M KOH.[118] It has been known that neither Au nor Cu is suitable for catalysis of ORR due to the weak affinity between Au and O_2 or OH^-[118–120] and a too-strong binding energy between Cu and oxygen.[118,119,121] Figure 8a shows that Cu/C and Au/C have very poor ORR kinetics. However, based on the DFT calculation model in Figure 8b, the adsorption energy of the $AuCu_3$ alloy with oxygen (−1.04 eV) is very close to that of Pt (−1.06 eV). In other words, the balance of oxygen adsorption and intermediate desorption was perfectly reached by changing the atomic ratio of Au and Cu, which opens a new gate for design of novel catalyst materials using a combination having elements of weak and strong oxygen affinities.

Non-noble-metal electrocatalysts.—Carbon supported M-N_x matrix (M = 3d transition metals).—Fundamental overview.— Different from the noble metal electrocatlalysts discussed in the above sections, some earth-abundant 3d transition metals(e.g. Fe, Co, Ni) usually do not exhibit catalytic activity for ORR in their metallic forms such as metal crystals or nanoparticles simply due to their strong reactivity or affinities with oxygen.[122] Instead, they are typically used to

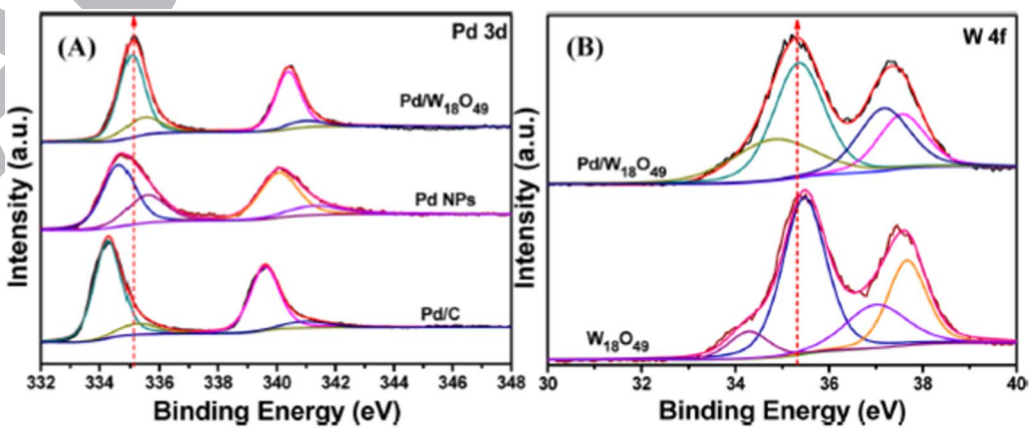

Figure 7. (A) XPS patterns of Pd 3d in $Pd/W_{18}O_{49}$, Pd NPs, and commercial Pd/C. (B) XPS pattern of W 4f in $Pd/W_{18}O_{49}$ and $W_{18}O_{49}$. Reprinted with permission from Ref. 95 Copyright 2014 American Chemical Society.

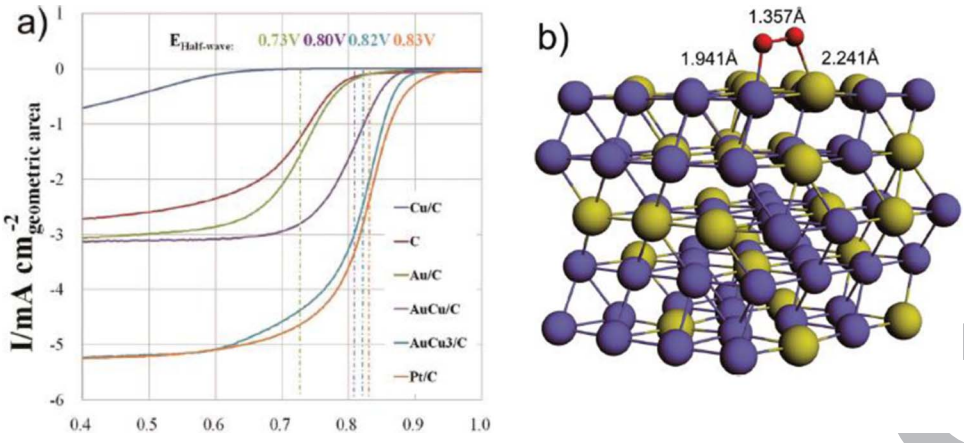

Figure 8. (a) LSV curves (background corrected and IR-compensated) of a series of catalysts: carbon, Cu/C, Au/C, Pt/C, intermetallic AuCu/C and intermetallic $AuCu_3$/C, normalised by the geometric area of the working electrodes. RDE measurements were tested in O_2–saturated 0.1 M KOH, scan rate: 10 mV/s, RDE rotation rate: 1600 rpm. Reprinted with permission from Ref. 118 Copyright 2014 Wiley-VCH. (b) The most probable adsorption mode of oxygen on AuCu (111) (rotated bridge mode); Cu (blue), Au (yellow) and O (red). Reprinted with permission from Ref. 118 Copyright 2014 Wiley-VCH.

form alloys with noble metals to enhance ORR kinetics by changing the crystal lattice structure, electron density, surface morphology, ensemble effects, and synergetic effects, etc. Recently, some novel carbon-supported (with or without doping elements of N, S, P and B) first row transition metal and metal oxides,[123–126] chalcogenides,[127–129] spinels,[130–132] pyrochlores[115,133,134] have been reported to show some activity for ORR in alkaline media. Among them, similar and ever faster ORR kinetics than Pt based electrocatalysts have been widely seen on this class of materials by stabilizing the metal or metal oxides with surface nitrogen (or other elements) functionalities on graphitic surfaces, which are the main focus of this section due to their direct applicability in AAEMFCs.

After the ground-breaking discovery of the metal macrocycle compounds,[135] a consensus of the key role of the N-metal bond on exhibiting ORR catalytic activity has generally formed.[136] It is accepted that in the macrocycles the ORR electrocatalysis active center is located on the central metal ion with sufficient d-character to coordinate O_2 molecules. And that is verified by the fact that the ORR normally operates at the potential of reduction of the metal-O_2^- adduct[137,138] and the onset potential of ORR is closely linked to the redox potential of the central metal.[137–139] However, the catalysts would not be stable without the strong anchoring effect caused by the large bonding energy between the central metal and the surrounding N.[140–143] More importantly, the metal-N bond serves as the bridge for the π-conjugated ligands on the outer periphery to relocate its redox potential by modifying the electronic structure.[136,144] For Example, cobalt porphyrins can be converted to a 4-electron transfer catalyst for ORR by placing pendant electron-withdrawing groups on the periphery of the macrocyclic ligands.[145] Indeed, electron-withdrawing groups on the macrocycle ring may shift the energy of the d orbitals away from the Fermi level, resulting in a higher ORR onset potential and higher turnover numbers due to a more suitable binding energy for ORR intermediates. In addition, it was found that adsorption of metal porphyrins on a carbon black support can dramatically enhance the ORR activity and shift the onset potential toward in the positive direction.[146]

The effect of the carbon support was attributed to the strong π-π interaction between the metal macrocycle ring and the carbon basal plane, for which the delocalized π electrons on the metal macrocycles could not exist without the metal-N_x matrix. And it was confirmed that the axial coordination on the central metal ions themselves does not contribute much to the strong binding.[146] At low pH, it is surprising to see that a dramatic anodic shift for the ORR onset potential can be achieved by pyrolysis of a mixture of metal macrocycles and carbon black at certain high temperatures (e.g. 700–900°C) under inert Ar or N_2 atmosphere.[33,147–149] Contrarily, the heat treatment effect on the positive shift of the onset and half wave potentials of ORR is less prominent in alkaline media than its counterpart in acidic media.[11,12] This difference has not been explained and needs due consideration because an even larger positive shift of the redox potential of $Fe^{2+}/^{3+}$ was noticed in 0.1 M NaOH as compared to 0.1 M $HClO_4$ from a square-wave voltammetry measurement.[33] Nevertheless, the stability and selectivity of metal macrocycle catalysts for ORR can be largely improved after pyrolysis.[12,150–152] As a result, it is generally required to conduct the step of heat treatment during synthesis of transition metal macrocycle based electrocatalysts to achieve optimized ORR performance, from which some alternative ways to form metal-N_x composites were derived and developed (*voyez-infra*). Not the entire organic framework can survive after treatment under such harsh conditions. However, at least partial metal-N_x moieties can remain in light of recent evidence by HR-XPS.[96,153] It is the expectation that the metal-N bond still plays a key role in the catalytic properties of the pyrolyzed macrocycles. However, this must not be the complete story because the pristine compounds with more optimized d characters should have higher activity otherwise. There have been continuous efforts on the identification of the active-site structure of pyrolyzed metal macrocycles (especially the ones supported on carbon).

Some representative theories such as van Veen et al.'s secondary structures containing M-N_4/C moieties,[154–160] Yeager et al.'s C–N_x–Me complex with reabsorption of metal species,[161–166] Wiesener's metal free C–N_x functional groups,[167,168] and Dodelet's metal ion-pyridinic nitrogen-edges of graphitic sheets,[149] were proposed and may be true under their specific preparation conditions. This debatable topic and the obscurity surrounding the nature of the active site after pyrolysis of metal macrocycles have been given considerable attention in recent years. Indeed some theoretical and experimental works have advanced our understanding of the common nature and original causes of activity of this class of electrocatalysts. Nagappan et al.[33] combined electrochemical and spectroscopic studies to unravel the nature of the active sites and ORR mechanisms on heat treated porphyrin catalysts in both acidic and alkaline media. Although the in situ XAS delta-mu ($\Delta\mu$) technique is literarily meant to remove the background of the bulk electrode and obtain specific information about surface adsorbates,[169–174] the nature of the sites where O_2 adsorbs can be still clarified with the assistance of theoretical simulations since any adsorbates cannot stand alone with the direct effect of local symmetrical and coordinating environments of the electrode surface. By careful comparison of Figure 9a and Figure 9c, one may notice that the active site for ORR has changed from a FeN_4C_{12} cluster to a FeN_4C_z cluster ($z = 10$ or 8), whereas the number z is correlated to the degree of the destruction of the carbon methine bridges. The simulated structures (Figures 9b and 9d) before and after pyrolysis

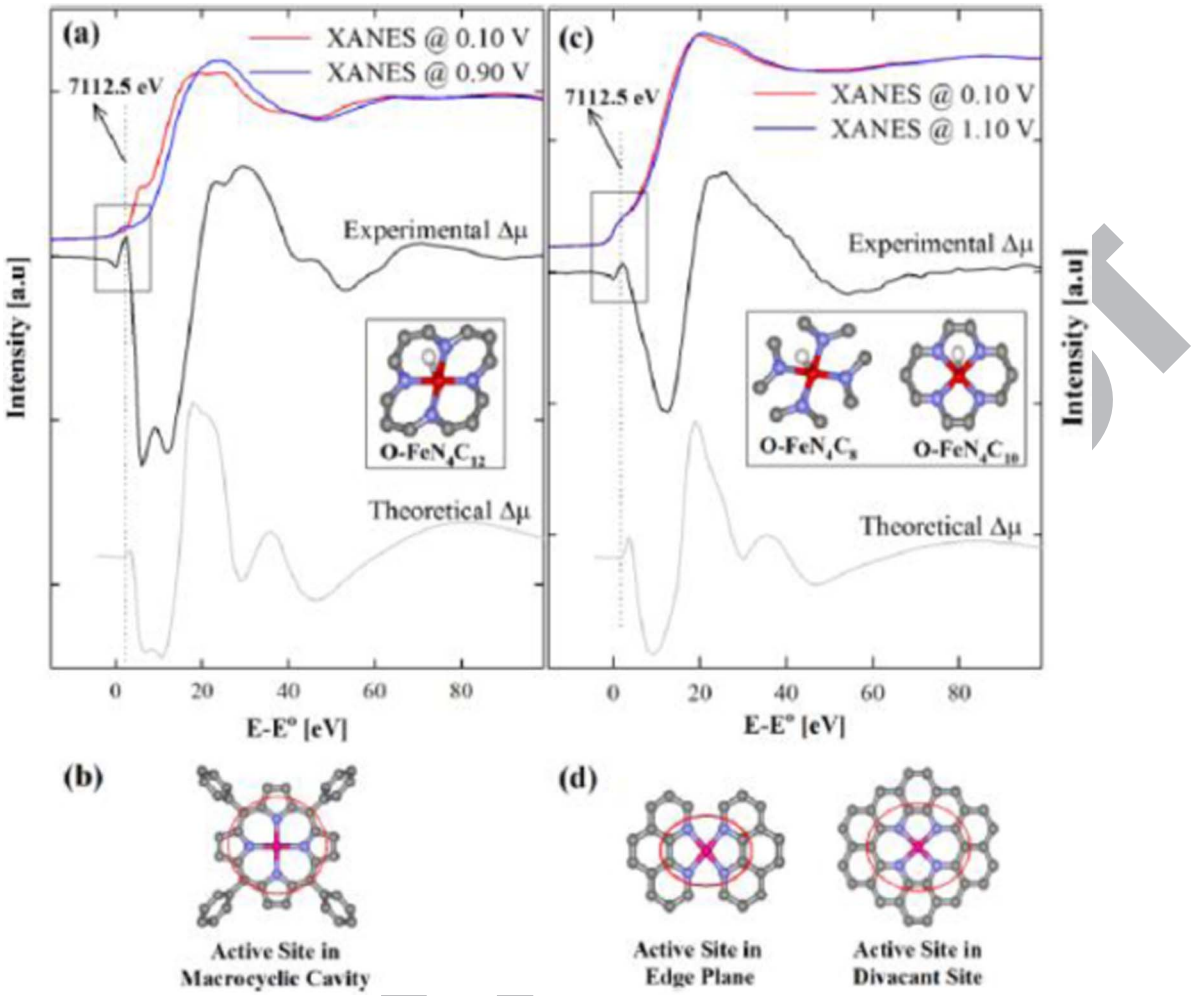

Figure 9. Active site structure identification. Experimental XANES and Δμ signatures of Fe−N_x/C catalyst pyrolyzed at (a) 300 and (c) 800°C. The Δμ signatures were obtained by subtracting the XANES signatures according to Δμ = μ(0.90 (or) 1.10 V) − μ(0.10 V). Experiments were conducted at Fe K-edge under in situ conditions in argon saturated 0.1 M NaOH electrolyte. Vertical dotted line indicates the pre-edge position at 7112.5 eV. Structural models shown in the insets of panels a and c were utilized for Δμ analysis using FEFF8 simulation. Also shown are the complete structural models of active site structures before (b) and after (d) pyrolysis at 800°C. Color codes in structural models: red, iron; blue, nitrogen; gray, carbon; white, oxygen. Reprinted with permission from Ref. 33 Copyright 2013 American Chemical Society.

are reminiscent of some crystallographic zones (e.g. divacancy) of carbon supports, indicating that the Fe-N_4 active sites are covalently integrated into the π-conjugated carbon basal plane. As a result, not only the adsorption energy of O_2 and intermediates on the catalytically active sites can be modulated by the delocalized π-electron system of the entire carbon basal plane, but also more efficient electron transfer between the reactants (O_2 molecule) and the electrode can be realized. This could be the fundamental reason for the dramatic shift of redox potential of Fe^{2+}/Fe^{3+} and the corresponding onset potential of the ORR.

In spite of the fact that the desired coordination number of N surrounding the central metal ions is still unclear,[175–177] the anchoring of Metal-N_x (e.g. Fe-N_4[33] or Co-N_4[177] on some defects or interplane regions of the carbon support seems to be the original cause of enhanced ORR activity. The active sites can be formed by other methods in addition to pyrolysis of metal macrocycles. Xu et al.[178] prepared different transition metal (Co, Fe, Cu, Mn, and Ni) incorporated nitrogen-containing electrocatalysts by pyrolysis of inorganic metal salts and aminopyrine (Apyr) as the nitrogen precursor. Besides the finding of significant enhancement by the pyrolysis due to formation of surface carbon-bonded pyridinic-N and metal, different metal elements exhibited discrepancy of ordering in terms of ORR activity and selectivity. This might be attributed to a higher content of sulfur in Mn- and Fe- incorporated catalysts, which is indicative of the importance of the appropriate choice of metal salts for pyrolysis. Asazawa et al.[179] synthesized Co-polypyrrole-based electrocatalysts using $Co(NO_3)_2$ as the starting metal salt. Moreover, two kinds of nitrogen structures (pyrrolic and pyridinic) were found to be coordinated with Co to form active sites for ORR using Hard X-ray Photo Electron Spectroscopy (HAXPES) analysis and DFT calculations. Consistent with the deteriorated performance by treatment of the pristine CoP-PyC catalyst with sulfuric acid, Domínguez et al.[180] also found the activity of Fe based electrocatalysts was decreased when subjected to acid treatment, possibly due to removal of active sites and blockage by adsorbed sulfates.

From Nagappan et al.'s study[33] it is the pyrolysis process that integrates Fe-N_4 active sites into defective pockets on the carbon support that can be either induced by pre-pyrolysis[181–186] or during the heat treatment by carbothermic reactions,[182,184] providing a large shift of redox potential of the Fe^{2+}/Fe^{3+} couple and much lowered ORR overpotential. Beyond that the pyrolyzing atmosphere was found to be important to the catalytic activity, and the Co-based catalysts heat treated in N_2 show better results than those in Ar or CO_2.[187] The pyrolysis temperature was also found to be important in maximizing the ORR performance of cobalt-polypyrrole and cobalt-phthalocyanine based catalysts, because metallic Co that is not ORR active may be

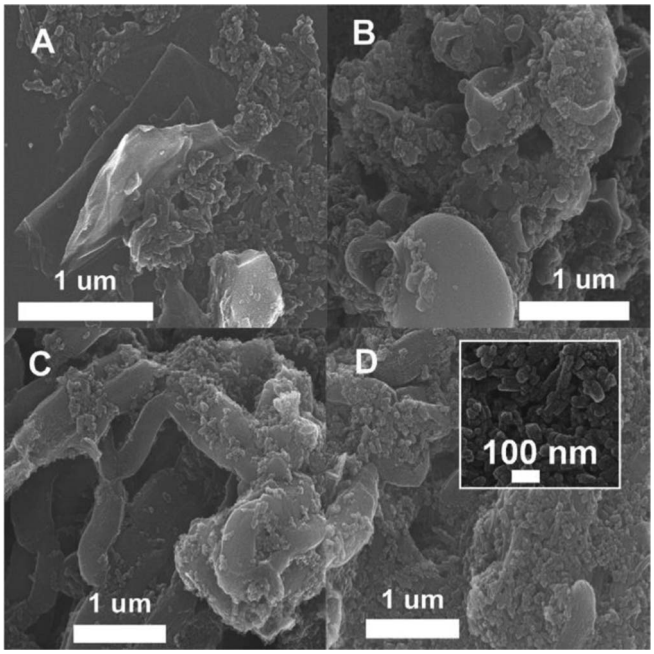

Figure 10. SEM images of the FePc/RGO (reduced graphene oxide) (A), FePc/MCV (mesoporous carbon vesicle) (B), and FePc/OMC (ordered mesoporous carbon) (C) with the mass ratio (FePc: carbon matrix) of 1:1. (D) SEM image of FePc/OMC with the mass ratio (FePc: OMC) of 3:1, inset is SEM image of FePc. Reprinted with permission from Ref. 189 Copyright 2014 Elsevier.

generated when the temperature is above a certain value.[150,188] The crucial role of pyrolysis on improvement of ORR activity of non-noble-metal catalysts did not seem to be debatable until a recent report about the effect of carbon support with varying microporous surface area on the catalytic activity of iron phthalocyanines (FePc) came out. Li et al.[189] prepared FePc/MVC (mesoporous carbon vesicle), FePc/OMC (ordered mesoporous carbon) and FePc/rGO (reduced graphene oxide) simply by mixing FePc and different carbon matrixes at room temperature. The as-synthesized catalysts with the SEM images shown in Figure 10, all display the 4-electron pathway for ORR and FePc/OMC shows comparable catalytic activity and better stability than Pt/OMC. It will be very interesting to see if edge plane-like defect sites on the OMC are truly the anchor zones for Fe-N_4 active sites via non-covalent π-π interaction. If true, the limitation in the active site density and low effective metal loading (≤ 3 wt.%)[33,190] on the current non-noble metal electrocatalysts can be overcome. This can have a significant impact on the overall fuel cells' performance by increasing the turnover number for the ORR while keeping the thickness of the electrodes unchanged.[191]

It has been demonstrated that the activation of solvated O_2 molecules can be facilitated by OH^- ions located at the electrode-electrolyte interface, leading to more facile ORR kinetics and electrode-independent outer-sphere electron transfer.[12,18] As the main fundamental reason for a broad choice of electrode materials for ORR electrocatalysts in high pH environment, however, it obviously cannot explain the complete O_2 reduction results with 4-electron transfer on numerous carbon supported non-noble-metal electrocatalysts.[36,192–194] In fact, as illustrated in Figure 11, the first 2-electron outer-sphere transfer process has been suppressed by efficient displacement of axial OH^- anions on the catalytically active site of Fe(II)-N_4 by molecular O_2. This clearly indicates that the ORR has switched to an inner-sphere electron transfer mechanism, in which the ferrous-hydroperoxyl adduct is stabilized and oxidized further to a ferric-hydoxyl species with the aid of a Frumkin-type double-layer effect.[195] Consistent with this study, Robson et al.[196] performed ORR mechanistic research on Fe-aminoantipyrine pyrolyzed electrocatalysts. A 2 × 2 pathway that mimics the direct 4-electron pathway was proposed and deferred by the evidence of rapid reduction of H_2O_2 in both acidic and alkaline media.

Novel synthesis methods for metal-Nx/C electrocatalysts.—Knowing the original causes of activity, it becomes unnecessary to prepare the catalysts by pyrolysis of organometallic compounds, which may raise the cost significantly with expensive precursors in large scale production. One feasible alternative way to prepare metal-N_x/C catalysts is to change the precursors or sources of nitrogen, metal ions and carbon for ensuing high temperature pyrolysis. Recently evolved heat-treatment precursors along with synthesis parameters and ORR results are summarized in Table III.

Aside from thermal annealing, it is always more favorable to conduct the synthesis at relatively low temperatures. As shown in Figure 12, a poly(sodium-p-styrenesulfonate) modified reduced graphene oxide support (PSS-rGO) was first fabricated at 95°C with the assistance of hydrazine hydrate. Then metal 5,10,15,20-tetrakis(4-hydroxyphenyl)porphyrin (M-THPP) was grown in situ on the PSS-rGO hybrid using a solvothermal method at 150°C. The unique

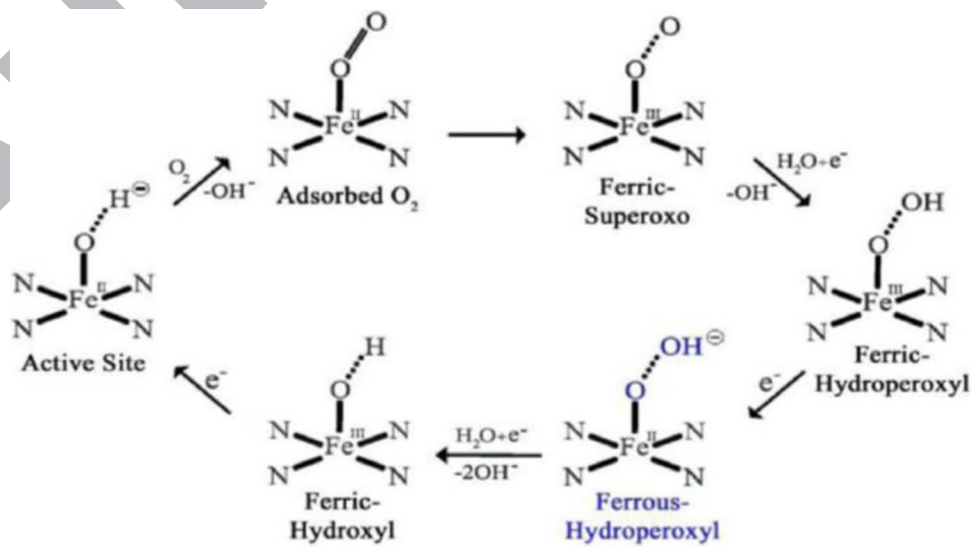

Figure 11. Proposed ORR mechanism. Catalyst cycle showing the redox mechanism involved in ORR on pyrolyzed Fe−N_x/C active sites in dilute alkaline medium. Reprinted with permission from Ref. 33 Copyright 2013 American Chemical Society.

Table III. Novel Metal-N_x electrocatalysts synthesized by pyrolysis at high temperature.

Material	Precursors for pyrolysis	Synthesis parameters	ORR performance	Ref.
Fe-N_x/C	Prussian blue nanocubes on carbon	1 h, 3 h at the pyrolysis temperature (700°C) without gas flow, HCl washing	• 0.313 mA mg^{-1} @0.775 V (the best catalyst in Ref. 401)	401
Fe-N/C	Methylenediantipyrine mixed with $Fe(NO_3)_3 \cdot 9H_2O$	Pyrolyzed at 800, 900, 950°C with different time under N_2, H_2 and NH_3, HF washing	• j_d at 0.9 V: −2.15 $mAcm^{-2}$ (the catalyst treated at 900°C in NH_3)	374
Fe-N/C	2,2-Pyridylbenzimidazole mixed with ferrous sulfate	Pyrolysis at different temperatures in NH_3	• $E_{1/2}$ V (vs. SHE), HT-PBZ/Fe-700 : 0.058 V	402
Fe-N/C	11,11′-bis(dipyrido[3,2-a:2′,3′-c] phenazinyl (bidppz) mixed with $FeSO_4 \cdot 7H_2O$	Heated to 700, 750, 800, 850 and 900°C for 1.5 h, HCl washing	• $E_{1/2}$, Fe−N/C-800 : 809 mV (Pt/C: 818 mV) • Superior durability than Pt/C	36
Fe-N/C	4,40,400-s-Triazine-1,3,5-triyltri-p-aminobenzoic acid mixed with $FeCl_2 \cdot 4H_2O$ and carbon black	Pyrolyzed at 800°C for 120 min at a rate of 3°C min^{-1} under a nitrogen atmosphere	• Kinetic current density: 4.1 mA cm^{-2} at 0.6 V • Comparable stability and tolerance to methanol with other Fe-N/C catalysts	403
Fe-N/C	FeTEPA chelate mixed with pretreated BP 2000 powder	Pyrolyzed at 800°C for 90 min with a heating ramp of 5°C min^{-1} in N_2	• E @ −0.6 mA, 47 mV higher than that of Pt/C	404
Fe-N/C	Hemin	Pyrolyzed at 500–950°C in an argon atmosphere for 2 h	• Current density at −0.1 V (vs. Hg/HgO), Self-assembly-HM (950°C): 3.3 mA/cm^2	405
Fe-N/C	MIL-88B-NH3 (MOF)	Pyrolyzed at 900°C in an argon atmosphere for 6 h	• $E_{1/2}$, 0.92 V	406
Fe-N/C	CPM-99 (MOF)	Pyrolyzed at different temperatures for 4 h in Ar gas	• $E_{1/2,}$ 0.802 V for CPM-99(Fe)/C	407
Fe-N/C	Mixture of ferrocene and melamine	Pyrolyzed at 600°C for 10 h with a heating ramp of 10°C/min	• Kinetic current density (j_k) • NC-600: 4.02 mA/cm^2 • Better methanol tolerance than Pt/C	408
Fe-N/graphene	Mixture of precipitates (ZnO/GO), $FeCl_3 \cdot 6H_2O$ and melamine	Pyrolyzed at 900°C for 2 h under Ar, H_2SO_4 leaching	• Cathodic current, −1.80 mA /cm^2 for Fe/N/GR-50-(0.10) • Better stability and methanol tolerance than Pt/C	409
	Iron (II) 1-cyclopenta-2,4-dienyl reduced graphene oxide	Pyrolyzed at 800°C for 2 h under nitrogen flow followed by treatment at 800°C for 10 min under NH_3	• Onset potential is 13 mV lower than that of Pt/C	410
	2,2-bipyridine and $FeCl_3 \cdot 6H_2O$ encapsulated in SBA-15	Pyrolysis at the given temperature for 3 h in high pure N_2, a heating rate of 2°C min^{-1}, HF etching	• $E_{1/2}$, Fe−N−GC-900: 0.86 V	411
Fe-N/CNTs	Mixture of $FeCl_3$, Polypyrrole and carbon nanotubes	Heat treated in N_2 flow at different temperatures (700, 800, and 900°C) for 2 h, H_2SO_4 leaching	• E_{onset} and E_h of NCNT-800 are comparable to Pt/C • Tolerant to MeOH	412
N-Fe CNT/CNP	Mixture of iron acetate, cyanamide and BP 2000	Pyrolyzed at 950°C in nitrogen for 1 h, H_2SO_4 leaching	• $E_{1/2}$, 0.87 ± 0.01 V at the loading of 0.2 mg cm^{-2}, 0.93 V at the loading of 1.0 mg cm^{-2} • Superior stability than Pt/C	252
Co-N/C	Mixture of pyrrole, carbon dots and $Co(NO_3)_2 \cdot 6H_2O$	800°C for 2 h	• Onset potential: −0.005 V vs. Ag/AgCl) • Number of Electron transfer: 3.8 • High cycling stability and tolerance to MeOH	413
Co-N/C	Mixture of ethylenediaminetetra acetic acid (EDTA), melamine, KOH and $Co(NO_3 \cdot 6H_2O)$	700°C for 2 h with a heating rate of 10°C min^{-1} under N_2	• $E_{1/2}$, NPC-Co_{45}: 0.79 V • e^- selectivity	414
Co-N/C	Mixture of N,N′-bis(salicylidene)ethylenediamine and $CoSO_4 \cdot 7H_2O$	Heat treated at different temperature for 2 h under N_2	• j_k at −0.10 V (mA cm^{-2}), Co-N-S/C-700: 4.80	415
Co-N/C	Co-COF	Pyrolyzed for 2 h under N_2	• Number of Electron transfer: 3.86 for Co-COF-900	416

Table III. (***Continued.***)

Material	Precursors for pyrolysis	Synthesis parameters	ORR performance	Ref
Co-N/C	Vitamin B12 (VB12) and carbon quantum dots	Heat treated at 500, 700 or 900°C for 4 h under N_2, at the rate of 5°C min^{-1}	• Number of Electron transfer: 3.56 for $Co_{1.12}/N_{2.92}$/C-700 • Onset potential: −0.1 V (vs. SCE) for $Co_{1.12}/N_{2.92}$/C-700 • Outperformed methanol tolerance and stability	417
	Vitamin B12 (VB12) and graphene	Heat treated at 600–800°C for 2 h under Ar, a heating rate of 5°C min^{-1}	• $E_{1/2}$, 0.833 V for g-VB12 • High stability	418
	Vitamin B12 (VB12) and BP2000	Heated at different temperatures for 2 h under NH_3	• $E_{1/2}$ (vs. Hg/HgO), 0.072 V for g-VB12 • n = 3.9 • Superior methanol tolerance to Pt/C	419
Co-N-graphene	Mixture of cobalt dichloride, GuHCl (guanidine hydrochloride) and GO (graphene oxide)	Heat treatment at 650, 750, 850 and 950°C for 1 h in an Ar atmosphere	• $E_{1/2}$ (vs. SCE), Co-NG 850: −0.164 V (Pt/C: −0.181 V)	420
Co-N-graphene	Mixture of melamine, cobalt nitrate and GO	Heat treatment at 850°C for 30 min under Ar	• Number of electron transfer: 3.97 for Co–N-GX • Onset potential: −0.05 V (vs. Ag/AgCl) for Co–N-GX	421
Mg-Co-Al-N/C	Mg-Co-Al layered double hydroxides	Heat-treated at 600, 700 and 800°C for 3 h, in acetonitrile vapor	• 2-electron pathway	422
Metal-N-C	Poly(ethyleneimine) mixed with $Co(NO_3)_2 \cdot 6H_2O$, $Fe(NO_3)_3 \cdot 9H_2O$, $Ce(NO_3)_3 \cdot 6H_2O$, and $CoSO_4 \cdot 7H_2O$	Heat-treated at 800°C for 1 h under a nitrogen atmosphere	• $E_{1/2}$ (vs. SHE), Co-PEI: 0 mV	423
Metal-N-graphene	Metal oxides–Polyaniline–Graphene	Heat-treated at 800°C under a nitrogen atmosphere	• $E_{1/2}$ (vs. Ag/AgCl), Fe–NCG: −0.19 V, Co–NMCG: −0.18 V, FeCo–NMCG: −0.18 V • Number of electron transfer: Fe–NCG: 3.9, Co–NMCG: 3.4, FeCo–NMCG: 3.8	424

*ORR kinetics parameters were obtained at room T, 1 atmosphere. Potentials were referred to the reversible hydrogen electrode (RHE) unless they are addressed otherwise.

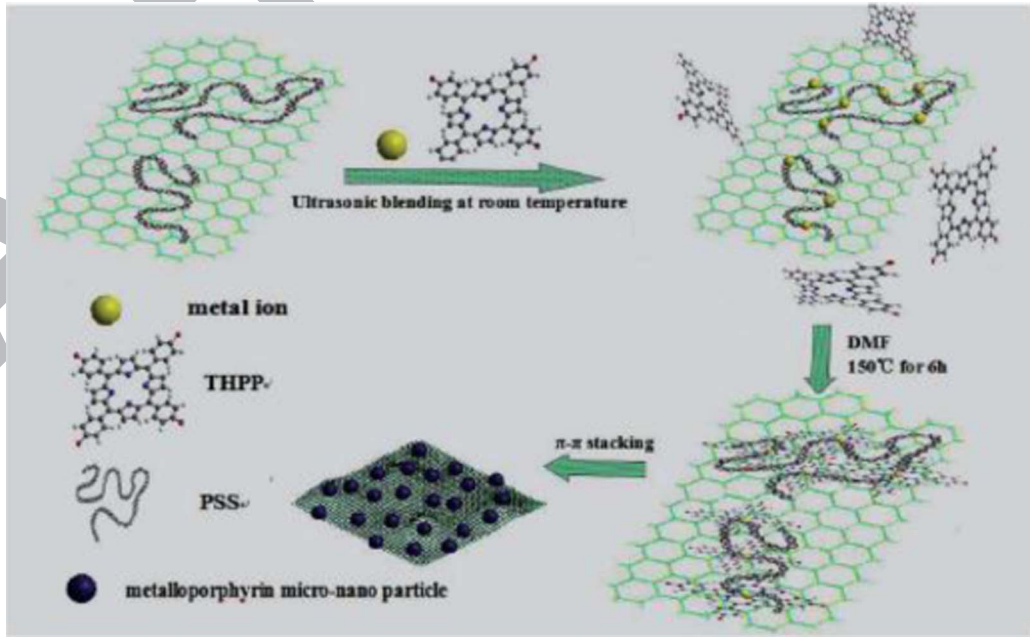

Figure 12. The synthesis routes to M-THPP/PSS-rGO composites Reprinted with permission from Ref. 488 Copyright 2014 Royal Society of Chemistry.

2-dimensional structure of rGO and the intact M-THPP moieties may provide a stronger π-π interaction than that between Co porphyrins and regular carbon black,[146] resulting in a $E_{1/2}$ of −0.22 V (vs. SCE) for the CoTHPP/PSS-rGO close to Pt/C (−0.20 V vs. SCE). In another work, Liu et al.[197] synthesized a FePc-graphene catalyst through an amidation reaction between carboxyl-functionalized graphene oxide and iron(II) tetra-aminophthalocyanine at 90°C. After being covalently bonded onto the graphene surface, the catalyst shows comparable catalytic activity with Pt/C as well as high stability and tolerance to crossover of methanol. Within the same category, a hybrid metal framework type of Fe porphyrin based catalyst ((G-dye-FeP)nMOF) was synthesized by the combination of $(Fe-P)_n$ MOF and G-dye (pyridine-functionalized graphene) that is terminated with pyridinium moieties.[198] The catalyst synthesized at 150°C shows a favored 4-electron ORR pathway with a n value of 3.82 and superior durability to that of Pt/C. The strong π-π stacking interaction may remain without any linker between the graphene sheets and the macrocycles. Graphene nanosheets and chemically reduced graphene supported iron phthalocyanine electrocatalysts were prepared by simple mixing under ultrasonication at room temperature.[199,200] The resulting catalyst exhibits excellent ORR activity and a long-term stability and tolerance to CO in alkaline solution.

The special synergic effect has also been found on other 2-dimensional carbon materials such as carbon nanotubes.[201–204] For example, after subjection of a mixture of nanoFeTSPc and MWCNTs to microwave irradiation, both hydroxyl/carboxyl (o) and sulfonate-functionalized (s) MWCNTs supported electrocatalysts were formed. The nanoFeTSPc-o-MWCNT catalyst gives the best ORR performance in terms of the half wave potential and the catalytic rate constant.[201] In another example,[202] FePc/SWCNTs composite synthesized by direct mixing of individual components shows high activity and perfect selectivity for ORR as well as insensitivity to methanol. Apart from the 2-dimensional carbon materials such as graphene and carbon nanobutes with conjugated π electron character, it is intriguing and surprising to see that some regular carbon supported organometallic complexes showing fast ORR kinetics were prepared at low temperatures. For example, Quernheim et al.[205] used regular carbon black to support a series of cobalt phenanthroline–indole macrocycles without any heat treatment and found that the catalysts show very close $E_{1/2}$ values to Pt/C as well as long term stability and tolerance to MeOH.

Metal-N_x/C electrocatalysts with novel compositions or shapes.—It is more common to see Fe- or Co-N_x coordinates than other metal-N complexes as ORR electrocatalysts. However, recently, it has been found that other third row transition metals can also be used to form metal-N composite catalysts with outstanding ORR activity and stability. For example, Kang et al.[206] prepared nitrogen-doped carbon from glycine and performed heat treatment with a mixture of $KMnO_4$ and the N-carbon support. The obtained Mn-CN_x catalyst shows an ORR $E_{1/2}$ potential that is only 12 mV lower than Pt/C. Ding et al.[207] synthesized carbon-supported nickel phthalocyanine catalysts by a solvent-impregnation and milling procedure followed by heat treatment at different temperatures. Although both metallic and N-coordinated Ni were formed, only incomplete oxygen reduction was observed on these catalysts.

In addition to single core metal-N_x complexes, bimetallic or nitrogen-coordinated catalysts have drawn more and more attention for further improvement of the catalytic activity and selectivity for ORR. Fu et al.[208] pyrolyzed a paste of a mixture of PANI modified GO sheet, $FeCl_3$ and $Co(NO_3)_2$ and obtained the FeCo–N–rGO catalysts with a striking positive shift of $E_{1/2}$ of 46 mV as compared to Pt/C. It was believed that the enhancement is from facilitation of incorporation of Fe–N_x moieties into graphene sheets by the Co–N_x moieties.[208] In another work, an Fe co-added CoPc-/C catalyst exhibits more than 40 mV positive shift for the onset potential and the half-wave potential as compared to the CoPc-/C pretreated under the same conditions.[209] The enhancement of performance was attributed to generation of Fe-N_x moieties, indicating that the Co-N_x framework may allow for rearrangement of N coordination during the pyrolysis process. In addition to combination of intrinsically active elements of Co and Fe, a bi-core CuFe–N_x/C composite electrocatalyst was synthesized by simple pyrolysis of FePc and CuPc precursors.[96,153] Although the Cu–N_x/C catalyst shows very limited ORR catalytic activity, a synergistic interaction between Cu and Fe was confirmed by high resolution X-ray photoelectron spectroscopy (HR-XPS) and soft X-ray absorption spectroscopy (XAS) measurements, resulting in enhancement of the ORR performance over that of the single core Fe-N_x/C catalyst.

Although the metal-N_x catalysts typically are amorphous in the tens of nanometer range, some pioneering work has been done to prepare ORR catalysts with special shapes at the submicrometer or micrometer range. Chao et al.[210] polymerized melamine with formaldehyde and doped with Co. The hierarchical peanut-like catalyst (Figure 13a) generated after hydrothermal reaction followed by heat treatment shows high catalytic activity (Figure 13b) for ORR in alkaline media. By heat treatment of a mixture of melamine, polyacrylonitrile (PA) and ferric chloride ($FeCl_3$), another fog-like fluffy structured Fe-N_x/C (Figure 13c) catalyst was prepared. The added melamine was found to be responsible for an increase of the porosity and defects in the carbon matrix and modification of the N content and distribution, leading to high ORR performance (Figure 13d) and outstanding stability for the catalysts. Furthermore, an ordered hierarchically porous structure (Figure 13e) seems to be beneficial to achieve a higher onset potential and higher current density than Pt/C on a N and Fe codoped catalyst(Figure 13f). Without any carbon support, a hollowed-out octahedral Co(II)-N complex (Figure 13g) with comparable ORR activity to that of Pt/C (Figure 13h) was formed by a two-step synthesis process (self-assembly at room T and carbonization at 800°C).

Other types of non-noble-metal electrocatalysts.—Metal oxides.—It is plausible that the ORR catalytic activity of the first row transition metals relies on multiple and reversible oxidation states that operate near the equilibrium potentials of ORR, providing that nitrogen coordinated metal ions instead of metallic forms can be used as efficient catalyst materials. Analogously, transition metal oxides that remain stable in alkaline media are expected to show similar intrinsic properties for ORR. Indeed, Chatenet et al. have studied a series of nanostructured MnO_x compounds that not only exhibited excellent ORR activity in alkaline media but also showed high tolerance to sodium borohydride and ethanol that could be used as fuels for alkaline direct liquid fuel cells.[211–213] In Su et al.'s DFT and electrochemical study,[214] a nanostructured a-Mn_2O_3 has been shown to be an excellent bi-functional catalyst for both oxygen reduction and oxygen evolution reactions (OER). Figure 14a depicts a general MnO_x Pourbaix diagram and clearly shows that the MnO_x electrode exhibits different oxidation states with various surface adsorbates at various potentials and pH values. From 0.69 V to 0.98 V, the onset potential region for ORR, the MnO_x catalyst is oxidized into 1/2 ML HO^* covered $Mn_2O_3(110)$ that is indicative of an active surface. It is a reminiscent of the active site of square-planar $Fe^{2+}-N_4$ with the axial adsorbate of labile OH^- anion for the Fe-N_x/C catalysts.[33] From Figure 14b, it is interesting to observe that bulk $Mn_3O_4(001)$, $Mn_2O_3(110)$ and $MnO_2(110)$ show only a marginal difference in terms of activity for ORR. That means, unlike most of noble-metal and metal-Nx electrocatalysts, the ORR is possibly much less sensitive to the starting oxidation states, which is further evidenced by examples including metal oxides and hydroxides shown in Table IV.

Nevertheless, it has been found that the ORR activity can be significantly influenced by the nanostructure on metal oxide catalysts with the same composition.[215] Meng et al.[215] synthesized α-, β-, δ- and amorphous MnO_2 and found that only α-MnO_2 can catalyze ORR in a 4-electron transfer mechanism as opposed to 2 e^- transfer on other MnO_2 samples. In another work, Selvakumar et al.[216] synthesized different types of α-MnO_2 nanostructures by a hydrothermal method, and found that ORR activity follows an order of nanowire > nanorod > nanotube> nanoparticle > nanoflower. This is in line with the finding that a long belt-like a-MnO_2 catalyst shows doubled and 4 times higher mass activity than a mixed tremella and short belt-like a-MnO_2 catalyst and a Tremella-like d-MnO_2 catalyst respectively (Figure 15).

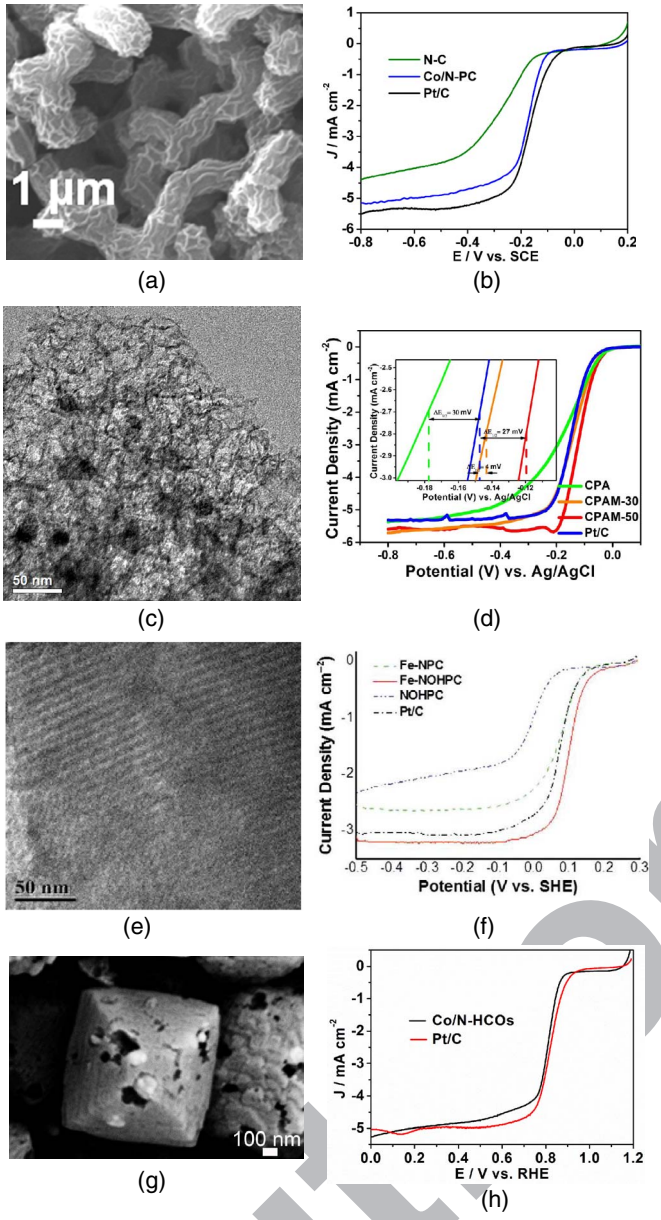

Figure 13. (a) A SEM image of the peanut-like Co/N-PC Reprinted with permission from Ref. 210 Copyright 2015 Elsevier. (b) ORR polarization curves of the N-C, peanut-like Co/N-PC and commercial Pt/C catalysts at a scan rate of 10 mVs^{-1} at 1600 rpm. Reprinted with permission from Ref. 210 Copyright 2015 Elsevier. (c) A TEM image of Fog-like fluffy CPAM-50. Reprinted with permission from Ref4.89 Copyright 2015 Royal Society of Chemistry. (d) LSV curves of fog-like fluffy CPA, CPAM-30, and CPAM-50. Reprinted with permission from Ref. 489 Copyright 2015 Royal Society of Chemistry. e. A TEM image of ordered hierarchically porous Fe-NOHPC. Reprinted with permission from Ref. 490 Copyright 2014 Wiley-VCH. f. ORR polarization curves for ordered hierarchically porous Fe-NOHPC, Fe-NPC, NOHPC, and Pt/C catalysts at a rotation rate of 1600 rpm in O_2-saturated 1 M NaOH. Reprinted with permission from Ref. 490 Copyright 2014 Wiley-VCH. g. A FE-SEM image of hollowed-out octahedral Co/N-HCOs. Reprinted with permission from Ref4.91 Copyright 2015 Elsevier. h. Polarization curves of Co/N-HCOs and Pt/C at 1600 rpm in O_2-saturated 0.1 M KOH solution. The polarization curveswere measured in O_2-saturated 0.1 M KOH at a scan rate of 10 mVs^{-1}. Reprinted with permission from Ref. 491 Copyright 2015 Elsevier.

The models described in Su et al.'s work[214] may be applicable to other transition metal oxides with prevalent phase changes on the electrode surface and in the sub-surface region with examples summarized in Table IV.

For noble-metal and metal-N_x types of ORR electrocatalysts, the carbon support has been widely used to improve the dispersion of metal nanoparticles and provide specific anchoring sites for metal-N_x active centers or synergic interactions between catalysts and the support. Although in some cases in Table IV, decent ORR kinetics can also be achieved on the metal oxide catalysts themselves, this does not mean that the carbon support is a reductant. Not only can the conductivity be enhanced by mixing with carbon for electronic percolation, but also some synergic effects might exist for achievement of better ORR performance in terms of both activity and stability.[217] It has been found that the MnO_x nanoparticles shape/phase and activity can be changed by using different carbon substrates.[218–221] Many types of carbon materials including carbon black,[222–225] mesoporous carbon,[226,227] carbon nanotubes[228–230] have been employed as supports for transition metal oxide composites. A recent review has also thoroughly covered the "starred" graphene supported non-noble-metal oxide electrocatalysts.[231]

Transition metal chalcogenides and sulfur doped non-noble-metal catalysts.— Transition metal based chalcogenides are an important class of alternative materials to Pt based electrocatalysts in acidic media due to their promising ORR activity and tolerance to crossover of methanol, and received continuous exploration in PEMFCs for the past two decades.[232–234] Nonetheless, the enthusiasm for utilization of transition metal chalcogenides in alkaline media seems to be surpassed by other types of transition metal electrocatalysts (*vide ante*), given the very few reports in the literature during the last three years. All the same, some attempts to develop transition metal chalcogenides with novel compositions and structures have been put into practice, which help to better understand some fundamental functions of this class of materials for ORR in alkaline media. Tetragonal and cubic phase Cu_2Se nanowires (NWs) were synthesized using a self-assembling method at 220°C and 280°C respectively.[127] From the kinetics study, the ORR pathway is structure-dependent with a direct $4e^-$ mechanism on the tetragonal Cu_2Se NWs and a dual-path mode that comprises both $2e^-$ and $4e^-$ mechanisms on the cubic Cu_2Se NWs. However, no further investigation follows the hypothesis that the spatial arrangement of Cu and Se atoms affects the adsorption and activation of O_2 molecules and modulates the electrocatalytic ORR performance of Cu_2Se NWs. Different from the synthesis route using surfactants for phase structure control of Cu_2Se NWs, $CoSe_2$/C was prepared via a two-step heating reaction method in p-xylene without any surfactants.[235] The as-synthesized cubic $CoSe_2$ catalyst shows a four-electron transfer pathway for ORR in alkaline media and higher tolerance to methanol than Pt/C. Analogous to selenium, transition metal sulfur chalcogenides were also studied for the catalytic reduction of oxygen in alkaline media.

With a general goal of improvement of conductivity and investigation of possible synergetic coupling effects between metal sulfides and nitrogen doped graphene, aerogel-supported NiS_2 nanoparticles were prepared by a one-pot hydrothermal method.[236] Only nitrogen was doped into the graphene support, and the existence of a synergetic effect between NiS_2 and NG was inferred according to the more positive onset potential and higher current density of ORR on NiS_2/NG as compared to stand-alone NiS_2 and NG. In another example, Periasamy et al.[237] prepared Cu_9S_8/CNT nanocomposites by a one-step wet chemical method. In spite of some catalytic activity for ORR and good tolerance to MeOH and CO, a hypothesis of formation of oxy-hydroxyl species of Cu(II) on the Cu_9S_8/CNT loaded electrode surface requires further attention with regard to the stability of this catalyst material.

From the above Carbon supported M-N_x matrix (M = 3d transition metals) and Metal oxides section, it can be seen that N-doped carbon has been commonly used as a support material. For the purpose of increasing new non-electroneutral sites on carbon backbones, some recent works have focused on adding another doping heteroatom of sulfur during the synthesis of non-noble-metal electrocatalysts. Xu et al.[192] found that a N and S co-doped Fe–N/C–TsOH catalyst using TsOH (p-toluenesulfonic acid) as the S precursor shows better ORR activity than the sulfur free catalyst. The enhancement was ascribed

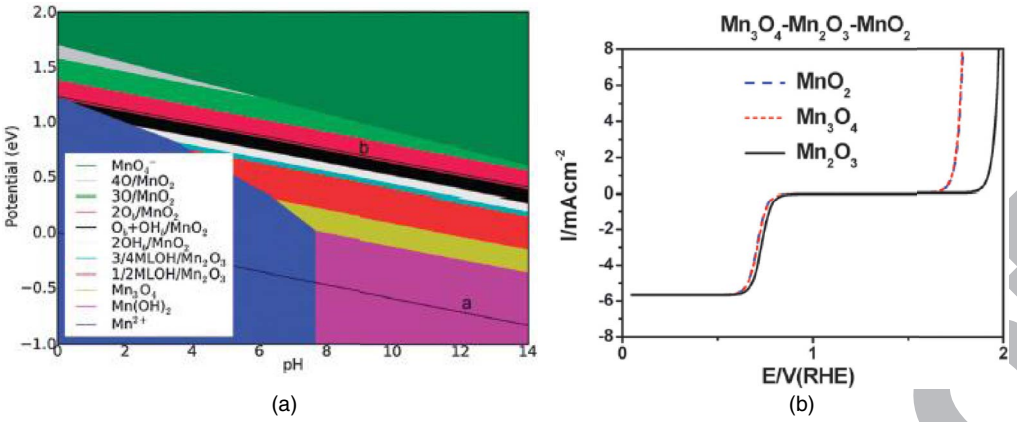

Figure 14. (a) General surface Pourbaix diagram for MnO_x catalysts. The oxidation state of the surface and the ORR and OER potential are constant versus the reversible hydrogen electrode (RHE). Lines a and b represent the RHE line and the O_2/H_2O equilibrium line. Reprinted with permission from Ref. 214 Copyright 2012 Royal Society of Chemistry. (b) Calculated current density for Mn_3O_4, Mn_2O_3 and MnO_2. Reprinted with permission from Ref. 214 Copyright 2012 Royal Society of Chemistry.

Table IV. Novel non-noble metal oxides electrocatalysts for ORR in alkaline media.

Metal element	Electrocatalyst	Doping elements	Preparation method; Precursors	Catalyst morphology /shape	ORR kinetics parameters	Ref.
	Manganese oxide octahedral molecular sieve	–	One-pot wet synthesis, calcination at different temperatures for 8 h; $KMnO_4$	Short nanorods (with CTAB), Nanofiber (without CTAB)	$E_{1/2}$ (vs. SCE) HT-OMS-2_{500}°C : −0.2 V	425
	Cu-α-MnO_2	Cu	A hydrothermal method; $KMnO_4$, $MnSO_4 \cdot H_2O$, $Cu(NO_3)_2 \cdot 3H_2O$	Nanowire	$E_{1/2}$ (vs. Ag/AgCl) [Cu% = 2.92] : −0.292 ± 0.018 V	426
	Mn_3O_4/NrGO	N	Electrodeposition process; $Mn(CH_3COO)_2$	Hierarchical nanoflakes network	$E_{1/2}$ (vs. Ag/AgCl) Mn_3O_4/NrGO: −0.2 V	427
Mn	Mn_3O_4/NrGO	N	In situ reduction of both graphene oxide (GO) and Mn(VII)	Nanoparticles	Onset potential for ORR, −0.175 V (vs. SCE)	428
	MnO_2	–	Using graphene oxide as the template	Layered nanosheets	The number of electrons transferred: 3.4	429
	Mn_2O_3	–	Calcination; Shewanella loihica PV-4 in the presence of MnO_4^-	Micro-/nanocubes	$E_{1/2}$ (vs. Ag/AgCl), Mn_2O_3-500: −0.24 ± 0.003 V	430
Fe	$FeO_{1.4}$/N-C	N	Hydrothermal reaction at 180°C and a thermal treatment at 800°C for 2 h under nitrogen atmosphere; $Fe(NO_3)_3 \cdot 9H_2O$	Wires with ultrafine particles	$J_k = 0.9$ mA $mg^{-1}_{Catalysts}$ @ −0.1 V (vs. Ag/AgCl)	431
	Fe_3O_4/N-C	N	Solvothermal carbonization process; Ferric chloride	Granular-like	$E_{1/2}$ (vs. Ag/AgCl), Fe_3O_4/N–C-900: −0.184 V	432
	Fe_3O_4/N-C	N	Fe^{3+}- mediated polymerization of dopamine on SiO_2 nanospheres, carbonization and subsequent KOH etching of the SiO_2 template	Hollow nano-spheres	The number of electrons transferred, 3.8	433
	Fe_X@NOMC (X = 25, 10, 5)	N	Precursors (FcN][NTf_2 and [MCNIm][$N(CN)_2$]] filling in SBA-15, calcination and subsequent template removal	Semiexposure morphology	$J_k = 5.30$ mA cm^{-1} @ −0.5 V (vs. MMO) for Fe_{10}@NOMC	434
	Fe_3O_4/N-GAs	N	Hydrothermally assembled at 180°C, iron acetate	Nanoparticles	Onset potential for ORR, −0.19 V (vs. Ag/AgCl)	435
Co	Fe-doped Co_3O_4 nanofilms	Fe	Electrodeposition at −0.8 V for 600 s, annealing at 400°C for 4 h; $Co(NO_3)_2 \cdot 6H_2O$, $FeCl_3 \cdot 4H_2O$, FTO conductive substrates	Flower-like architecture	Onset potential of −0.162 V (vs. Ag/AgCl)	436
	$Co(OH)_2$ / graphene	–	Electrodeposition from $Co(NO_3)_2$	Interlaced nanowalls	$E_{1/2}$, positive shift of 190 mV compared to GC	437

Table IV. (***Continued.***)

Metal element	Electrocatalyst	Doping elements	Preparation method; Precursors	Catalyst morphology /shape	ORR kinetics parameters	Ref
	CoO/CNTs	N	Growing nanocrystals on oxidized multiwalled CNTs, annealing in NH_3; $Co(OAc)_2$	Cubic rock salt structure	–	230
	Co_3O_4/C	–	A solvent-mediated morphological control method, annealing at 330°C for 2 h; $CoCl_2 \cdot 6H_2O$	Nano-rods and spherical structures	$J_{-50,\ -600\ mV}$ / mA cm^{-2} Co_3O_4-11: 0.239, 3.54	438
	Co_3O_4/rGO	–	A one-pot hydrothermal procedure; $Co(Ac)_2 \cdot 4H_2O$	Nanorods	The number of electrons transferred: 3.5	439
	Co_3O_4/N-MG	N	Hydrothermal reaction at 150°C for 3 h; $Co(Ac)_2$	–	Onset potential, 0.93 V	440
	Co/Co_3O_4/C–N	Co, N	Sol-gel, annealed in N_2 at different temperatures; $Co(NO_3)_2 \cdot 6H_2O$	Nanoparticles	Onset potential, Co/Co_3O_4/C–N-750: −36.0 mV (vs. Hg/HgO)	441
	CoO@Co/N–C	Co, N	Reflux reaction at 90°C, annealed in Ar at 700°C; cobalt(II) chloride hexahydrate	Particles with diameter of about 30–50 nm	Onset potential, 0.99 V	442
	g-C_3N_4@CoO	C, N	Wet impregnation, 550°C under Ar; $Co(OAc)_2$, cyanamide	A core–shell structure	J_k, 16.78 mA cm^{-2} at −0.25 V (vs. Ag/AgCl)	443
	Co-gC_3N_4 / graphene	C, N	Wet impregnation, 600°C under Ar; Dicyandiamide and $Co(OAc)_2 \cdot 4H_2O$	Uniform porous morphology	$E_{1/2}$ (vs. Ag/AgCl), CCNG-600: −0.141 V	444
Ni	$Ni(OH)_2$/GO	–	A microwave irradiation approach; nickel(II) acetate	Platelets and rhombus particles	The number of electrons transferred, 3.5	445
Cu	Cu_2O	–	A reductive solution route; $Cu(Ac)_2$	Nanocubes	The number of electrons transferred, 3.7	446
	Cu/TiO_2	–	A hydrothermal method; copper acetate	Nanoparticles	The number of electrons transferred, 3.74	447
Bimetallic	NiO/$NiCo_2O_4$	–	Coaxial electrospinning, annealing treatment at 600°C in air; $Co(Ac)_2 \cdot 6H_2O$, $Ni(Ac)_2 \cdot 6H_2O$	Nanotubes	Onset potential for ORR, −0.05 V (vs. Ag/AgCl)	448
	MnO_x-Co_3O_4/C	–	Wet Chemistry; $Co(OAc)_2$, $KMnO_4$	Nanoparticles on nanosheets	$E_{1/2}$, 814 mV	223
	$Ni(OH)_2$-MnO_x/C	–	Reducing the amorphous MnO_2/C suspension in the presence of Ni^{2+} with NaBH4; $Mn(CH_3COO)_2 \cdot 4H_2O$, $KMnO_4$, $Ni(NO_3)_2$	Floccule	$E_{1/2}$, positive shift of 0.05 V compared to MnO_2/C and MnO_x/C; Unchanged electron transfer number after AAT testing	224
	Co_2FeO_4 /MWCNT	–	Wet chemistry, annealing at 350°C for 3 h under H_2 atmosphere; $CoCl_2 \cdot 6H_2O$, $FeCl_2 \cdot 4H_2O$	Hollow structured	$E_{1/2}$, 0.73 V	449
	$NiCo_2O_4$	–	A facile hydrothermal method at 180°C for 6 h; $Ni(NO_3)_2 \cdot 6H_2O$, $Co(NO_3)_2 \cdot 6H_2O$	Urchin-like sphere	Onset potential for ORR, 0.83 V	450
	$NiCo_2O_4$	–	A hydrothermal method at 180°C for 12 h, annealed 400°C for 2 h; $Ni(NO_3)_2 \cdot 6H_2O$, $Co(NO_3) \cdot 6H_2O$	Macroporous sheets	The number of electrons transferred, > 3.5	451
Spinel	$ZnCo_2O_4$/NCNT	N	Solvothermal preparation at 150°C for 10 h; $Co(OAc)_2 \cdot 6H_2O$, $Zn(NO_3)_2 \cdot 6H_2O$	–	The number of electrons transferred, > 3.7	452
	$CuCo_2O_4$/N-rGO)	N	A simple solvothermal method at 160°C for 3 h; $Co(OAc)_2$, $Cu(OAc)_2$	–	The number of electrons transferred, 3.8	453
	$CoMn_2O_4$/ PDDA-CNTs	–	A solvothermal method at 180°C for 10 h, $Co(OAc)_2 \cdot 6H_2O$ and $Mn(OAc)_2 \cdot 6H_2O$	–	E (V) @ I = −3 mA cm^{-2},-0.133	454
	$CoMn_2O_4$, $MnCo_2O_4$	–	Thermal degradation at 400°C	–	The number of electrons transferred, $CoMn_2O_4$: 3.68, $MnCo_2O_4$: 3.51	455

*ORR kinetics parameters were obtained at room T, 1 atmosphere. Potentials were referred to the reversible hydrogen electrode (RHE) unless they are addressed otherwise.

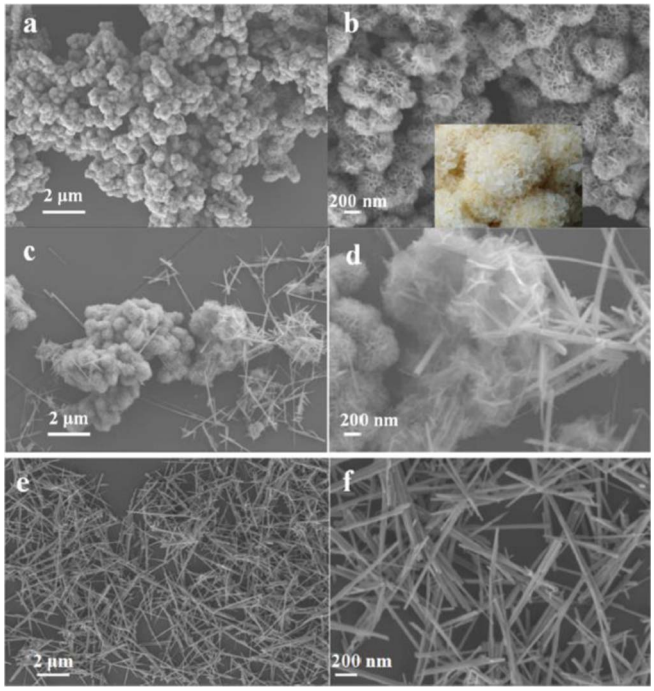

Figure 15. SEM images of Tremella-like δ-MnO_2 (a and b), mixed tremella and short belt-like α-MnO_2 (c and d), and long belt like α-MnO_2 (e and f). Inset in b: photograph of dried Tremella fuciformis fungi forcomparison (http://tupian.baike.com). Reprinted with permission from Ref. 492 Copyright 2015 Elsevier.

to the altering of electroneutrality of the carbon backbone, increase of support porosity, and assistance of trapping of Fe ions in a pyrole-type N enriched environment caused by formation of C–S–C and oxidized –SO_n–bonds. Qing et al.[238] used copper phthalocyanine tetrasulfonic acid tetrasodium salt as the single precursor for Cu, N, and S during a pyrolysis reaction. In addition to the increased porosity of the carbon support and C-S_n-C (n = 1,2) bonds formation, it was believed that the inhibition of creation of copper carbide in the presence of sulfur is also helpful in achieving the superior ORR performance. From the above studies and others in the literature,[37,128,239–243] there is no evidence yet to show that there is any coordination between sulfur and metal that is responsible or not for ORR catalytic activity as it does in the case of N and metal.

Similar to Ni-Co based spinel in Table IV, some thiospinel type $NiCo_2S_4$/rGO catalysts were prepared using a solvothermal strategy with NaS or thiourea as the reducing agents and sulfur precursors.[244,245] With more octahedral catalytically active sites of Co^{3+}[244], the as-synthesized sulfur doped catalysts show similar ORR activity to that of Pt/C and better durability and tolerance to MeOH than the spinel $NiCo_2O_4$–rGO counterpart. In addition, the improved ORR performance may be benefited by the enhanced conductivity resulting from doping S into graphene, as indicated by the XPS signals of thiophenic-S (aromatic C–S–C).

Carbides & nitrides/oxynitrides.— As indicated in Table III, a large number of active metal-N_x/C catalysts can be synthesized by a high temperature pyrolysis process. Aside from the formation or rearrangement of metal-N bonds and anchoring in some specific sites on the carbon support, it is inevitable to encapsulate some metallic particles in graphitic carbon shells,[246–249] which are thought to be spectators for ORR.[249] The important role of the metal carbide phase in the ORR had not been paid much attention until some recent studies on this specific topic came out. Hu et al.[246] placed a mixture of cyanamide and ferrocene in an autoclave and pyrolyzed the sealed raw materials at 700°C–800°C. While the pressure inside the autoclave reached 600 bar, Fe_3C nanoparticles encased by uniform graphitic layers (Figure 16) instead of Fe-N moieties were formed unexpectedly.

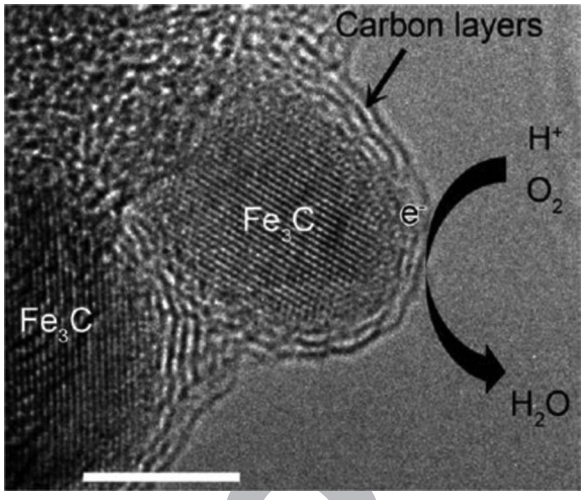

Figure 16. Oxygen reduction process on Fe_3C/C-700 (scale bar = 5.00 nm). Reprinted with permission from Ref. 246 Copyright 2014 Wiley-VCH.

The "high- temperature, high-pressure" obtained Fe_3C/C catalysts showed very similar ORR behavior to that of Pt/C in 0.1M KOH even after hot acid leaching, indicating that there remains a synergic interaction between the Fe_3C particles and the surrounding protective graphic layers. Yang et al.[250] added PEG-PPG-PEG Pluronic P123 into a mixture of melamine and $Fe(NO_3)_3$ (no carbon support) and successfully prepared bamboo-like carbon nanotube/Fe_3C nanoparticle hybrids after pyrolysis at 800°C in N_2 under normal pressure. The ORR half-wave potential on the PMF-800 catalyst showed a positive shift of 49 mV compared to a 20 wt% Pt/C catalyst and much higher stability and better methanol tolerance. In line with the Fe_3C/C catalysts in Hu et al.'s study,[246] it was found that the Fe_3C nanoparticles were encapsulated in b-CNTs, leading to a change of local work functions of CNT walls and strong stability in both acidic and alkaline media.[251–255]

For electrocatalysis in fuel cells, group IVB to VIB transition metal carbides such as TiC,[256–258] ZrC,[259] WC/W_2C[260–262], VC,[263] Mo_2C[264] have been typically used as support materials to improve the stability of the electrocatalysts. Nevertheless, using a one-step hydrothermal method, TiC nanowires were synthesized and exhibited doubled exchange current density in comparison to the TiC powder sample.[256] As expected, the one dimensional TiC catalyst also showed very good stability and tolerance to MeOH. In addition to the above monometallic transition metal carbides, a bimetallic CoWC@C catalyst was synthesized by a reduction and carbonization method in a flow of H_2 and Ar.[265] The higher catalytic activity of the bimetallic CoWC@C catalyst as compared to WC@C and Co@C was attributed to the formation of a Co_3W_3C phase as the active site for ORR.

In the large family of metal nitrides and oxynitrides, the composites with metal elements from the groups from IVB to VIB have been widely used as ORR electrocatalysts in both acidic and basic media due to their stability and the capability to push electron density towards the Fermi level by contraction of d-bands.[266,267] Using mpg-C_3N_4 templates to control the particle size, TiN nanoparticles with particle sizes in diameter of 7 nm, 12 nm and 23 nm were prepared with a wet chemistry and a calcination step and tested for ORR in 0.1M NaOH.[268] The ORR current follows the order of 7 nm >12 nm > 23 nm, which is consistent with the order of surface area on the TiN nanoparticles. However, more than 50% of H_2O_2 content for the ORR products on the best TiN-7 nm catalyst indicates that only a two-electron transfer process was taking place on the oxynitrided electrode surface. Recently, it was found that the ORR selectivity of TiN can be dramatically improved by formation of a hierarchical TiN/TiCN structure using a chemical vapor deposition approach.[258] The interface between TiN and TiCN layers as shown in Figures 17a and 17b was believed to be active for oxygen adsorption. The TiN/TiCN sample

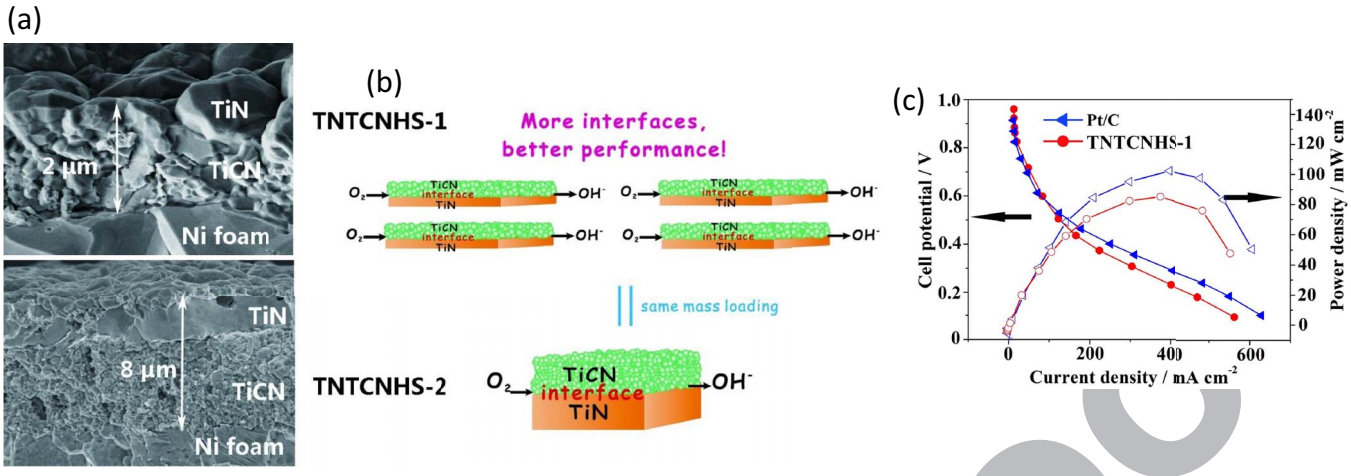

Figure 17. (a) SEM images of the cross-view of titanium nitride/titanium carbonitride hierarchical structures (TNTCNHS-1 and TNTCNHS-2) before Ni template removed. (b) Schematic the active interfaces of TNTCNHS. Reprinted with permission from Ref. 258 Copyright 2014 Nature Publishing Group. (c) Single cell testing of the TNTCNHS-1 and commercial Pt/C as cathode catalysts with a loading of 4 mg cm^{-2} and 2 mg cm^{-2}, respectively. Anode catalysts are both platinum on carbon ($m_{Pt} = \sim 0.4$ mg cm^{-2}). Reprinted with permission from Ref. 258 Copyright 2014 Nature Publishing Group.

(TNTCNHS) with Ni template removed was employed and examined as cathodic catalyst in a single cell. From Figure 17c, with a catalyst loading of 0.1 mg cm^{-2} it shows a higher open circuit potential and comparable maximum power density to that of a Pt/C cathode.

Other than metals from groups IVB to VIB, recently, late transition metals such as copper have been used to form nitrides for use as ORR electrocatalysts in alkaline media. Wu et al.[269] prepared copper nitride nanocubes in a nonaqueous system with programmed increasing temperature up to 250°C. The Cu_3N nanocubes had an average size of 26.0 ± 5.6 nm and exhibited electrocatalytic activity for ORR in 0.1 M KOH, though much lower than a Pd/C catalyst. Regarding the catalytic activity of metal nitrides/oxynitrides, it may be further improved by forming bimetallic composites to obtain multiple active species and tuning of electronic states.[267,270] A $Co_{0.50}Mo_{1-x}Mo_{0.50}O_yN_z$ synthesized by an impregnation method followed by ammonolysis demonstrated an onset potential of 0.918 V for ORR in 0.1 M KOH. From XPS and EXAFS measurements, it was concluded that the integration of CoO into the rock-salt structure of Mo_2N correlates with the enhanced activity.

Perovskites.— Although the perovskite materials were proposed as ORR electrocatalysts in fuel cells in the 1970s, their performance has been limited dramatically by their high ohmic losses, low specific surface area and crystallite agglomeration.[271–274] In pursuit of minimizing the size of crystallites and the degree of their agglomeration, combinations with carbon based materials have been investigated. Perovskite–carbon nanocomposites were prepared via an in situ autocombustion route with Vulcan–XC72 carbon and La and Mn–glycine complex as the precursors.[274] By comparison of particle sizes in Figures 18A, 18B and Figures 18C, 18D, smaller particles were formed by the in situ autocombustion method than the sol-gel method. From Figures 18E–18H, the degree of agglomeration of oxide perovskite crystalline materials was significantly suppressed on the nanocomposites, leading to a factor of 2.4 activity enhancement. Importantly, a dual role of the carbon support to improve the electrical contact and catalyze O_2 to H_2O_2 was also concluded from the study of $LaCoO_3$/C and $La_{0.8}Sr_{0.2}MnO_3$/C composites.[275]

Others have attempted to improve the intrinsic catalytic activity by modifying the compositions. Suntivich et al.[276] correlated the ORR activity with e_g electron numbers of different transition metal oxide perovskites and obtained a volcano plot. It indicates that the B-O (B = Cr, Mn, Fe, Co, and Ni) bond strength that governs the rate-determining step of ORR has a maximum value. Notably different from this finding for oxide perovskites, it is worthwhile to recall that a downshift in energy level of e_g-orbitals generally

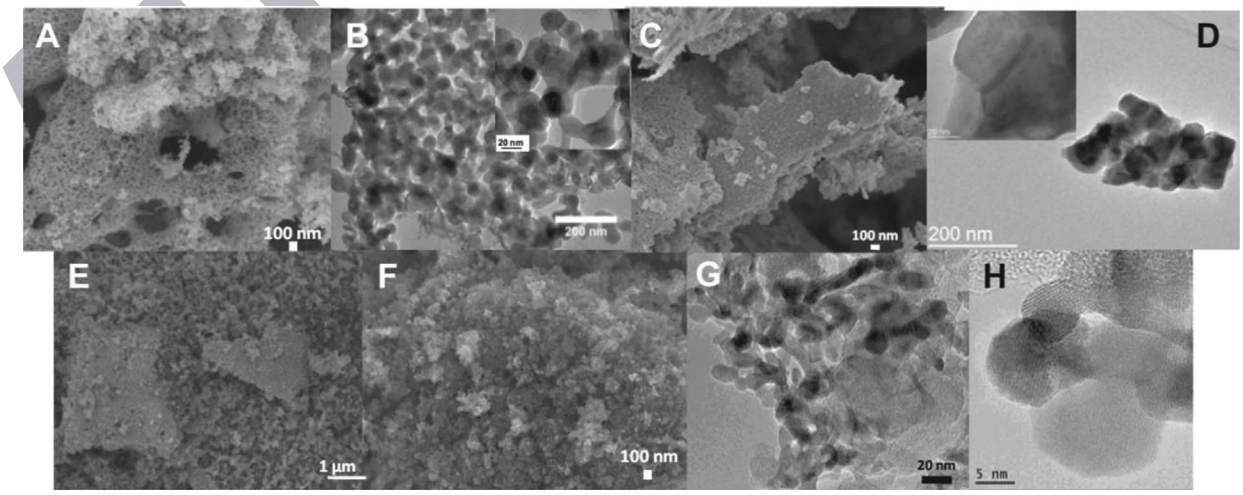

Figure 18. SEM Images recorded by: SEM (A) and TEM (B) for LaMn-AC; SEM (C) and TEM (D) for LaMn-SG; SEM (E) for LaMn-AC manually mixed with Vulcan–XC72 in 1:1 mass ratio; and SEM (F) and TEM (G, H) for 50-LaMn–ISAC–Vulcan. Reprinted with permission from Ref. 274 Copyright 2015 Elsevier.

leads to higher ORR onset potentials and higher turnover numbers in the case of metal-N electrocatalysts.[33,139,146,277] Practically, Sunarso et al.[278] synthesized $LaMO_3$ and $LaNi_{0.5}M_{0.5}O_3$ (M = Ni, Co, Fe, Mn and Cr) perovskite oxide electrocatalysts via a combined ethylenediaminetetraacetic acidcitrate complexation technique and subsequent calcinations. Among them $LaCoO_3$ and $LaNi_{0.5}Mn_{0.5}O_3$ showed the best ORR kinetics with a 4-electron transfer pathway within each class of materials.

Metal-free electrocatalysts.— From the above sections, transition metal based materials (noble-metal and non-noble metal) with characteristics such as partially filled d band orbitals, multiple and reversible oxidation states, and suitable adsorption energy with O_2 and intermediates may serve as electrocatalyts for ORR in alkaline media. Of all the non-metal elements in the periodic table, carbon is probably the only element that can possibly be used as the main component of a metal-free electrocatalyst for ORR, provided that some prerequisites such as sufficient conductivity, large surface area, and reasonable stability in extreme pH environments are met. However, a good electrocatalyst for ORR needs to have much more special properties than a simple conductor or current collector. Figure 3c illustrates the double-layer structure at an ideal Pt polycrystalline (or single crystal) electrode in alkaline media. However, in the case of an ideal graphite electrode (with solely sp^2-hybridized carbon) there is one electron residing in the unhybridized p orbital that can pair up with one of the O_2 electron pair in the π orbital. This means that O_2 will have to approach the graphite surface horizontally to form an O-C bond via π-π interaction and rearrangement of electron density. It has been theoretically calculated and concluded that O_2 in its triplet state has weaker chemisorption compared to O_2 in its singlet state on graphite and the chemisorbed species are highly unstable.[279] As a result, the amount of chemisorbed O_2 at the IHP near an ideal graphite electrode is negligible.

Thanks to the dramatic decrease of overpotential (ca. 0.83 V) for the first electron transfer ($O_{2,aq} + e^- \rightarrow (O_2^{\cdot -})_{aq}$) during ORR with pH changed from 0 to 14, an outer-sphere electron transfer can still be facilely conducted with the rather small overpotential that can be overcome by noncovalent forces such as hydrogen bonding. The hydrogen bond formation between non-specifically adsorbed OH^- and solvated O_2 molecules can be further promoted by modification of the carbon surface with quinone/hydroquinone functional groups.[280–282] Nevertheless, for the aforementioned carbon surface, the oxygen reduction has to stop at the second electron transfer step with HO_2^- as the major product because there is a lack of proper adsorption sites for HO_2^- to continue the following electron transfer steps.[283] It is therefore necessary to modify the crystallographic structure of the graphite in order to pursue a fundamental change from an outer-sphere electron transfer path to a favored inner-sphere electron path for oxygen reduction.

As it is generally known that transition metal-N_x moieties anchored at carbon crystallographic atomic defects such as the divacancy and armchair edges are key active sites for ORR after a pyrolysis process with a mixture of precursors of metal and nitrogen and carbon materials, tremendous efforts have been devoted to the investigation of ORR performance of all kinds of carbon materials with doped heteroatoms to create defects. Indeed, all metal-free carbon based electrocatalysts

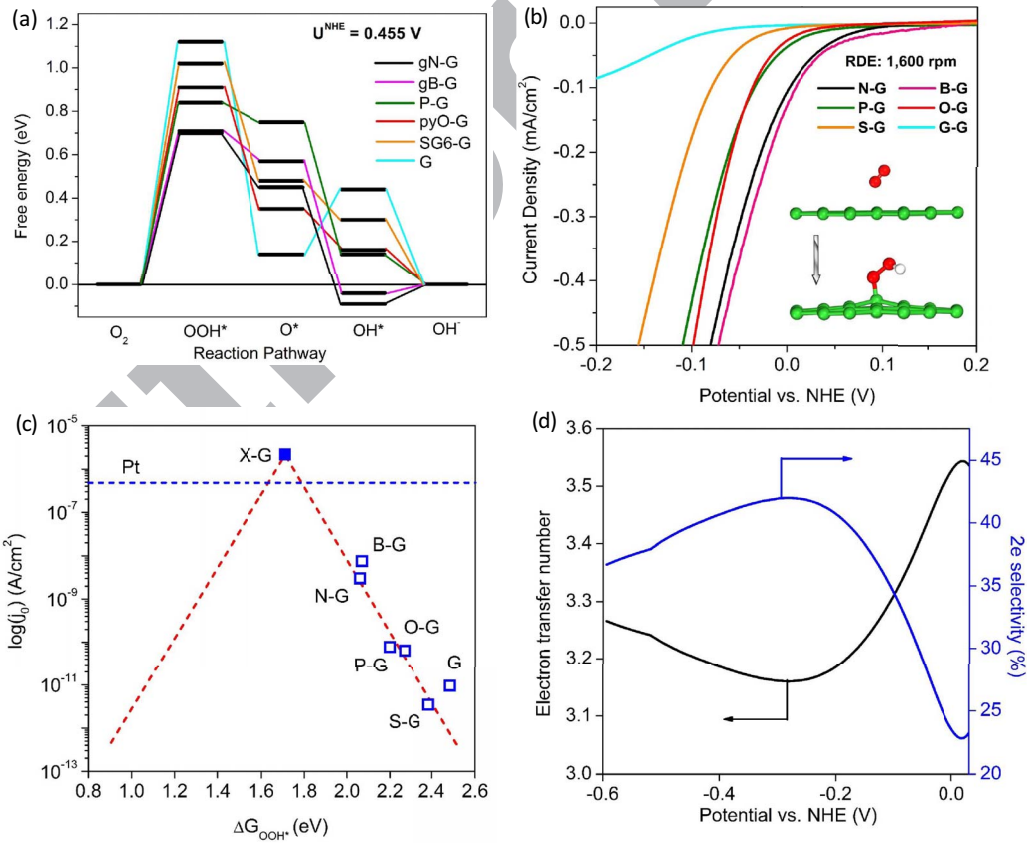

Figure 19. (a) Free energy diagram of different heteroatom-doped graphenes at the equilibrium potential U^0. Reprinted with permission from Ref. 34 Copyright 2014 American Chemical Society. (b) Enlarged LSVs plots at the ORR initial region for different catalysts on RDE at 1600 rpm in an O_2-saturated 0.1 M solution of KOH. Inset illustrates the first electron transfer step that is O_2 to adsorbed OOH*. Reprinted with permission from Ref. 34 Copyright 2014 American Chemical Society. (c) Volcano plot between j_0 theory and ΔG_{OOH^*} with charge-transfer coefficient $\alpha = 0.5$ (red dashed line). Blue hollow squares are j_0^{expt} obtained from Tafel plots and DFT-derived ΔG_{OOH^*} for each doped graphene catalyst. Reprinted with permission from Ref. 34 Copyright 2014 American Chemical Society. (d) RRDE measured electron transfer numbers (black) and corresponding $2e^-$ pathway selectivity (blue) for N-graphene catalyst. Reprinted with permission from Ref. 34 Copyright 2014 American Chemical Society.

with promising ORR performance reported so far have doped elements such as N, O, B, S, and P (infra vide), whereas the graphene or reduced graphene oxide catalysts only show limited activity and selectivity for ORR.[284,285] Though categorized by the type of carbon materials in morphology in this section, the importance of dopant for achievement of complete reduction of oxygen on metal free electrocatalysts will be discussed in each subsection. A more detailed review about the effect of different doping elements was also published recently.[286]

Graphene based metal-free electrocatalysts.—As the most shining "star" in the carbon family in the last decade, graphene and functionalized graphene materials have been widely used as supports for ORR electrocatalysts.[105] Only recently has the "secondary role" of graphene in a cathodic eletrocatlayst for ORR been reconsidered, and a large number of reports has appeared dealing with the identification of the basic mechanism of ORR, new synthesis technologies, improvement of some features like easy stacking, effects of different heteroatoms and other aspects. Jiao et al.[34] constructed models for 13 configurations of graphene clusters doped with 5 different heteroatoms (N, S, O, B, and P) and conducted both electrochemical measurements and density functional theory (DFT) calculations. From Figure 19a, all heteroatom-doped graphene electrodes have the same rate-determining step, i.e., the first electron transfer to form OOH^*, which is consistent with that on other types of metal based electrocatalysts[12,19–21] and dictates the order of onset potentials for ORR (see Figure 19b). However, due to weak adsorption of OOH^* on these doped graphene surfaces, the theoretical exchange current density (j_0) values were all located on the right branch of a volcano plot as shown in Figure 19c. The weak adsorption of OOH^* also leads to an exothermic desorption process, which is the fundamental reason for the lack of selectivity for ORR and a mixed $2e^-$ (33%) and $4e^-$ (67%) pathway on the gN-G model (Figure 19d).

Although a molecular orbital origin involving hybridization of the valence band (v) of the active sites with the (σ) orbital of the adsorbed oxygen-containing species was proposed,[34] the exact identification of the "active sites" is still quite elusive. It has been demonstrated that chemisorption of O_2 on N-functionalized carbon is more facilitated than for N-free carbon surfaces with a ketone formed on the carbon atoms next to the graphitic-N group.[286,287] Raman and XPS are two major techniques for characterization of the basic structure of the graphene substrate and different types of doped N. For example, using the D/G band intensity ratio of a Raman spectrum as an index of the disorder degree and the average size of the sp^2 domains,[217,288–290] Lu et al.[290] studied the degree of structural defects and edge plane exposure of N-doped reduced graphene oxides with various N contents. It was found that more defected N-RGO in few-layer flakes was produced after doping with N, which is responsible for the higher ORR activity on N-RGO than that on RGO.

Lai el al.[291] prepared various N-graphene samples with different N precursors and pyrolysis at different temperatures. Pyrodinc N, pyrrolic N and quaternary N (graphitic N) were identified by their characteristic peaks corresponding to different binding energy values in XPS spectra. From the ORR results, it was concluded that the ORR limiting current can be enhanced by graphitic N and the ORR selectivity for $4e^-$ pathway can be improved by pyridinic N species. In spite of the controversial role of the type of N (with graphitic N[292–294], pyridinc N[295, 296] and pyrolic N[297–300] as the dominating factor for ORR), the overall ORR activity should positively rely on the N content in heterogeneous nanocarbon materials with the limit of conductivity and active sites considered, assuming the carbon atoms adjacent to doped N are the active site for O_2 interaction.[301,302] Zhang et al.[283] employed a two-step pyrolysis method to synthesize N-doped graphene with various N contents showing electrocatalytic activity and long-term stability for ORR in 0.1 M KOH. From both experimental and theoretical studies, it was concluded that an optimized N content should be around 25% to achieve sufficient carbon active sites with high spin density and charge transfer[283,298,303] as well as good conductivity.

Of all heteroatom-doped graphene catalysts, the B-doped is the most competitive alternative to the N-doped.[34] Through a DFT calculation on a model of graphic B-doped graphene, Fazio et al.[304] inferred that the positively charged boron atom is the active center for ORR in the B-doped graphene catalysts. For both dissociative and associative mechanisms of ORR, they conceived that the very first step is the adsorption of molecular oxygen on B atoms with an end-on adsorption mode. In addition to single element doped graphene, there have appeared a number of studies of bi-element co-doped graphene catalysts for ORR and the enhanced ORR activity as compared to N-doped samples was usually attributed to a "synergic effect" between N and the other elements.[296,305–308] Although it is probably true that the overall ORR activity may be benefited from an increased number of active sites, improved surface area and conductivity, and other factors under their specific preparation and testing conditions, the essence and the actual effect of the so called "synergic interaction" between different doping atoms needs further investigation.

Although the thorough understanding of adsorption and desorption modes of O_2 and the reduction intermediates on heteroatom doped graphene is still pending, the synthesis and evaluation of ORR performance have continued. Table V shows the recent work on ORR in alkaline media using heteroatom-doped graphene-based electrocatalysts without any metal salt added during preparation. It can be seen that the overall performance of the graphene metal-free catalysts is still quite far from the standard Pt/C catalyst except the ones with highly porous structure.[309] It has been noticed that bulk graphene layers typically suffer from serious stacking due to strong π-π interactions, which may cause dramatically reduced specific surface area and reduced ORR performance.[310,311] In order to increase the porosity of heteroatom doped graphene catalysts, a template adding-removal strategy was usually employed during the doping process prior to high temperature pyrolysis. For example, an aqueous dispersion of melamine and GO was dipped into liquid nitrogen to form ice crystal templates.[312] After sublimation of the ice and heat treatment, an N-doped graphene sample with 30 times higher specific surface area than that without ice crystal templates was formed. The obtained catalyst showed a decrease of overpotential of 60 mV and produced an oxygen reduction intermediate of $HO\cdot$ radical. It is also very interesting to find that graphene like carbon nanosheets can be produced without the precursor of graphene oxide. As a typical example, Liu et al.[313] used chitosan and urea as the precursors and conducted pyrolysis without any other treatment. The TEM image in Figure 20a shows that a transparent texture and crumpled-sheet morphology were formed. Due to the large specific area of $\sim$1510 $m^2\ g^{-1}$ and high ratio of graphitic/pyridinic nitrogen structure, the carbon nanosheet catalyst showed ORR performance close to that of Pt/C (Figure 20b).

Carbon nanotube based metal-free electrocatalysts.—In principle, the original cause of ORR activity from carbon nanotubes (CNTs) should be similar to that of graphene because the latter can be considered as the configuration of CNT unzipped longitudinally along its axis. As described in the above section, superior electrocatalytic activity for ORR on graphene may come from the defects and doping heteroatoms (for altering the charge density and increase of active sites), which leads to the major difference of preparation of these two types of electrocatalysts. From Table V, it can be seen that the synthesis of heteroatom doped graphene catalysts usually starts from the precursor of graphene oxide. It is not only because reduction of graphene oxide is a well-established protocol for preparation of graphene layers, but also because structure defects in bulk and facile replacement of oxygen by other heteroatoms can be realized, considering the fact that no report on the treatment of heteroatom sources (e.g. NH_3 or urea) with pristine graphene can be found.

In contrast, heteroatom-doped CNTs are commonly produced according to the following methods. (i) In situ CVD growth of N-CNTs. It has been widely employed to grow CNTs on transition metal particles (catalysts) using a chemical vapor deposition method and a precursor containing C such as acetylene, ethylene, and methane. As such an N-doped CNT catalyst can be easily produced with a precursor

Table V. Novel heteroatom-doped graphene based "metal-free" electrocatalysts for ORR in alkaline media.

Material	Content of doped elements	Preparation method	Morphology	Novelty/merits	Ref.
N-doped graphene	Typical atomic content, 3.5%	A silica templating approach, growing silica on GO, coating of polydopamine, pyrolysis and removal of template	Nanosheet	Uniform and tunable mesoporous structure; More positive onset potential and $E_{1/2}$ than Pt/C; Long term stability	309
N-doped rGO	At.% = 1.81 – 2.82%	A thermal annealing approach, pyrolysis of the mixture of GO and urea under N_2	Crumpled sheets	A 2-electron transfer pathway is dominant	290
N-doped graphene	At.% = 8.59 – 20.59%	Pyrolysis of the mixture of GO and urea under Ar	Three-dimensional stacked structures	The NG700 showed better ORR performance than others treated at lower temperature	456
N-doped graphene	At.% = 6.8 – 6.9%	Hydrothermal reduction of GO and urea, annealing at 600°C	Graphene sheet structure	Selectivity for ORR was improved after annealing	293
N-doped graphene	3.27–15.28 wt.%	Wet-chemical approach with GO and 2,3-diaminopyridine	Nanoplatelets	Higher stability than Pt/C	457
	At.% = 4 – 12%	Thermal annealing with a mixture of cyanamide and GO	Crumpled slate-like	Stable methanol crossover effect, high current density and durability	458
N-doped graphene	At.% = 2 – 3%	One step pyrolysis method with a GO-ppy composite	3D porous structure	A predominant four-electron ORR; Superior stability and tolerance to crossover effect than Pt/C	292
	6.24 – 8.55%	One step pyrolysis method with a GO-melamine composite	Micron-sized flake	Optimized pyrolysis temperature is 900°C	294
N-doped carbon nanosheet	At.% = 2.91 – 3.89%	Pyrolysis of chitosan and urea	Crumpled-sheet	Large BET surface area of ~1510 $m^2\ g^{-1}$; The onset potential is only 18 mV less positive than that of Pt/C; Higher stability and tolerance to MeOH than Pt/C	313
	At.% = 3.02 – 11.2%	Pyrolysis of crystal sugar and urea	Entangled and crumpled morphology	Large BET surface area of 565.1 $m^2\ g^{-1}$ for NG1000; Higher kinetic current density than Pt/C	459
	1.55 wt. %	Pyrolysis of folic acid	Porous	BET surface area is 1358 $m^2\ g^{-1}$; Similar limiting current density with Pt/C; Higher stability and tolerance to MeOH than Pt/C	460
N-doped carbon nanoribbon	4.1–8.3 wt. %	Pyrolysis of graphene nanoribbons (GNR)/polyaniline (PANI) compo-Sites	Nanoribbon	Carbon nanoribbon was prepared from unzipping CNTs; Four-electron transfer process	461
N-Doped graphene quantum dots/graphene	At.% = 4.3%	An electrochemical method for preparation of N-GQDs, followed by a hydrothermal treatment for preparation of N-GQDs/graphene	–	Comparable activity to Pt/C	462
N-doped graphene; N,S-codoped graphene	–	An organic condensation method using 1,2-diaminobenzene as the N source and 2-aminothiophenol as the source of N and S	Edge-rich	Lack of π-π stacking; SNG exhibits a higher catalytic activity than NG	463
B-doped graphene	At.% = 3.2%	Annealing of GO and B_2O_3	Flake-like structure	On-set potential is 100 mV more positive than graphene.	336
	At.% = 0.57 – 1.92%	Annealing of GO and boric acid	Lamella structure	The BG700 showed better ORR performance than others treated at lower temperature.	456
S-doped graphene	S level: 1.30%–1.53%	Annealing of GO and benzyl disulfide	Sheets with wrinkled and folded features	Catalytic activity of S-graphene-1050 is better than Pt/C; J_k value is 9.34 mA/ cm^{-2} at −0.30 V (vs. Ag/AgCl)	464

Table V. Novel heteroatom-doped graphene based "metal-free" electrocatalysts for ORR in alkaline media.

Material	Content of doped elements	Preparation method	Morphology	Novelty/merits	Ref.
Carbon black/S-doped graphene	–	Annealing of GO, sodium polysulfide and carbon black	Highly developed porous structure	Higher exchange current density than Pt/C	465
I-doped graphene	–	Annealing of GO and iodine	A wrinkled and voile-like feature	Catalytic activity of I-graphene-900 w is better than Pt/C; J_k value is 9.21 mA/ cm^{-2} at −0.30 V (vs. Ag/AgCl)	466
N/B co-doped graphene	6.80% of N and 4.82% of S	Annealing the mixture of H_3BO_3 and NG	Slice-like	Onset potential of BNG was −0.17 V (vs. Ag/AgCl)	467
N/B co-doped graphene	2.5 at.% of B; 3.4 at.% of N;	Doping B with BH_3 and GO followed by doping N with hydrazine	Nano-platelets	No annealing process; The number of electrons transferred is 3.86	308
N/B co-doped graphene	5.4% B and 5.3% N	Annealing with a GO-CBP composite	2D morphology	$E_{1/2}$ = −0.27 V (vs. Ag/AgCl)	468
N/B co-doped carbon nanosheet	∼ 5.64 – 13.07 at.% N and 1.23 – 7.76 at.% B	Annealing with a mixture of urea-PEG-boric acid	A crumpled, cross-linked thin film	J_k value, BCN-2.5-1000: 26.62 mA cm^{-2}	469
N/B co-doped Graphene Quantum Dots / Graphene Hybrid	∼18.3 at. % nitrogen and ∼13.6 at. % boron	Annealing of GQD/GO and boric acid under NH_3/Ar	Flake-like	∼15 mV more positive onset potential than Pt/C	470
N/S co-doped graphene	2.12% of N and 1.70% of S	Annealing with a Cys-PDA-rGO composite	Porous 3D network	No evident restacking of graphene sheets; higher ORR activity than NG	305
N/S co-doped graphene	0.89–1.25% of N, 0.17–0.34% of S	Pyrolyzing GO and poly[3-amino-5-mercapto-1,2,4-triazole] composite (PAMTa)	Wrinkled structure	$E_{1/2}$ is comparable with Pt/C	306
SN-rGO	Atomic ratio: N/C = 0.12; S/C = 0.08	Reflux reaction with thiourea and GO	Wrinkled single sheet	No annealing treatment; onset potential on SN-rGO is very close to that of the Pt/C	296

containing both C and N. For example, Li et al.[314] prepared N-CNTs using ethanediamine as a precursor and conducted heat treatment at different temperatures. Interestingly, the N-CNTs sample (800°C) with the highest content of pyridinic N shows the best catalytic activity for ORR (approaching Pt/C). In sharp contrast, the N-CNTs sample (900°C) with the highest content of quaternary/graphitic N gives the worst performance. (ii) Post doping of N (or other elements) on CNTs. After pretreatment of CNTs with concentrated H_2SO_4/HNO_3, N-doped CNTs were prepared by heat treating oxidized CNTs and tripyrrolyl[1,3,5]triazine at different temperatures.[315] As opposed to the findings by Li et al.,[314] as-prepared NCNT-900 with the highest graphitic-N content exhibits the highest kinetic current density for ORR in 0.1 M KOH. In addition, the NCNT-1000 sample with a total N content of 0.70 at.% (vs. 2.40% for NCNT-900) shows a *n* value of 3.1 for ORR, indicating that the active sites for complete oxygen reduction are not sufficient after annealing at 1000°C. Other examples using alterative N precursors such as ammonia,[316] polymers,[317] triazole and tetrazole derivatives,[318] cyanamide,[319] dual nitrogen sources,[320] and other heteroatom resources for B[321] and S[322] can be found in the literature. (iii) Surface decoration of N. Giambastiani et al.[323,324] functionalized MWCNTs with different N-containing heterocycles under mild conditions (see Figure 21a). Because the CNTs surface was solely functionalized by pyridinic moieties, it is possible to study the effect of electronic properties of the heterocycle on the kinetics of ORR. It was found that polarization values of the N−C_α bond shown in the Figure 21b must be located in a range of 4.0–4.5 in order to trigger complete oxygen reduction paths.

Aside from the existing recognition that the catalytic activity of ORR on CNTs can be enhanced by doping heteroatoms into the basal or edge plane, a recent work has shown that surface modification to

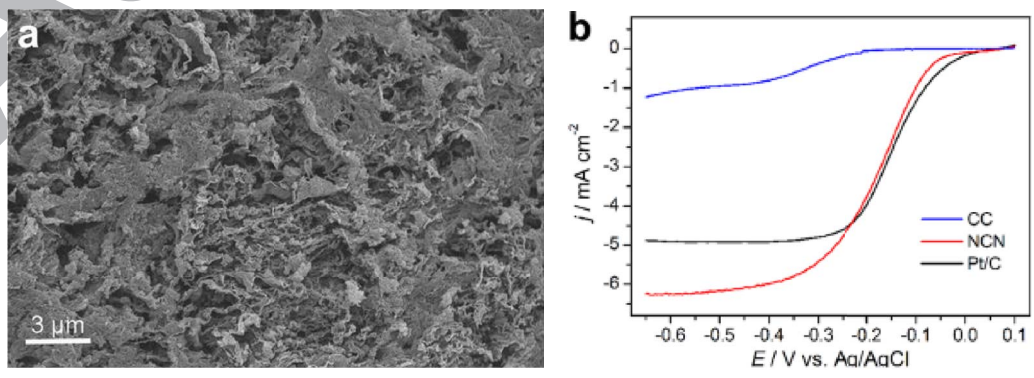

Figure 20. (a) SEM images of Nitrogen-Doped Carbon Nanosheets (NCN). Reprinted with permission from Ref. 313 Copyright 2014 American Chemical Society. (b) LSV curves of carbonized chitosan (CC), NCN, and Pt/C electrodes in O_2-saturated 0.1 M KOH at a scan rate of 5 mVs^{-1} and a rotational rate of 1600 rpm. Reprinted with permission from Ref. 313 Copyright 2014 American Chemical Society.

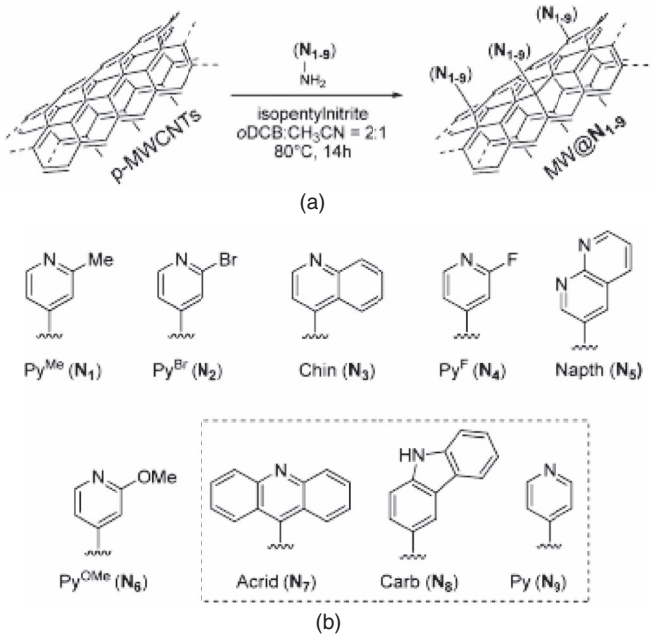

Figure 21. (a) MWCNT N-Decoration via Aryldiazonium Salt (Tour) Protocol. Reprinted with permission from Ref. 323 Copyright 2014 American Chemical Society. (b) N-Containing Heterocycles Used for the MWCNT Decoration. Reprinted with permission from Ref. 323 Copyright 2014 American Chemical Society.

generate C-O groups may also help to improve the ORR performance significantly. Dumitru et al.[325] treated CNTs with citric acid, diazonium salts and peroxymonosulfuric acid separately and conducted heat treatment at moderate temperature (up to 450°C) in some cases. Though not obvious from Figures 22a and 22b, an increase of the signal of COO on citric acid treated CNTs and C-O (or hydroxyl) on peroxymonosulfuric acid treated CNTs, and the presence of the 4-nitrophenyl group on diazonium salts treated CNTs can be found based on deconvolution calculations (Figure 22c). From the K-L plots in Figure 22d, the C-O (or hydroxyl) enriched sample shows a four-electron pathway for ORR, whereas others show only a dominate two-electron pathway. It is very interesting to explore the special role of the surface C-O (or hydroxyl) function on the improvement of ORR selectivity and activity, given that non-specific adsorbed OH^- on any electrode surface is quite abundant and responsible for promotion of mediated outer-sphere electron transfer for ORR.[11,280–282,326–329]

Other types of carbon materials.—Apart from the heteroatom doped or surface functionalized graphene and carbon nanotubes as metal-free ORR electrocatalysts, numerous and miscellaneous carbon materials such as carbon fiber, mesoporous carbon, graphyne and graphdiyne, aerogels, nanoparticles, quantum dots, and others with special morphology or structure have been reported. Nevertheless, a general strategy to change the pristinely inefficient (2-electron transfer for ORR) into efficient (4-electron transfer) electrocatalysts for ORR is still focused on doping heteroatoms, creating structural defects, and surface functionalization, given that there remain inconsistent results concerning the active sites, role of heteroatoms and their content under different preparation conditions.

Other than the typical examples about preparation methods, structure, ORR kinetics performance, etc. summarized in Table VI, some

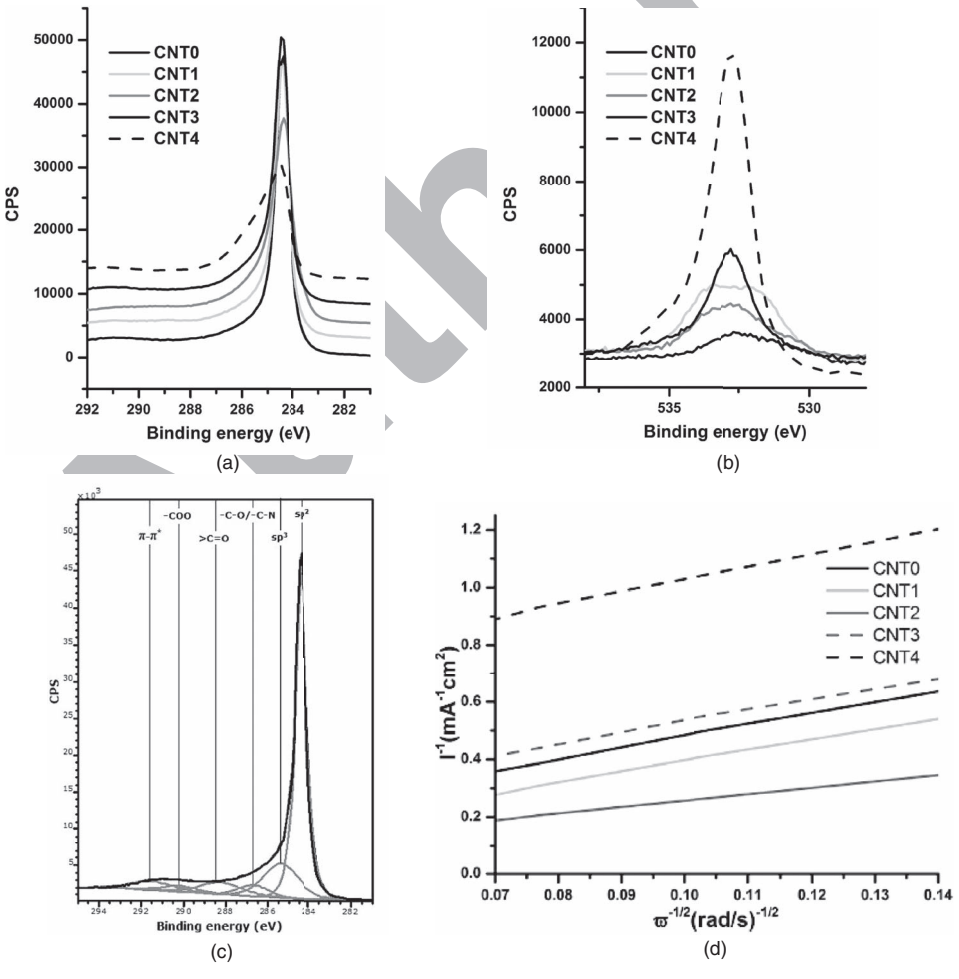

Figure 22. (a) C1s core level spectra of unmodified and modified CNTs. Reprinted with permission from Ref. 325 Copyright 2014 Elsevier. (b) O1s core level spectra of unmodified and modified CNTs. Reprinted with permission from Ref. 325 Copyright 2014 Elsevier. (c) Deconvolution of C1s core level spectra of CNT0. Reprinted with permission from Ref. 325 Copyright 2014 Elsevier. (d) K-L plot for unmodified and modified carbon nanotubes at −0.6 V. Reprinted with permission from Ref. 325 Copyright 2014 Elsevier.

Table VI. Recently developed metal-free carbon electrocatalysts other than graphene or carbon nanotubes for ORR in alkaline media.

Material	Content of doped elements	Preparation method	Structure/Morphology	Surface area	Novelty/Merits	Ref.
N-doped carbon fiber	1.3%–3.4 at.% of N	Carbonizing the electronspun polyacrylonitrile carbon fiber at 1000°C, followed by acidification and NH_3 etching	Fiber	–	Improvement of wettability, diameter reduction, highly porous structure, more exposed edge planes, and higher proportion of pyridinic-N by post acidification and NH_3 etching	471
	31.6–44.1 at.% of pyrrolic-N content	Thermal treatment of electronspun polyacrylonitrile carbon fiber under NH_3	Fiber	–	The NCNFs sample with the best catalytic activity for ORR has the highest content of pyrrolic-N	472
N-doped mesoporous carbons	–	Carbonizing a composite of honey- SBA-15 at different temperature	Mesopores with short rod-like microstructures	1059 – 1273 m^2/g	The best catalyst of N-OMCs-800 has the highest pyridinic N and graphitic N content and the largest surface area.	473
N-doped mesoporous carbons	–	Pyrolyzing polymerized ethylenediamine nanocasted into a SBA-15 hard template	Mesoporous structure with a hexagonal porous network	473–517 m^2/g	Higher j_k value than Pt/C	474
B-doped mesoporous carbons	1.30 at.% of B	Carbonization of sucrose and 4-hydroxyphenylboronic acid into SBA-15 silica template	Rod-like morphology	778–1040 m^2/g	It needs to reach a balance between B content and surface area.	475
N-doped graphdiyne	3.04 – 3.35 at.% of N	Cross-coupling reaction, followed by heating under ammonia/Ar	Loose, spongy structure	–	N-doping leads to high positive charges on the carbon atoms	476
N/S codoped carbon aerogels	5 wt.% of N; 1 wt.% – 4 wt.% of S	Hydrothermal synthesis, followed by pyrolysis	Homogeneous interconnected particle matrix	224.5–266.7 $m^2\ g^{-1}$	Synergistic effect of co-doped sulfur- and nitrogen	477
N doped graphene nanoribbons aerogel	2.8 at.% of N	Unzipping of CNTs, hydrothermal treatment, annealing	Interconnected, porous structure with hierarchical pores	617 $m^2\ g^{-1}$	Superb electrocatalytic activity and better stability than commercial Pt/C	478
N doped carbon nanoparticle	0.39–0.58 at.% of N	A solution plasma process	Turbostratic structure	–	In situ nitrogen doping	479
N doped carbon nanoball	0.23–0.49 at.% of N	A solution plasma process, followed by annealing	Ball-shaped structure	–	ORR activity can be improved by thermal annealing	480
N/P doped carbon foams	–	Copyrolyzing of poly(vinyl alcohol)/polystyrene (PVA/PS) hydrogel composites	Hierarchical interconnected macroporous structure	1083 $m^2\ g^{-1}$	First report on N and P dual-doped hierarchical porous carbon foams for ORR	339
N doped carbon spheres	0–1.58% of N	Pyrolysis of hollow poly(o-phenylenediamine) spheres	Hollow microspheres	–	Higher activity than MWCNTs or NCNTs	481
N doped carbon spheres	2.35 – 4.82 wt.% of N	Carbonizing a MV/HMS composite, following by removal of silica	Hierarchically micro-meso-macroporous structure	1413 $m^2\ g^{-1}$	Higher J_k value than Pt/C	482
N/S doped carbon nanospheres	4.25–9.52 wt.% of S; Up to 74.7 at.% of N	Pyrolysis of a mixture of polyacrylonitrile nanospheres and S	Nanospheres	653 $m^2\ g^{-1}$	Sulfur helps to improve the ORR activity	483
N-doped carbon hemispheres	10.9 wt.% of N	IL coating on silica, followed by removal of silica and annealing	Honeycomb-like	65.1 $m^2\ g^{-1}$	Ionic liquids were used as the carbon source	484
Sulfur-containing carbon soot	1.0–3.4 at.% of S	Flame synthesis	Disordered, nonporous	–	The first report using flame pyrolysis method	485
(N, P, and B)-codoped nanocarbons	–	Pyrolysis of a mixture of urea, phosphoric acid and boracic acid	Nanoporous morphology	89.5 $m^2 \cdot g^{-1}$	ORR activity is higher than single- or dual-doped nanocarbons	486
N doped carbon	3.15 at.% of N	Polymerization of *o*PD using a hard template of silica colloid, followed by pyrolysis, removal of silica and activation by NH_3	Hierarchical porous structure	1280 $m^2\ g^{-1}$	Highest ORR activity among metal-free catalysts	487

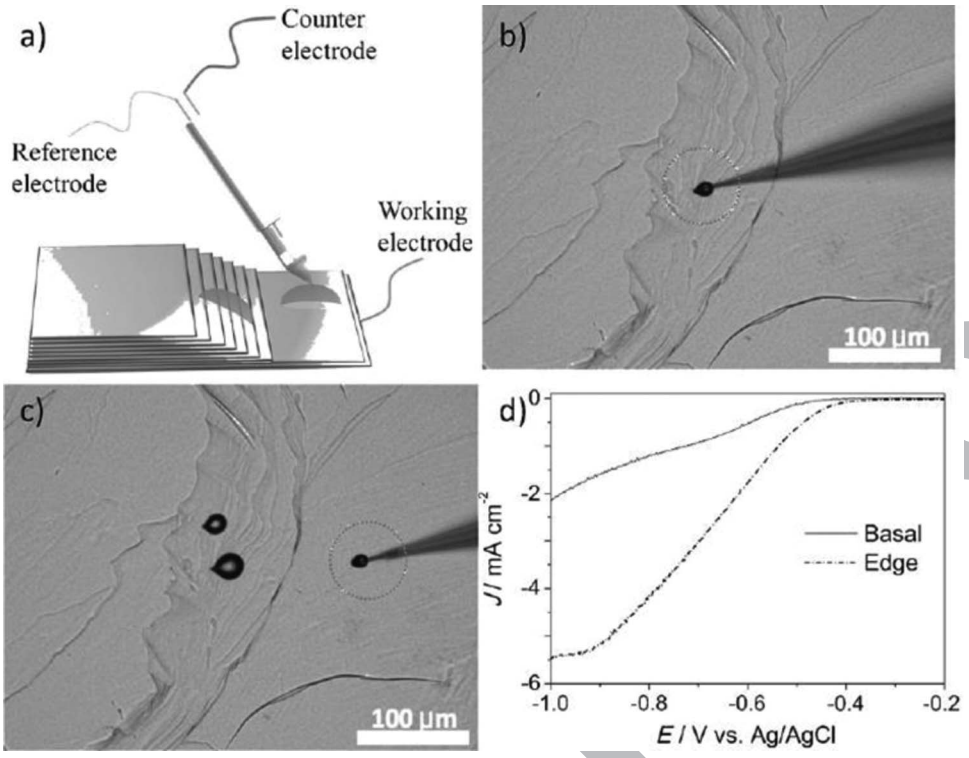

Figure 23. a) Micro apparatus for the ORR electrochemical experiment. b) Optical photograph of the HOPG as the working electrode with the air-saturated droplet deposited on the edge of the HOPG. c) The air saturated droplet was deposited on the basal plane of the HOPG electrode. d) LSV curves of the ORR tested for a droplet located either on the edge (as shown in Figure 23b) or on the basal plane (as shown in Figure 23c) of the HOPG. Reprinted with permission from Ref. 341 Copyright 2014 Wiley-VCH

new fundamental findings need to be emphasized in the following. It is generally accepted that the charge neutrality of pristine carbon materials can be changed by doping or surface modification with more electronegative elements like F[330, 331], N[332, 333], O[286, 334], electronegativity similar elements like S[123, 335] or less electronegative elements like B[336, 337], P[338, 339], endowing a shift of the Fermi level, availability of active sites, and improvement of ORR towards the 4e⁻ pathway. In addition, ORR can be significantly benefited by an increase of surface area and porosity of carbonaceous electrocatalysts. For example, P doped ordered mesoporous carbon with different lengths and thicknesses were prepared by pyrolyzing of triphenylphosphine (P source) and phenol (C source) using SBA-15 templates with different rod lengths. The POMC-3 sample with the shortest channel length exhibits the largest surface area of 1182 $m^2\ g^{-1}$ and pore volume of 1.87 $cm^3\ g^{-1}$, leading to an increase in activity for ORR in 0.1 M KOH.[340]

In addition to the changes by dopants, the carbon materials themselves may exhibit structural effects on ORR activity. With an electrochemical micromanipulator–microinjection system in Figure 23a, air-saturated 1 M KOH micro-droplets were deposited either on the edge (Figure 23b) or on the basal plane (Figure 23c) of HOPG. From the LSV curves in Figure 23d, the edge is more active than the basal plane for ORR, which is an important guideline for design of better metal-free carbon based ORR electrocatalysts. Indeed, the graphite sample prepared by ball-milling with more edges exposed shows much enhanced electrocatalytic activity and selectivity than the pristine graphite.[341] It is true that carbon in its elementary substance form is the most attractive kind of material to be used as metal-free electrocatalyst for ORR. Besides that, the development of conducting polymer based electrocatalysts cannot be ignored due to their unique properties and promising performance for ORR in alkaline media.[342,343] Kerr et al.[343] prepared two poly(3,4-ethylenedioxythiophene) (PEDOT) samples using a vapor-phase polymerization and an electrodeposition method. Although the PEDOT samples prepared by both methods have similar structure, it is surprising to observe that ORR undergoes a transition from a 2-electron process to a 4-electron 'series' on vapor-phase polymerized PEDOT, whereas it proceeds via a 2-electron pathway on electrodeposited PEDOT.

Composites and natural resourced carbon materials.—Outstanding intrinsic ORR activity has been observed on the aforementioned carbon materials. However, some of them may suffer from practical problems when being used as electrodes for ORR. For instance, heteroatom-doped graphene materials showing high ORR catalytic activity have a common limitation of re-stacking of layers by π–π interactions and vander Waals forces.[231,344] The electrode surface area may drop dramatically when a high loading is needed, which will cause a significant decrease of current density for ORR. One strategy to overcome this problem is to incorporate carbon nanotubes as a spacer into graphene layers and form a composite so that restacking of graphene can be avoided. Ratso et al.[344] pyrolyzed a mixture of GO and MWCNTs at 800°C for 2 h using urea or DCDA as the N source for doping. As-synthesized electrocatalysts showed remarkable electrocatalytic activity that is close to a commercial Pt/C as well as good long-term stability.

In another example, Young et al.[345] synthesized a core-sheath structured CNT/N-carbon composite by pyrolysis of a monolithic CNT-ionic liquid-silica composite and subsequent removal of silica by HF. From RDE and alkaline fuel cell testing, the nanocomposite catalyst displayed one of the best performances among metal-free electrocatalysts for ORR. Unfortunately, the comparison of CNT/N-carbon composite and N-carbon prepared under similar conditions is missing, which makes the role of CNT in this composite sample unclear. Additionally, (N and S) doped mesoporous carbon/graphene composites were prepared by calcining mesoporous silica/graphene composites in the presence of different types of amino acids as heteroatoms sources.[346] In this case, mesoporous carbon was formed on graphene sheets as shown in Figure 24. As-prepared single doped and dual doped composite catalysts exhibited similarly high

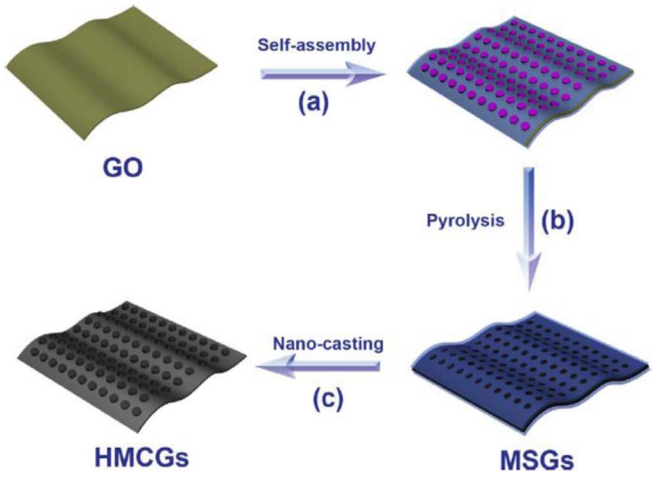

Figure 24. The synthesis procedure of Heteroatom doped mesoporous carbon/graphene nanosheets (HMCGs) (a) self-assembly of mesoporous TEOS on GO, (b) removal of CTAB and (c) nanocasting approach of each amino acid. Reprinted with permission from Ref. 346 Copyright 2014 Elsevier.

electrocatalytic activity and kinetics for ORR and superior durability as compared to Pt/C.

From the perspective of environmental protection, it would be desirable to prepare metal-free carbon based electrocatalysts using some earth-abundant materials or even waste materials. Chen et al.[347] prepared N doped carbon nanosheets by a two-step hydrothermal reaction and pyrolysis process (under NH_3) using typha orientalis as the only starting material. The sample heat treated at 800°C shows a 3D interpenetrated network structure (see Figures 25a and 25b), and similar catalytic activity but higher durability than Pt/C (Figures 25c and 25d). Various carbon materials based electrocatalysts with different stuctures and dopants have been also prepared by pyrolysis of Escherichia coli,[348] natural seaweed,[349] water hyacinth,[350] gelatin,[351] and protein-rich pulse flour,[352] etc.

Practical Considerations

The transplantation speed for cathodic electrocatalysts into real AAEMFCs falls far behind that for development of novel materials, as evidenced by the extremely scarce reports about real alkaline fuel cell testing. This may be partially due to the unsatisfactory overall cell performance caused by the intrinsic limited properties of anion exchange membranes.[353,354] On the other hand, more attention has to be paid to some remaining electrocatalysis issues. Rotating ring disk electrode (RRDE) measurements have become a routine way to evaluate and compare the catalytic activity of ORR electrocatalysts along with their function as the tool to study ORR kinetics without the effect of solution diffusion limitations. However, a very important but often omitted difference between RRDE measurement and AAEM fuel cell testing is the effective contact with the electrolyte. In the case of RRDE, an electrode covered or modified with anodic electrocatalysts is usually fully immersed in the alkaline electrolyte (typically 0.1 M KOH). This creates a big advantage of almost complete utilization of the active sites by wetting the electrode with liquid electrolyte solution that is saturated by O_2. In a sharp contrast, a solid-phase anion

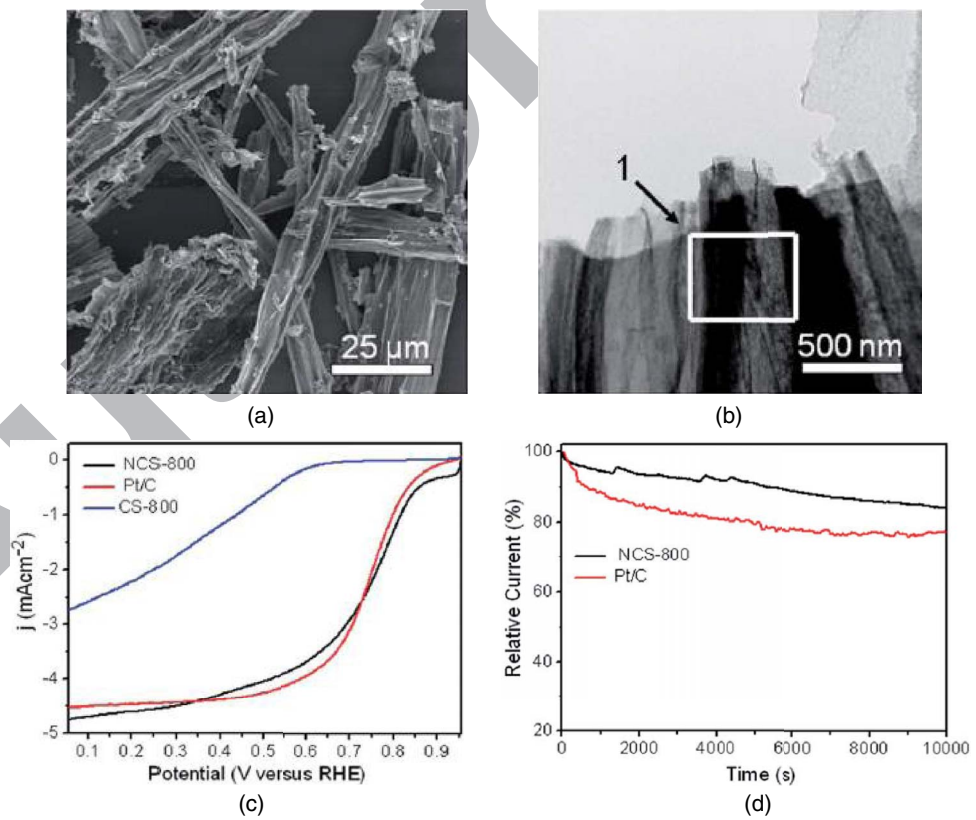

Figure 25. (a) The SEM image of Nitrogen-doped nanoporous carbon nanosheets (NCS-800). Reprinted with permission from Ref. 347 Copyright 2014 Royal Society of Chemistry. (b) The STEM image of NCS-800. Reprinted with permission from Ref. 347 Copyright 2014 Royal Society of Chemistry. (c) RDE voltammograms in O_2-saturated 0.1 M KOH solution at room temperature (rotation speed 1600 rpm, sweep rate 20 mV s^{-1}) for NCS-800, CS-800 and Pt/C. Reprinted with permission from Ref. 347 Copyright 2014 Royal Society of Chemistry. (d) Current–time (i–t) chronoamperometric response of NCS-800 and Pt/C electrodes at 0.10 V (vs. RHE) in O_2-saturated 0.1 M KOH solution at a rotation rate of 800 rpm. Reprinted with permission from 347 Copyright 2014 Royal Society of Chemistry.

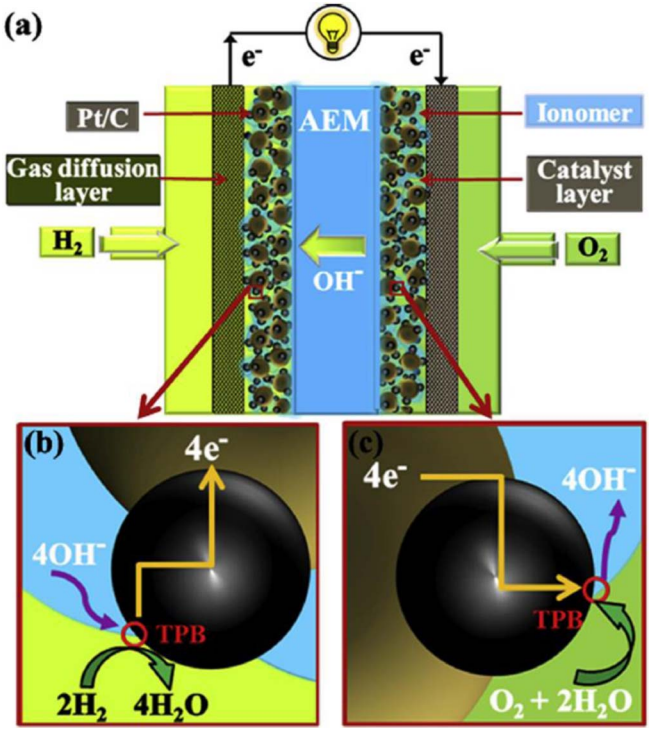

Figure 26. Schematic illustration of (a) an AAEMFC, (b) the three phase boundary in the anode and (c) the three phase boundary in the cathode. Reprinted with permission from Ref. 361 Copyright 2014 Elsevier.

exchange membrane is used as both OH^- conductor and electrode separator in an AAEMFC.

Current anion exchange membranes are typically composed of polymer backbones with hydrophobic side chains terminated with quaternary ammonium groups. Upon adsorption of water, ionic clusters and ionic channels can be formed inside the bulk membrane and the surface by proper alignment of the hydrophilic quaternary ammonium groups.[355–357] It has been shown that good electrochemical performance of a composite electrode cannot be obtained unless there is direct contact between catalyst and ionic channels in the solid membrane electrolyte for facile reactions and mass transport.[354,358,359] It is not difficult to imagine that only the top surface of the catalyst layer with direct contract to ionic channels of the membrane can be utilized no matter whether the catalyst layer is prepared by depositing catalyst materials on a gas diffusion layer (e.g. carbon cloth) or spraying them directly on the membrane. It is the blending of liquid ionomer in the catalyst layer with the membrane material that dramatically helps to extend the reaction zone deep into the catalyst layer.[360] From Figure 26, a three-phase boundary can be formed inside the catalyst layer and the transport of electrons, hydroxide ions, and molecular oxygen can be significantly promoted, resulting in significant enhancement of the ORR kinetics. For example, the highest peak power density of 358 mW cm^{-2} was achieved with a 20 wt.% ionomer content in the catalyst layers in AAEMFC tests by minimizing the active, ohmic and mass diffusion polarization losses.[361] In addition, the ORR pathway on silver nanowire catalysts may be shifted towards the $4e^-$ mechanism by increasing the ionomer content during preparation of the catalyst ink.[362] Even so, considering the very limited conductivity of current ionomers and electrode architectures, the thickness of the electrodes (especially the cathode) plays a critical role in the overall performance of an AAEMFC.

During the operation of a real AAEMFC mass-transport limitations and cooperative issues inside the catalyst layer have to be addressed in order to increase the utilization rate of electrocatalysts. On this perspective some experimental and modeling work in acidic media can be used as reference for future investigation of similar problems in alkaline media.[363–365] Durand et al.[366,367] studied kinetic parameters and the mechanism of ORR inside Nafion using RDE and electrochemical impedance spectroscopy (EIS). Not only the diffusion limitation in aqueous electrolyte but also the diffusion limitation in the active layer was fully considered to obtain the electrode kinetic parameters. In practice, the diffusion in aqueous electrolyte was corrected by RDE with a Levich plot.[367] On the other hand a homogeneous flooded model[367–370] was employed to correct for diffusion limitations in the active layer assuming that the mass transport in the gas layer is fast enough. From the dc and ac experiments it was found that an "ECE-Damjanovic" mechanism is valid on Pt nanoparticles inside the Nafion, and a direct four-electron transfer mechanism was confirmed. Durand et al.[369,370] further studied the diffusion, ohmic, spatial discrete distribution drop and other effects in a gas diffusion electrode (GDE, illustrated in Figure 27) that is the most important component for catalysis in all kinds of fuel cells. From Figure 27, the catalyst active layer of a GDE is made of catalyst nanoparticles, PTFE binder and Nafion ionomer in the voids. It is reasonable to infer that the thinner active layer leads to better ORR performance because ORR takes place only on the catalytically active sites having contact with both the carbon and electrolyte phases, and the gas (oxygen) diffusion resistance and ohmic drop are smaller. Using a modified flooded homogeneous model and EIS analysis, it was concluded that the restricted diffusion behavior for a GDE is not completely induced by the concentration gradient within the active layer.[370]

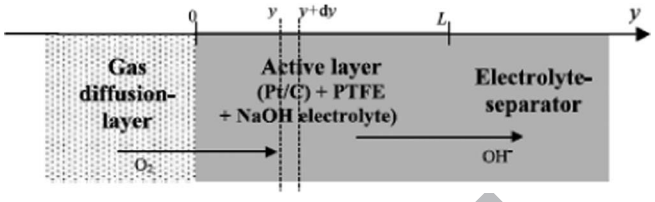

Figure 27. GDE-example of an oxygen cathode in alkaline media. Reprinted with permission from Ref. 370 Copyright 2002 Elsevier.

For the state-of-the-art Pt/C catalysts, the catalyst layer thickness of a 30% Pt/C is about 10 μm with a loading of 0.5 mgPt/cm^2.[371] However, for the non-precious metal catalysts prepared by pyrolysis of metal macrocycle compounds, the "active" transition metal loading in the form of metal-N_x instead of metallic form is usually lower than 3%. In order to increase the number of active sites and absolute current value, a strategy of increasing the catalyst loading is always pursued.[192,235,238,372] As a result, a catalyst layer thickness of ~50–100 μm will easily be reached, which makes the volumetric current density 125–1000 times lower than that of a Pt/C electrode under the best scenario of equal current. Unfortunately, the absolute current will be decreased dramatically with significant mass transport issues within the catalyst layer even with the best ionomer and electrode architectures to date.[356] Consequently, in general, an electrocatalyst with excellent ORR performance during RRDE measurements is promising but may not be qualified to be used in AAEMFCs.[373] New approaches are needed for changing the microstructure of electrodes that are made of electrocatalysts of lower active-site density than Pt.

Recently, there have been some pioneering attempts to test and study the ORR performance of cathodic electrocatalysts in AAEMFCs. He et al.[217] fabricated AAEMFCs with an A201 Tokuyama anion exchange membrane and either a commercial Pt/C catalyst or a high metal loading (24.7 wt.%) CoO/rGO(N) non-precious metal catalyst as the cathode. The large metal loading of CoO endows increased active sites of CoO strongly coupled with pyridinic nitrogens in rGO(N) and reduced thickness of the catalyst layer. The cell voltage-current polarization curves shown in Figure 28 were obtained with a CoO/rGO(N) cathode of 7.8 μm and a Pt/C cathode of 6.0 μm. With a comparable thickness of catalyst layer, the power density on CoO/rGO(N) catalyst is closely approaching that of the Pt catalysts at practical voltages (e.g. 0.6 V).

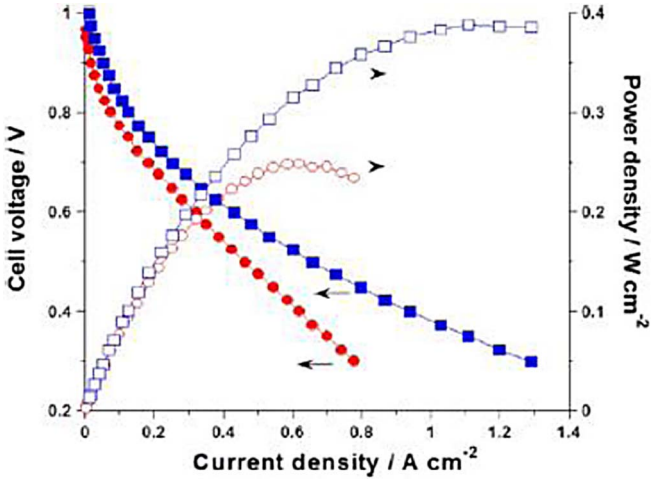

Figure 28. Performance of anion-exchange-membrane fuel cells using identical Pt/C anodes with Pt/C (square symbols) and CoO/rGO(N) cathodes (circle symbols) tested at 60°C with H_2 (at 1 atm, 57% RH) feed at the anode and O_2 (at 1 atm, 100% RH) at the cathode. The cell voltage−current polarization curves (filled symbols) on the left axis and the power current curves (open symbols) on the right axis. Reprinted with permission from Ref. 217 Copyright 2013 American Chemical Society.

In line with the preparation of the cathode in He et al.'s report, an OH^- type ionomer was added into the N-CNTs and Pt/C catalyst ink to make gas diffusion electrodes.[317] Without the reporting of catalyst layer thickness, the metal-free N-CNTs cathode shows a maximum power density of 37 mW/cm^2 as compared to that of 62 mW/cm^2 on Pt/C, and good stability over 30 h under fuel cell operating conditions. A better result that approaches the power density of transition metal based catalysts[217] was achieved by spraying CNTs/HDC catalysts with ionomer directly onto pore-filling anion conducting membranes.[345] During the preparation of a cathode for an AAEM single cell, the catalyst powder is usually mixed with ionomer in a volatile organic solvent and sprayed or coated onto carbon paper/cloth or membranes.[374] Alternatively, in a recent work, the PdNi/C catalyst ink with the binder of PTFE was sprayed onto GDLs and post-treated with poly(vinybenzyl chloride) which is the backbone of the anion exchange membrane.[375] As-prepared gas diffusion electrodes were submerged in undiluted N,N,N′,N′-tetramethylhexane-1,6-diamine for 24 h and KOH solution for 1h before fuel cell testing. With a catalyst loading of 0.4 mg cm^{-2}, the PdNi/C electrode showed a 1.7 times higher power density at 0.4 V than that of a commercial Pt/C electrode. For further improvement of the cell performance, a few constructive suggestions such as maximization of active sites of electrocatalysts, minimization of thickness of the AAEM, and optimization of fuel cell conditions were proposed.[317]

It is beyond the scope of this paper to introduce the status of development of anion exchange membranes and some engineering issues about AAEMFCs, and readers are referred to some more relevant reviews published recently.[5,353] However, some forward-looking work has to be specially emphasized here for smoother and faster implementation of various promising electrocatalysts materials into real AAEMFC applications. It has been pointed out that the degradation of head groups of AAEM in quaternary ammonium types or imidazolium-types can occur under strong basic conditions over a long period of time.[4,376–379] To study the influence of these mobile cationic head groups on the ORR performance of electrocatalysts, Ong et al.[379] added 1 mM of different quaternary ammonium-, imidazolium-, and DABCO-based cationic groups in 1 M KOH and measured cyclic voltammetry in the absence of O_2 and hydrodynamic voltammetry in the presence of O_2 on a Pt disk RDE. It was found that the hindrance of ORR activity by cationic groups follows the same order as for the suppression of hydrogen adsorption and electrochemical surface area of the Pt electrode. Considering the largest impact on ORR kinetics by imidazolium-based functional groups, it was believed that AAEMs containing these moieties may not be suitable for fuel cell applications.

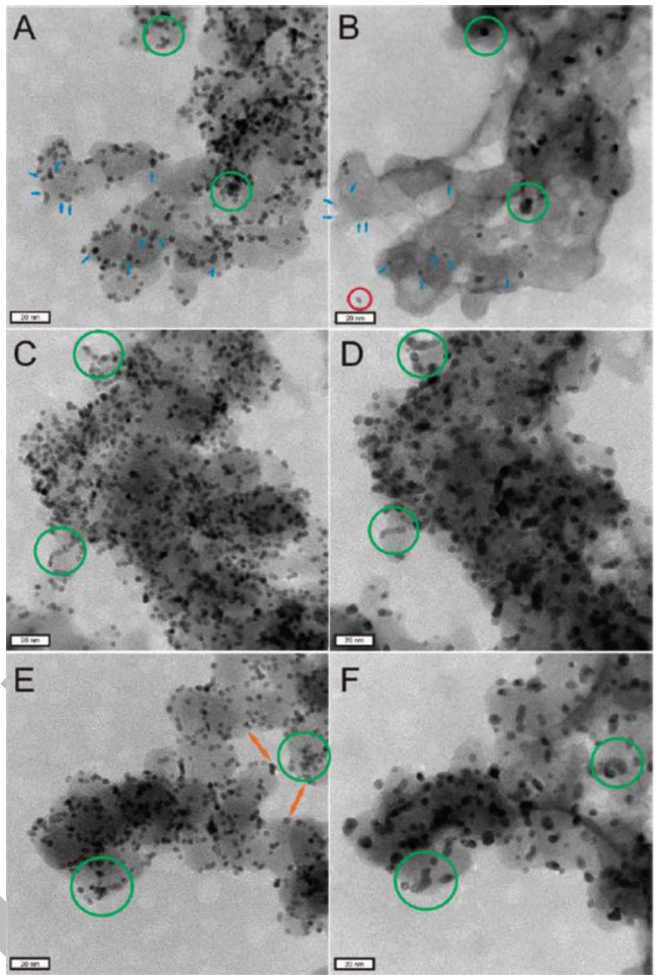

Figure 29. IL-TEM images after 0 (A, C, E) and after 3600 (B, D, F) degradation cycles. Green circles indicate agglomeration, the red circle shows a detached platinum particle, blue arrows point at platinum particles that decrease in size due to dissolution, and orange arrows emphasize massive changes in the support structure. Reprinted with permission from Ref. 380 Copyright 2012 American Chemical Society.

Another crucial aspect that must be considered for fuel cell operation is the stability of the electrocatalysts especially under the drastic operating conditions such as sudden change of potentials on the cathode. Therefore, it is necessary to investigate the degradation mechanism of cathode electrocalysts over a long period of time under extreme pH environments. To save time for assembling polymer electrode assemblies and testing in fuel cell systems, Meier et al.[380] developed an "accelerated aging tests" protocol with a combination of an electrochemical half-cell and a technology of identical location transmission electron microscopy (IL-TEM). By means of precise identification of a specific area of a TEM gold grid coated with Pt/C electrocatalyst pre- and post-test cycles in acidic solutions, the degradation processes were monitored in an ex-situ manner (see Figure 29) and several different degradation pathways were observed. By changing the electrolyte from acid to base, this advanced technique is highly applicable for evaluation and study of the stability of noble-metal, transition metal, and metal-free electrocatlysts materials quickly and reliably, devoid of the use of anion exchange membranes. By means of the same technique of IL-TEM, Zadick et al.[381] found that cubic Pd nanoparticles (NPs) turned into coalesced and near-spherical NPs after a hundred scans of CVs due to the intensive hydrogen

insertion/desinsertion process and further electrooxidation on the Pd surface. In another report of Pt/C degradation in alkaline medium, a three-times faster degradation rate was measured as compared to the same material in acidic medium.[382] This was ascribed to a modification of the carbon surface chemistry anchoring sites of the particles on the support in alkaline media.

Conclusions and Perspectives

Among many constraints on the overall alkaline anion exchange membrane fuel cells (AAEMFCs) performance, electrocatalysis and the sluggish oxygen reduction reaction (ORR) are especially prominent. In spite of the disadvantages of cost and scarcity and numerous studies of replacement candidates (for decades) of Pt/C electrocatalysts for ORR, Pt/C is still the state-of-the-art and most practically used ORR electrocatalyst in the fuel cell industry and serves as the benchmark for evaluation of novel catalysts in the scientific community. The lack of sufficient understanding of the details of the ORR processes in alkaline media makes the investigations focused on fundamental mechanisms especially valuable. The new inputs on ORR mechanisms summarized in this review help to unravel the complex interconnections and effects of such variables as surface structure, the shape of nanoparticles, and other factors like temperature and pressure and adsorption of OH^- anion and quaternary ammonium cations.

The endeavor of searching for alternative materials to Pt-based catalysts for ORR in alkaline media has never stopped. Among the non-Pt noble metals, Pd and Ag based catalysts are two promising groups, showing comparable ORR activity with commercial Pt/C catalysts. Progressive achievements have been made in recent years on preparing Pd and Ag nanoparticles with different shapes, facets and sizes using novel synthesis routes, enhancing the metal-support interactions, development of novel catalysts in oxide forms, alloying with a broad range of noble or non-noble metals, etc. Nevertheless, the detailed and solid information on the intrinsic origin of dramatic enchantment of ORR activity and stability on Pd and Ag based electrocatalysts as pH increases is unavailable, which makes it difficult to conduct a bottom-up strategy for the design of novel catalysts of these families. Some in situ electrochemical spectroscopy investigations and fuel cell testing are required to accelerate the process of utilizing these materials in practical applications. In contrast to the large number of reports of Pd and Ag based cathode catalysts, it is much less common to see studies on other non-Pt noble metals such Au, Ru and Ir. However, an important discovery of an $AuCu_3$ alloy[118] showing higher mass activity than Pt has opened the gate of designing novel active ORR electrocatalysts with combinations of elements having strong and weak affinity for oxygen.

Inspired by the natural capability of organometallic compounds for ORR, tremendous efforts have been devoted to searching and studying an important class of non-precious metal electrocatalysts with central transition metal ions coordinated with nitrogen functionalities. Some general viewpoints, consensus and controversies are summarized here. First of all, for metal-N_x-C electrocatalysts prepared by pyrolysis of metal macrocycles or metal salts with N precursors and carbon supports, it is reasonable to assign the metal-N_x moieties anchored on some graphitic defects or inter-plane regions of the carbon support as the active sites for ORR. Secondly, it is generally assumed that an optimal pyrolysis temperature exists for achievement of covalent bonds and avoiding the formation of metallic particles. In addition, to obtain catalytically active and stable metal-N_x/C electrocatalysts, the heat treatment atmosphere, metal and N precursors and follow-up acid leaching procedures all matter to some but less extent, given enough specific cavities on carbon. Thirdly, aside from high temperature heat treatment, some intriguing work has been done to prepare functionalized mesoporous and two-dimensional carbon (e.g. CNTs and graphene) supported metal-N_x electrocatalysts via solvothemal or even reactions at room temperature. The obtained comparable ORR performance was attributed to the strong non-covalent π-π interaction between the active metal center and the carbon support, which is not fully evidenced and deserve further attention and investigation.

Among other types of non-noble-metal electrocatlalysts for ORR in alkaline media, the first row transition metal oxides are the most important class of materials in view of their excellent activity, superior stability and feasibility of synthesis, etc. Unlike the confined coordination in the metal-N_x/C, more freedom and merits can be given to form transition metal oxide catalysts. Firstly, the stoichiometric ratio of metal and oxygen can vary in a large range in that MO, MO_2, M_2O_3, M_3O_4 and other compositions (or combination of different metal elements) can be seen in the literature. Secondly, by simple modification of precursor salts, concentration, pH, temperature of hydrothermal and possible calcination reactions, etc. various designed shapes of metal oxides can be made, in which a prolonged morphology like nanowires or long belts generally shows better ORR kinetics. Thirdly, unlike most of the pyrolyzed metal-N_x/C electrocatlysts with very low effective metal loading limited by total defect sites of carbon supports, a much higher catalyst loading (up to ca. 20 wt.%) can be obtained for the carbon supported metal oxide catalysts, potentially leading to smaller ohmic resistance and facile mass transport and turn over frequency in a real AAEMFC.

Though less intensively reported, some transition metal chalcogenides, sulfur-doped non-noble-metal catalysts, transition metal carbides and nitrides/oxynitrides and perovskites have attracted more and more attentions due to promising ORR performance in alkaline media. From some recent reports on late transition metal chalcogenides composed of selenium and sulfur, variously structured nanoparticles or nanocomposites can be formed with a wet chemical method under mild temperatures. Only some hypothesis about structure-activity relation and possible synergetic effects between chalcogenides and carbon supports were proposed, which makes it urgently needed to do systematical studies on this class of materials with compositions, microstructures, surface chemistry, support, stability of electrode, intermediates of ORR and other variables fully considered.

In contrast to chalcogenides, better ORR kinetics was obtained on some sulfur-doped non-noble-metal catalysts. These materials were prepared by doping sulfur into carbon backbones with a pyrolysis process or forming thiospinels with a solvothermal method. The enhancement of ORR kinetics may be caused by improved porosity and conductivity by doping heteroatoms of sulfur into carbon backbones and altering of oxidation status of transition metals. However, there is some vague or missing information that needs clarification, including the coordination effect of metal and sulfur in the cases of doping sulfur into carbon support and the distinct roles of metal-S bonds in thiospinels as opposed to those in chalcogenides.

Some transition metal carbides and nitride/oxynitride electrocatalysts have evolved recently with decent (comparable or even better than Pt/C) ORR performance and durability in the absence or presence of methanol in alkaline media. The catalysts of Fe_3C encapsulated in graphic layers or CNT walls have shown superior ORR kinetics to that of Pt/C and stability provided by the protective carbon layers, indicating that the metal carbide phases presumed as ORR inactive phases previously deserve urgent re-visit and thorough exploration. Transition metal carbides and nitrides/oxynitrides with metal elements from IVB to VIB groups have shown catalytic activity but incomplete oxygen reduction typically. For further improvement of the catalytic activity of the transition metal carbides and nitrides/oxynitrides, it may be beneficial to form bimetallic composites for obtaining multiple active species and tuning of electronic states.

Without the "acid-stability' requirement, some attempts have been made on the utilization of perovskite materials as elelctrocatalysts for ORR in alkaline media. Some disadvantages of perovskite materials such as high ohmic loss, low specific surface area and crystallite agglomeration have been alleviated by combination of carbon support, new synthesis technologies, etc. Although the intrinsic catalytic activity of transition metal oxide perovskites can be improved by adjusting the metallic compositions, these materials have lower activity than the state-of-the-art cathodic catalysts for ORR considering the best performing perovskite materials reported thus far.

For preparation of metal-free carbon material based electrocatalysts for ORR in alkaline medial, it is generally required to modify

the electron neutrality of the carbon plane with highly delocalized SP^2 electron properties by doping with heteroatoms such as N, O, P, B, S, I and so on. And it is quite interesting to notice that the electronegativity of the doping elements seems to be irrelevant for surface modification of electronic structures, since more electronegative elements like N, more electron-deficient elements like P and B, and electronegatively similar elements like S can all serve the purpose of changing the local electron density and Fermi level of the carbon substrate very well. Nevertheless, a theoretical and experimental study has proved that heteroatom doped graphene with five different commonly used atoms (N, S, O, B, and P) all exhibit inferior exchange current densities than an ideal X-graphene catalyst,[34] indicating that there is still opportunity for further improvement of the catalytic properties of doped carbon materials towards ORR.

While urgent investigations of ORR mechanisms and precise identification of the nature of the active sites on metal-free electrocatalysts need to be conducted, some common properties can be obtained for the design of improved electrocatalysts for ORR in alkaline medial after reviewing a large variety of carbonaceous materials such as doped graphene, carbon nanotubes, carbon fibers, mesoporous carbons, and carbon aerogels (see Tables V and VI). First of all, there is no doubt that the active sites on carbon substrates for ORR are introduced by the heteroatoms (X) although some non-active X-C moieties may also be formed. Consequently, it is beneficial to increase the content of heteroatoms as long as the conductivity is sufficient and the maximum number of active sites is not reached. Secondly, outstanding ORR performance can be usually seen on those heteroatom- doped carbon materials with large surface area (typically $> 600\ m^2/g$). For instance, low overpotentials, fast kinetics and $4e^-$ pathway, and good long-term durability were found on many mesoporous carbon electrocatalysts prepared by pyrolysis of a mixture of precursors for C and heteroatoms and a silica substrate followed by removal of silica with HF or strong base. To overcome the problem of re-stacking of graphene layers due to strong π-π interactions, some composite materials like graphene/CNTs have shown much improved catalytic properties. Last but not least, edges and topological defects have shown better catalytic activity than basal planes on carbon, which needs to be considered during design and preparation of novel metal-free electrocatalyst materials.

To the end, from the point of view of practical applications, although RRDE measurement is a fast and reliable method for screening electrocatalysts for ORR, one must realize that the RRDE results may not necessarily be transferable to a real AAEMFC. By mixing the catalyst powder with hydroxide-conducting ionomer during the preparation of membrane electrode assemblies (MEAs), the reaction zone has been largely extended into the catalyst layer instead of being localized on the surface with direct contact to ionic clusters and ionic channels of the anion exchange membranes. However, the "higher catalyst loading - better ORR performance" phenomenon as seen during RRDE measurements is no longer available in AAEM fuel cell testing, due to the significantly deteriorated performance with a large mass transport resistance and low conductivity ionomers. Therefore, from the point of view of electrocatalysis, the next step to advance the AAEMFC technology relies on the development of electrode architectures with significantly increased active site density and/or greatly improved ionomer conductivity.

In addition to activity and kinetics for ORR, the stability of a cathode electrocatalyst is equally important in order to be employed in AAEMFCs. Similar to the situation in PEMFCs, the conventional Pt/C electrodes still suffer from aggregation of metal nanoparticles and degradation of the carbon support in AAEMFCs, and methanol crossover in the case when methanol is the fuel. From the literature, it is not unusual to see largely improved stability for alternative electrocatalysts for Pt/C in diluted base (e.g. 0.1 M KOH). Nevertheless, real long-term alkaline fuel cell testing or accelerated aging tests under strongly basic conditions are desirable. For a better understanding of the degradation mechanism of ORR, some pioneering studies such as the impact of mobile ionomer head groups and some advanced technologies like identical location- TEM are also highly needed.

Acknowledgment

This work was supported by "The Recruitment Program of Global Youth Experts" from the Chinese government and the "Hundred Talents Program" of Zhejiang University. We thank Dr. S. Khene and Dr. J.-P Dodelet for valuable discussions.

References

1. T. Burchardt, J. H. Miners, P. Gouerec, and W. Stinissen, *Prepr. Symp. - Am. Chem. Soc., Div. Fuel Chem.*, **46**, 473 (2001).
2. E. De Geeter, M. Mangan, S. Spaepen, W. Stinissen, and G. Vennekens, *J. Power Sources*, **80**, 207 (1999).
3. G. F. McLean, T. Niet, S. Prince-Richard, and N. Djilali, *Int. J. Hydrogen Energy*, **27**, 507 (2002).
4. O. I. Deavin, S. Murphy, A. L. Ong, S. D. Poynton, R. Zeng, H. Herman, and J. R. Varcoe, *Energy Environ. Sci.*, **5**, 8584 (2012).
5. R. Slade, J. P. Kizewski, S. D. Poynton, R. Zeng, and J. R. Varcoe, in *Fuel Cells: Selected Entries from the Encyclopedia of Sustainability Science and Technology*, K. D. Kreuer Editor, Springer Science+Business Media, New York (2013).
6. J. R. Varcoe and R. C. T. Slade, *Fuel Cells (Weinheim, Ger.)*, **5**, 187 (2005).
7. L. A. Adams, S. D. Poynton, C. Tamain, R. C. T. Slade, and J. R. Varcoe, *ChemSusChem*, **1**, 79 (2008).
8. S. Gu, R. Cai, T. Luo, Z. Chen, M. Sun, Y. Liu, G. He, and Y. Yan, *Angew. Chem., Int. Ed.*, **48**, 6499 (2009).
9. S. Lu, J. Pan, A. Huang, L. Zhuang, and J. Lu, *Proc. Natl. Acad. Sci. U. S. A.*, **105**, 20611 (2008).
10. A. Wieckowski and J. Spendelow, in *Encyclopedia of Applied Electrochemistry* G. Kreysa, K.-I. Ota, and R. F. Savinell Editors, Springer New York (2014).
11. N. Ramaswamy and S. Mukerjee, *J. Phys. Chem. C*, **115**, 18015 (2011).
12. N. Ramaswamy and S. Mukerjee, *Advances in Physical Chemistry*, **2012**, 1 (2012).
13. K. Wan, Z.-P. Yu, X.-H. Li, M.-Y. Liu, G. Yang, J.-H. Piao, and Z.-X. Liang, *ACS Catal.*, **5**, 4325 (2015).
14. F. Moureaux, P. Stevens, and M. Chatenet, *Electrocatalysis*, **4**, 123 (2013).
15. W. Y. Wong, W. R. W. Daud, A. B. Mohamad, and K. S. Loh, *Int. J. Hydrogen Energy*, **40**, 11444 (2015).
16. E. Antolini and E. R. Gonzalez, *J. Power Sources*, **195**, 3431 (2010).
17. J. S. Spendelow and A. Wieckowski, *Phys. Chem. Chem. Phys.*, **9**, 2654 (2007).
18. B. B. Blizanac, P. N. Ross, and N. M. Markovic, *Electrochim. Acta*, **52**, 2264 (2007).
19. D. B. Sepa, M. V. Vojnovic, and A. Damjanovic, *Electrochim. Acta*, **25**, 1491 (1980).
20. D. B. Sepa, M. V. Vojnovic, L. M. Vracar, and A. Damjanovic, *Electrochim. Acta*, **32**, 129 (1987).
21. A. Damjanovic, A. Dey, and J. O. M. Bockris, *Electrochim. Acta*, **11**, 791 (1966).
22. P. N. Ross, in *Handbook of Fuel Cells: Fundamentals, Technology, Applications, V2*, W. Vielstich, A. Lamm, and H. Gasteiger Editors, p. 465, Wiley (2003).
23. E. Yeager, M. Razaq, D. Gervasio, A. Razaq, and D. Tryk, in *Proceedings of the Electrochemical Society*, D. Scherson, D. Tryk, M. Daroux, and X. Xing Editors, p. 440 (1992).
24. S. J. Clouser, J. C. Huang, and E. Yeager, *J. Appl. Electrochem.*, **23**, 597 (1993).
25. E. Yeager, M. Razaq, D. Gervasio, A. Razaq, and D. Tryk, *J. Serb. Chem. Soc.*, **57**, 819 (1992).
26. A. J. Appleby, *Compr. Treatise Electrochem.*, **7**, 173 (1983).
27. L. M. Torres, A. F. Gil, L. Gallcia, and I. Gonzalez, *J. Chem. Educ.*, **73**, 808 (1996).
28. N. M. Markovioc, H. A. Gasteiger, and P. N. Ross, Jr., *J. Phys. Chem.*, **100**, 6715 (1996).
29. N. Markovic, H. Gasteiger, and P. N. Ross, *J. Electrochem. Soc.*, **144**, 1591 (1997).
30. B. E. Conway, *Prog. Surf. Sci.*, **49**, 331 (1995).
31. G. Jerkiewicz, G. Vatankhah, J. Lessard, M. P. Soriaga, and Y.-S. Park, *Electrochim. Acta*, **49**, 1451 (2004).
32. C. Roth, A. J. Papworth, I. Hussain, R. J. Nichols, and D. J. Schiffrin, *J. Electroanal. Chem.*, **581**, 79 (2005).
33. N. Ramaswamy, U. Tylus, Q. Jia, and S. Mukerjee, *J. Am. Chem. Soc.*, **135**, 15443 (2013).
34. Y. Jiao, Y. Zheng, M. Jaroniec, and S. Z. Qiao, *J. Am. Chem. Soc.*, **136**, 4394 (2014).
35. D. Yu, E. Nagelli, F. Du, and L. Dai, *J. Phys. Chem. Lett.*, **1**, 2165 (2010).
36. L. Lin, Q. Zhu, and A.-W. Xu, *J. Am. Chem. Soc.*, **136**, 11027 (2014).
37. M. Li, X. Bo, Y. Zhang, C. Han, A. Nsabimana, and L. Guo, *J. Mater. Chem. A*, **2**, 11672 (2014).
38. N. R. K. Vilambi and E. J. Taylor, *Electrochim. Acta*, **34**, 1449 (1989).
39. C. A. C. Sequeira, D. M. F. Santos, and W. Baptista, *J. Braz. Chem. Soc.*, **17**, 910 (2006).
40. M. R. Tarasevich, A. Sadkowski, and E. Yeager, *Compr. Treatise Electrochem.*, **7**, 301 (1983).
41. S. Mukerjee, S. Srinivasan, and M. P. Soriaga, *J. Electrochem. Soc.*, **142**, 1409 (1995).
42. Q. He and S. Mukerjee, *Electrochim. Acta*, **55**, 1709 (2010).
43. C. Chen, Y. Kang, Z. Huo, Z. Zhu, W. Huang, H. L. Xin, J. D. Snyder, D. Li, J. A. Herron, M. Mavrikakis, M. Chi, K. L. More, Y. Li, N. M. Markovic, G. A. Somorjai, P. Yang, and V. R. Stamenkovic, *Science (Washington, DC, U. S.)*, **343**, 1339 (2014).
44. D. Aberdam, R. Durand, R. Faure, and F. El-Omar, *Surf. Sci.*, **171**, 303 (1986).
45. F. El Kadiri, R. Faure, and R. Durand, *J. Electroanal. Chem. Interfacial Electrochem.*, **301**, 177 (1991).

46. M. Pourbaix, *Atlas of Electrochemical Equilibria in Aqueous Solutions*, p. 638 pp (1966).
47. H. Duan and C. Xu, *Electrochim. Acta*, **152**, 417 (2015).
48. S. R. Calvo and P. B. Balbuena, *Surf. Sci.*, **601**, 4786 (2007).
49. Y. Wang and P. B. Balbuena, *J. Phys. Chem. B*, **109**, 18902 (2005).
50. I. A. Pasti, N. M. Gavrilov, M. Baljozovic, M. Mitric, and S. V. Mentus, *Electrochim. Acta*, **114**, 706 (2013).
51. X. Zhong, H. Yu, X. Wang, L. Liu, Y. Jiang, L. Wang, G. Zhuang, Y. Chu, X. Li, and J.-G. Wang, *ACS Appl Mater Interfaces*, **6**, 13448 (2014).
52. M. Stojmenovic, M. Momcilovic, N. Gavrilov, I. A. Pasti, S. Mentus, B. Jokic, and B. Babic, *Electrochim. Acta*, **153**, 130 (2015).
53. Y.-L. Tsai, K.-L. Huang, C.-C. Yang, J.-S. Ye, L.-S. Pan, and C.-L. Lee, *Int. J. Hydrogen Energy*, **39**, 5528 (2014).
54. M. Chatenet, M. Aurousseau, R. Durand, and F. Andolfatto, *J. Electrochem. Soc.*, **150**, D47 (2003).
55. B. N. Wanjala, B. Fang, R. Loukrakpam, Y. Chen, M. Engelhard, J. Luo, J. Yin, L. Yang, S. Shan, and C.-J. Zhong, *ACS Catal.*, **2**, 795 (2012).
56. D. A. Robinson and K. J. Stevenson, *J. Mater. Chem. A*, **1**, 13443 (2013).
57. M. Oezaslan, F. Hasche, and P. Strasser, *J. Electrochem. Soc.*, **159**, B444 (2012).
58. R. Devivaraprasad, R. Ramesh, N. Naresh, T. Kar, K. Singh Ramesh, and M. Neergat, *Langmuir*, **30**, 8995 (2014).
59. R. Rizo, E. Herrero, and J. M. Feliu, *Phys. Chem. Chem. Phys.*, **15**, 15416 (2013).
60. X. Yu, H. Wang, L. Guo, and L. Wang, *Chem Asian J*, **9**, 3221 (2014).
61. L. Genies, R. Faure, and R. Durand, *Electrochim. Acta*, **44**, 1317 (1998).
62. C. Alegre, D. Sebastian, E. Baquedano, M. E. Galvez, R. Moliner, and M. J. Lazaro, *Catalysts*, **2**, 466 (2012).
63. S. Zhao, A. E. Wangstrom, Y. Liu, W. A. Rigdon, and W. E. Mustain, *Electrochim. Acta*, **157**, 175 (2015).
64. T. Huang, S. Mao, H. Pu, Z. Wen, X. Huang, S. Ci, and J. Chen, *J. Mater. Chem. A*, **1**, 13404 (2013).
65. N. R. Elezovic, B. M. Babic, L. Gajic-Krstajic, P. Ercius, V. R. Radmilovic, N. V. Krstajic, and L. M. Vracar, *Electrochim. Acta*, **69**, 239 (2012).
66. Z. Cui, M. Yang, H. Chen, M. Zhao, and F. J. Di Salvo, *ChemSusChem*, **7**, 3356 (2014).
67. Z. Cui, R. G. Burns, and F. J. Di Salvo, *Chem. Mater.*, **25**, 3782 (2013).
68. M. Nie, Z. J. Zeng, B. He, Q. Li, X. W. Liu, and C. S. Zheng, *Mater. Res. Innovations*, **18**, 255 (2014).
69. L. Truong-Phuoc, C. Pham-Huu, V. Da Costa, and I. Janowska, *Chem. Commun. (Cambridge, U. K.)*, **50**, 14433 (2014).
70. J. K. Norskov, J. Rossmeisl, A. Logadottir, L. Lindqvist, J. R. Kitchin, T. Bligaard, and H. Jonsson, *J. Phys. Chem. B*, **108**, 17886 (2004).
71. M. Chatenet, L. Genies-Bultel, M. Aurousseau, R. Durand, and F. Andolfatto, *J. Appl. Electrochem.*, **32**, 1131 (2002).
72. L. Jiang, A. Hsu, D. Chu, and R. Chen, *J. Electrochem. Soc.*, **156**, B643 (2009).
73. W. Zhou, M. Li, O. L. Ding, S. H. Chan, L. Zhang, and Y. Xue, *Int. J. Hydrogen Energy*, **39**, 6433 (2014).
74. H. Erikson, A. Sarapuu, K. Tammeveski, J. Solla-Gullon, and J. M. Feliu, *Electrochem. Commun.*, **13**, 734 (2011).
75. Y.-B. Cho, J. E. Kim, J. H. Shim, C. Lee, and Y. Lee, *Phys. Chem. Chem. Phys.*, **15**, 11461 (2013).
76. J. Ohyama, Y. Okata, N. Watabe, M. Katagiri, A. Nakamura, H. Arikawa, K.-I. Shimizu, T. Takeguchi, W. Ueda, and A. Satsuma, *J. Power Sources*, **245**, 998 (2014).
77. Q. Wang, X. Cui, W. Guan, L. Zhang, X. Fan, Z. Shi, and W. Zheng, *J. Power Sources*, **269**, 152 (2014).
78. S. M. Alia, K. Duong, T. Liu, K. Jensen, and Y. Yan, *ChemSusChem*, **5**, 1619 (2012).
79. J. Greeley, J. Rossmeisl, A. Hellman, and J. K. Noerskov, *Z. Phys. Chem. (Muenchen, Ger.)*, **221**, 1209 (2007).
80. J. E. Choe, M. S. Ahmed, and S. Jeon, *J. Power Sources*, **281**, 211 (2015).
81. K. Lee, M. S. Ahmed, and S. Jeon, *J. Electrochem. Soc.*, **162**, F1 (2015).
82. K.-L. Huang, Z.-T. Liu, and C.-L. Lee, *Electrochim. Acta*, **157**, 78 (2015).
83. M. Shao, J. Odell, M. Humbert, T. Yu, and Y. Xia, *J. Phys. Chem. C*, **117**, 4172 (2013).
84. G. Fu, X. Jiang, L. Tao, Y. Chen, J. Lin, Y. Zhou, Y. Tang, and T. Lu, *Langmuir*, **29**, 4413 (2013).
85. X. Yang, L. Gan, C. Zhu, B. Lou, L. Han, J. Wang, and E. Wang, *Chem. Commun. (Cambridge, U. K.)*, **50**, 234 (2014).
86. Q. Wu, Z. Rao, L. Yuan, L. Jiang, G. Sun, J. Ruan, Z. Zhou, and S. Sang, *Electrochim. Acta*, **150**, 157 (2014).
87. Q. He, B. Shyam, M. Nishijima, X. Yang, B. Koel, F. Ernst, D. Ramaker, and S. Mukerjee, *J. Phys. Chem. C*, **117**, 1457 (2013).
88. Y. Zheng, S. Zhao, S. Liu, H. Yin, Y.-Y. Chen, J. Bao, M. Han, and Z. Dai, *ACS Appl. Mater. Interfaces*, Ahead of Print (2015).
89. M. Han, S. Liu, L. Zhang, C. Zhang, W. Tu, Z. Dai, and J. Bao, *ACS Appl. Mater. Interfaces*, **4**, 6654 (2012).
90. D. A. Slanac, A. Lie, J. A. Paulson, K. J. Stevenson, and K. P. Johnston, *J. Phys. Chem. C*, **116**, 11032 (2012).
91. H.-Q. Dong, Y.-Y. Chen, M. Han, S.-L. Li, J. Zhang, J.-S. Li, Y.-Q. Lan, Z.-H. Dai, and J.-C. Bao, *J. Mater. Chem. A*, **2**, 1272 (2014).
92. S. Liu and X. Qin, *RSC Adv.*, **5**, 15627 (2015).
93. Q. Wu, L. Jiang, L. Qi, L. Yuan, E. Wang, and G. Sun, *Electrochim. Acta*, **123**, 167 (2014).
94. Y. Wang, X. Lu, Y. Liu, and Y. Deng, *Electrochem. Commun.*, **31**, 108 (2013).
95. Y. Lu, Y. Jiang, X. Gao, X. Wang, and W. Chen, *J Am Chem Soc*, **136**, 11687 (2014).
96. Q. He, X. Yang, R. He, A. Bueno-Lopez, H. Miller, X. Ren, W. Yang, and B. E. Koel, *J. Power Sources*, **213**, 169 (2012).
97. Z. Zhang, X. Wang, Z. Cui, C. Liu, T. Lu, and W. Xing, *J. Power Sources*, **185**, 941 (2008).
98. M. H. Seo, S. M. Choi, J. K. Seo, S. H. Noh, W. B. Kim, and B. Han, *Appl. Catal., B*, **129**, 163 (2013).
99. A. Sarkar, A. V. Murugan, and A. Manthiram, *J. Mater. Chem.*, **19**, 159 (2009).
100. S. Maheswari, P. Sridhar, and S. Pitchumani, *Electrochem. Commun.*, **26**, 97 (2013).
101. Q. Yi and L. Song, *Electroanalysis*, **24**, 1655 (2012).
102. R. M. Modibedi, M. K. Mathe, R. G. Motsoeneng, L. E. Khotseng, K. I. Ozoemena, and E. K. Louw, *Electrochim. Acta*, **128**, 406 (2014).
103. H. Wang, J. Zheng, L. Zhu, F. Peng, and H. Yu, *Adv. Mater. Res. (Durnten-Zurich, Switz.)*, 550, 238 (2012).
104. Q. Yi, H. Chu, M. Tang, Z. Yang, Q. Chen, and X. Liu, *J. Electroanal. Chem.*, **739**, 178 (2015).
105. M. Liu, R. Zhang, and W. Chen, *Chem. Rev. (Washington, DC, U. S.)*, **114**, 5117 (2014).
106. L. Yuan, L. Jiang, J. Liu, Z. Xia, S. Wang, and G. Sun, *Electrochim. Acta*, **135**, 168 (2014).
107. D. J. Davis, A.-R. O. Raji, T. N. Lambert, J. A. Vigil, L. Li, K. Nan, and J. M. Tour, *Electroanalysis*, **26**, 164 (2014).
108. H. Wang, D. Cao, Y. Xiang, D. Liang, and S. Lu, *RSC Adv.*, **4**, 51126 (2014).
109. L. Xu, H. Li, J. Xia, L. Wang, H. Xu, H. Ji, H. Li, and K. Sun, *Mater. Lett.*, **128**, 349 (2014).
110. C. Lai, P. Kolla, Y. Zhao, H. Fong, and A. L. Smirnova, *Electrochim. Acta*, **130**, 431 (2014).
111. F.-B. Wang, J. Wang, L. Shao, Y. Zhao, and X.-H. Xia, *Electrochem. Commun.*, **38**, 82 (2014).
112. W. Jin, M. S. Moats, S. Zheng, H. Du, Y. Zhang, and J. D. Miller, *J. Phys. Chem. B*, **116**, 7531 (2012).
113. J. Kang, S. Byun, S. Nam, S. Kang, T. Moon, and B. Park, *Int. J. Hydrogen Energy*, **39**, 10921 (2014).
114. L. F. Mabena, R. M. Modibedi, S. Sinha Ray, and N. J. Coville, *Fuel Cells (Weinheim, Ger.)*, **12**, 862 (2012).
115. K. Fujii, Y. Sato, S. Takase, and Y. Shimizu, *J. Electrochem. Soc.*, **162**, F129 (2015).
116. K. Chakrapani and S. Sampath, *Phys Chem Chem Phys*, **16**, 16815 (2014).
117. P. Rodriguez and T. M. Koper Marc, *Phys Chem Chem Phys*, **16**, 13583 (2014).
118. N. Zhang, X. Chen, Y. Lu, L. An, X. Li, D. Xia, Z. Zhang, and J. Li, *Small*, **10**, 2662 (2014).
119. P. Quaino, N. B. Luque, R. Nazmutdinov, E. Santos, and W. Schmickler, *Angew. Chem., Int. Ed.*, **51**, 12997 (2012).
120. F. Abild-Pedersen, J. Greeley, F. Studt, J. Rossmeisl, T. R. Munter, P. G. Moses, E. Skulason, T. Bligaard, and J. K. Noerskov, *Phys. Rev. Lett.*, **99**, 016105/1 (2007).
121. B. Hvolbæk, T. V. W. Janssens, B. S. Clausen, H. Falsig, C. H. Christensen, and J. K. Nørskov, *Nano Today*, **2**, 14 (2007).
122. D. A. McQuarrie, P. A. Rock, and E. B. Gallogly, *General chemistry*, Mill Valley, CA : University Science Books (2011).
123. Z. Yang, H. Nie, X. a. Chen, X. Chen, and S. Huang, *J. Power Sources*, **236**, 238 (2013).
124. K. Selvakumar, S. M. Senthil Kumar, R. Thangamuthu, G. Kruthika, and P. Murugan, *Int. J. Hydrogen Energy*, **39**, 21024 (2014).
125. N. Mahmood, C. Zhang, J. Jiang, F. Liu, and Y. Hou, *Chemistry*, **19**, 5183 (2013).
126. G. Wu and P. Zelenay, *Acc. Chem. Res.*, **46**, 1878 (2013).
127. S. Liu, Z. Zhang, J. Bao, Y. Lan, W. Tu, M. Han, and Z. Dai, *J. Phys. Chem. C*, **117**, 15164 (2013).
128. M. Shen, C. Ruan, Y. Chen, C. Jiang, K. Ai, and L. Lu, *ACS Appl Mater Interfaces*, **7**, 1207 (2015).
129. X. Wang, Y. Ke, H. Pan, K. Ma, Q. Xiao, D. Yin, G. Wu, and M. T. Swihart, *ACS Catal.*, **5**, 2534 (2015).
130. X. Bo, Y. Zhang, M. Li, A. Nsabimana, and L. Guo, *J. Power Sources*, **288**, 1 (2015).
131. W. Chu, D. Higgins, Z. Chen, and R. Cai, *Non-Noble Met. Fuel Cell Catal.*, 357 (2014).
132. W. Yan, W. Bian, C. Jin, J.-H. Tian, and R. Yang, *Electrochim. Acta*, Ahead of Print (2015).
133. C. A. Hancock, A. L. Ong, and J. R. Varcoe, *RSC Adv.*, **4**, 30035 (2014).
134. M. Saito, Y. Saito, T. Konishi, H. Kawai, J. Kuwano, H. Shiroishi, and Y. Uchimoto, *ECS Trans.*, **16**, 891 (2008).
135. R. J. Jasinski, *Nature (London, U. K.)*, **201**, 1212 (1964).
136. J. H. Zagal, M. A. Pa´ez, and J. F. Silva, in *N4-Macrocyclic Metal Complexes*, J. H. Zagal, F. Bedioui, and J.-P. Dodelet Editors, Springer Science+Business Media, Inc., New York (2006).
137. Q. He, T. Mugadza, G. S. Hwang, and T. Nyokong, *Int. J. Electrochem. Sci.*, **7**, 7045 (2012).
138. Q. He, X. Cheng, Y. Wang, R. Qiao, W. Yang, and J. Guo, *J. Porphyrins Phthalocyanines*, **17**, 252 (2013).
139. M.-S. Liao and S. Scheiner, *J. Chem. Phys.*, **117**, 205 (2002).
140. P. B. Armentrout, **428**, 18 (1990).
141. J. R. Fulton, A. W. Holland, D. J. Fox, and R. G. Bergman, *Acc. Chem. Res.*, **35**, 44 (2002).
142. Q. A. Acton, *Nitrogen Compounds—Advances in Research and Application*, Scholarlyeditions (2013).
143. V. Soukharev, N. Mano, and A. Heller, *J. Am. Chem. Soc.*, **126**, 8368 (2004).
144. K. Oyaizu, H. Murata, and M. Yuasa, in *Molecular Catalysts for Energy Conversion*, T. Okada and M. Kaneko Editors, Springer, Berlin Heidelberg (2009).
145. B. Steiger and F. C. Anson, *Inorg. Chem.*, **34**, 3355 (1995).
146. S.-I. Yamazaki, Y. Yamada, T. Ioroi, N. Fujiwara, Z. Siroma, K. Yasuda, and Y. Miyazaki, *J. Electroanal. Chem.*, **576**, 253 (2005).

147. A. H. C. Sirk, S. A. Campbell, and V. I. Birss, *Electrochemical and Solid-State Letters*, **8**, A104 (2005).
148. C. W. B. Bezerra, L. Zhang, H. Liu, K. Lee, A. L. B. Marques, E. P. Marques, H. Wang, and J. Zhang, *J. Power Sources*, **173**, 891 (2007).
149. J.-P. Dodelet, in *N4-Macrocyclic Metal Complexes*, J. H. Zagal, F. Bedioui, and J.-P. Dodelet Editors, Springer Science+Business Media, Inc, New York (2006).
150. X. Dai, J. Qiao, X. Zhou, J. Shi, P. Xu, L. Zhang, and J. Zhang, *Int. J. Electrochem. Sci.*, **8**, 3160 (2013).
151. R. Chen, H. Li, D. Chu, and G. Wang, *J. Phys. Chem. C*, **113**, 20689 (2009).
152. R. J. van Veen and C. Visser, *Electrochim. Acta*, **24**, 921 (1979).
153. Q. He, X. Yang, X. Ren, B. E. Koel, N. Ramaswamy, S. Mukerjee, and R. Kostecki, *J. Power Sources*, **196**, 7404 (2011).
154. J. A. R. Van Veen, H. A. Colijn, and J. F. Van Baar, *Electrochim. Acta*, **33**, 801 (1988).
155. J. A. R. Van Veen, J. F. Van Baar, and K. J. Kroese, *J. Chem. Soc., Faraday Trans. 1*, **77**, 2827 (1981).
156. A. L. Bouwkamp-Wijnoltz, W. Visscher, J. A. R. van Veen, E. Boellaard, A. M. van der Kraan, and S. C. Tang, *J. Phys. Chem. B*, **106**, 12993 (2002).
157. A. L. Bouwkamp-Wijnoltz, W. Visscher, and J. A. R. Van Veen, *Electrochim. Acta*, **43**, 3141 (1998).
158. A. L. Bouwkamp-Wijnoltz, W. Visscher, J. A. R. Van Veen, and S. C. Tang, *Electrochim. Acta*, **45**, 379 (1999).
159. J. McBreen, W. E. O'Grady, D. E. Sayers, C. Y. Yang, and K. I. Pandya, *Proc. - Electrochem. Soc.*, **87-12**, 182 (1987).
160. H. Schulenburg, S. Stankov, V. Schuenemann, J. Radnik, I. Dorbandt, S. Fiechter, P. Bogdanoff, and H. Tributsch, *J. Phys. Chem. B*, **107**, 9034 (2003).
161. D. A. Scherson, S. L. Gupta, C. Fierro, E. B. Yeager, M. E. Kordesch, J. Eldridge, R. W. Hoffman, and J. Blue, *Electrochim. Acta*, **28**, 1205 (1983).
162. A. Tanaka, S. L. Gupta, D. Tryk, C. Fierro, E. B. Yeager, and D. A. Scherson, *Proc. - Electrochem. Soc.*, **92-11**, 555 (1992).
163. E. Yeager, *Electrochim. Acta*, **29**, 1527 (1984).
164. I. T. Bae, D. A. Tryk, and D. A. Scherson, *J. Phys. Chem. B*, **102**, 4114 (1998).
165. S. Kim, I. T. Bae, M. Sandifer, P. N. Ross, R. Carr, J. Woicik, M. R. Antonio, and D. A. Scherson, *J. Am. Chem. Soc.*, **113**, 9063 (1991).
166. S. Kim, D. Tryk, I. T. Bae, M. Sandifer, R. Carr, M. R. Antonio, and D. A. Scherson, *J. Phys. Chem.*, **99**, 10359 (1995).
167. K. Wiesener, *Electrochim. Acta*, **31**, 1073 (1986).
168. R. Franke, D. Ohms, and K. Wiesener, *J. Electroanal. Chem. Interfacial Electrochem.*, **260**, 63 (1989).
169. Q. He, B. Shyam, M. Nishijima, D. Ramaker, and S. Mukerjee, *J. Phys. Chem. C*, **117**, 4877 (2013).
170. T. M. Arruda, B. Shyam, J. S. Lawton, N. Ramaswamy, D. E. Budil, D. E. Ramaker, and S. Mukerjee, *J. Phys. Chem. C*, **114**, 1028 (2010).
171. T. M. Arruda, B. Shyam, J. M. Ziegelbauer, S. Mukerjee, and D. E. Ramaker, *J. Phys. Chem. C*, **112**, 18087 (2008).
172. M. Teliska, V. S. Murthi, S. Mukerjee, and D. E. Ramaker, *J. Electrochem. Soc.*, **152**, A2159 (2005).
173. M. Teliska, W. E. O'Grady, and D. E. Ramaker, *J. Phys. Chem. B*, **109**, 8076 (2005).
174. Q. He, B. Shyam, K. Macounova, P. Krtil, D. Ramaker, and S. Mukerjee, *J. Am. Chem. Soc.*, **134**, 8655 (2012).
175. I. Kramm Ulrike, J. Herranz, N. Larouche, M. Arruda Thomas, M. Lefevre, F. Jaouen, P. Bogdanoff, S. Fiechter, I. Abs-Wurmbach, S. Mukerjee, and J.-P. Dodelet, *Phys Chem Chem Phys*, **14**, 11673 (2012).
176. Z. P. Li, Z. X. Liu, K. N. Zhu, Z. Li, and B. H. Liu, *J. Power Sources*, **219**, 163 (2012).
177. S. Kattel, P. Atanassov, and B. Kiefer, *Phys. Chem. Chem. Phys.*, **15**, 148 (2013).
178. P. Xu, W. Chen, Q. Wang, T. Zhu, M. Wu, J. Qiao, Z. Chen, and J. Zhang, *RSC Adv.*, **5**, 6195 (2015).
179. K. Asazawa, H. Kishi, H. Tanaka, D. Matsumura, K. Tamura, Y. Nishihata, A. G. Saputro, H. Nakanishi, H. Kasai, K. Artyushkova, and P. Atanassov, *J. Phys. Chem. C*, **118**, 25480 (2014).
180. C. Dominguez, F. J. Perez-Alonso, J. L. Gomez de la Fuente, S. A. Al-Thabaiti, S. N. Basahel, A. O. Alyoubi, A. A. Alshehri, M. A. Pena, and S. Rojas, *J. Power Sources*, **271**, 87 (2014).
181. H. Li, H.-J. Zhang, X. Li, S. Zheng, B. Zhao, and J. Yang, *Int. J. Hydrogen Energy*, **39**, 3198 (2014).
182. J. R. Hahn and H. Kang, *Phys. Rev. B Condens. Matter Mater. Phys.*, **60**, 6007 (1999).
183. S. L. Mielke, D. Troya, S. Zhang, J.-L. Li, S. Xiao, R. Car, R. S. Ruoff, G. C. Schatz, and T. Belytschko, *Chem. Phys. Lett.*, **390**, 413 (2004).
184. Y. Luo, Y. Heng, X. Dai, W. Chen, and J. Li, *J. Solid State Chem.*, **182**, 2521 (2009).
185. T. Kondo, T. Suzuki, and J. Nakamura, *J. Phys. Chem. Lett.*, **2**, 577 (2011).
186. P. Nemes-Incze, Z. Konya, I. Kiricsi, A. Pekker, Z. E. Horvath, K. Kamaras, and L. P. Biro, *J. Phys. Chem. C*, **115**, 3229 (2011).
187. H.-J. Zhang, H. Li, X. Li, B. Zhao, Z.-F. Ma, and J. Yang, *Electrochim. Acta*, **115**, 1 (2014).
188. L. Li, X. Yuan, Z. Ma, and Z.-F. Ma, *J. Electrochem. Soc.*, **162**, F359 (2015).
189. M. Li, X. Bo, Y. Zhang, C. Han, and L. Guo, *J. Power Sources*, **264**, 114 (2014).
190. M. Lefevre, J. P. Dodelet, and P. Bertrand, *J. Phys. Chem. B*, **104**, 11238 (2000).
191. H. A. Gasteiger, S. S. Kocha, B. Sompalli, and F. T. Wagner, *Appl. Catal., B*, **56**, 9 (2005).
192. L. Xu, G. Pan, and X. Liang, *RSC Adv.*, **4**, 19756 (2014).
193. J. Y. Cheon, T. Kim, Y. Choi, H. Y. Jeong, M. G. Kim, Y. J. Sa, J. Kim, Z. Lee, T. H. Yang, K. Kwon, O. Terasaki, G. G. Park, R. R. Adzic, and S. H. Joo, *Sci Rep*, **3**, 2715 (2013).
194. W. Y. Wong, W. R. W. Daud, A. B. Mohamad, A. A. H. Kadhum, K. S. Loh, and E. H. Majlan, *Int. J. Hydrogen Energy*, **38**, 9370 (2013).
195. Z. Samec and T. Kakiuchi, in *Advances in Electrochemical Science and Engineering*, H. Gerischer and C. W. Tobias Editors, VCH verlagsgesellschaft mbH. & VCH Publishers Inc. (2008).
196. M. H. Robson, A. Serov, K. Artyushkova, and P. Atanassov, *Electrochim. Acta*, **90**, 656 (2013).
197. Y. Liu, Y.-Y. Wu, G.-J. Lv, T. Pu, X.-Q. He, and L.-L. Cui, *Electrochim. Acta*, **112**, 269 (2013).
198. M. Jahan, Q. Bao, and K. P. Loh, *J. Am. Chem. Soc.*, **134**, 6707 (2012).
199. X. Gao, J. Wang, Z. Ma, and J. Ye, *Electrochim. Acta*, **130**, 543 (2014).
200. Y. Jiang, Y. Lu, X. Lv, D. Han, Q. Zhang, L. Niu, and W. Chen, *ACS Catal.*, **3**, 1263 (2013).
201. K. I. Ozoemena and O. Fashedemi, *RSC Adv.*, Ahead of Print (2015).
202. G. Dong, M. Huang, and L. Guan, *Phys. Chem. Chem. Phys.*, **14**, 2557 (2012).
203. P.-J. Wei, G.-Q. Yu, Y. Naruta, and J.-G. Liu, *Angew Chem Int Ed Engl*, **53**, 6659 (2014).
204. R. Cao, R. Thapa, H. Kim, X. Xu, M. Gyu Kim, Q. Li, N. Park, M. Liu, and J. Cho, *Nat Commun*, **4**, 2076 (2013).
205. M. Quernheim, H. Liang, Q. Su, M. Baumgarten, N. Koshino, H. Higashimura, and K. Mullen, *Chemistry*, **20**, 14178 (2014).
206. J. Kang, H. Wang, S. Ji, J. Key, and R. Wang, *J. Power Sources*, **251**, 363 (2014).
207. L. Ding, Q. Xin, X. Zhou, J. Qiao, H. Li, and H. Wang, *J. Appl. Electrochem.*, **43**, 43 (2013).
208. X. Fu, Y. Liu, X. Cao, J. Jin, Q. Liu, and J. Zhang, *Appl. Catal., B*, **130–131**, 143 (2013).
209. L. Ding, X. Dai, R. Lin, H. Wang, and J. Qiao, *J. Electrochem. Soc.*, **159**, F577 (2012).
210. S. Chao, Q. Cui, Z. Bai, K. Wang, and L. Yang, *Electrochim. Acta*, Ahead of Print (2015).
211. M. Chatenet, F. Micoud, I. Roche, E. Chainet, and J. Vondrak, *Electrochim. Acta*, **51**, 5452 (2006).
212. A. C. García, F. H. B. Lima, E. A. Ticianelli, and M. Chatenet, *J. Power Sources*, **222**, 305 (2013).
213. A. C. García, J. J. Linares, M. Chatenet, and E. A. Ticianelli, *Electrocatalysis*, **5**, 41 (2014).
214. H.-Y. Su, Y. Gorlin, I. C. Man, F. Calle-Vallejo, J. K. Norskov, T. F. Jaramillo, and J. Rossmeisl, *Phys. Chem. Chem. Phys.*, **14**, 14010 (2012).
215. Y. Meng, W. Song, H. Huang, Z. Ren, S.-Y. Chen, and S. L. Suib, *J. Am. Chem. Soc.*, **136**, 11452 (2014).
216. K. Selvakumar, S. M. Senthil Kumar, R. Thangamuthu, K. Ganesan, P. Murugan, P. Rajput, S. N. Jha, and D. Bhattacharyya, *J. Phys. Chem. C*, Ahead of Print (2015).
217. Q. He, Q. Li, S. Khene, X. Ren, F. E. Lopez-Suarez, D. Lozano-Castello, A. Bueno-Lopez, and G. Wu, *J. Phys. Chem. C*, **117**, 8697 (2013).
218. A. C. Garcia, A. D. Herrera, E. A. Ticianelli, M. Chatenet, and C. Poinsignon, *J. Electrochem. Soc.*, **158**, B290 (2011).
219. B. Klapste, J. Vondrak, and J. Velicka, *Electrochim. Acta*, **47**, 2365 (2002).
220. J. Vondrak, B. Klapste, J. Velicka, M. Sedlarikova, V. Novak, and J. Reiter, *Journal of New Materials for Electrochemical Systems*, **8**, 1 (2005).
221. J. Vondrak, B. Klapste, J. Velicka, M. Sedlarikova, J. Reiter, I. Roche, E. Chainet, J. F. Fauvarque, and M. Chatenet, *Journal of New Materials for Electrochemical Systems*, **8**, 209 (2005).
222. J. S. Lee, G. S. Park, H. I. Lee, S. T. Kim, R. Cao, M. Liu, and J. Cho, *Nano Lett*, **11**, 5362 (2011).
223. Y. Wang, X. Ma, L. Lu, Y. He, X. Qi, and Y. Deng, *Int. J. Hydrogen Energy*, **38**, 13611 (2013).
224. Q. Wu, L. Jiang, Q. Tang, J. Liu, S. Wang, and G. Sun, *Electrochim. Acta*, **91**, 314 (2013).
225. I. Roche, E. Chainet, M. Chatenet, and J. Vondrak, *J. Phys. Chem. C*, **111**, 1434 (2007).
226. Y. Tan, C. Xu, G. Chen, X. Fang, N. Zheng, and Q. Xie, *Advanced Functional Materials*, **22**, 4584 (2012).
227. J. Wei, Y. Liang, X. Zhang, G. P. Simon, D. Zhao, J. Zhang, S. Jiang, and H. Wang, *Nanoscale*, **7**, 6247 (2015).
228. H. Zhang, H. Qiao, H. Wang, N. Zhou, J. Chen, Y. Tang, J. Li, and C. Huang, *Nanoscale*, **6**, 10235 (2014).
229. N. I. Andersen, Synthesis and characterization of bi-functional ORR/OER nano-catalysts in alkaline media, in, The University of New Mexico, Albuquerque, New Mexico (2013).
230. Y. Liang, H. Wang, P. Diao, W. Chang, G. Hong, Y. Li, M. Gong, L. Xie, J. Zhou, J. Wang, Z. Regier Tom, F. Wei, and H. Dai, *J Am Chem Soc*, **134**, 15849 (2012).
231. C. Zhu and S. Dong, *Nanoscale*, **5**, 1753 (2013).
232. N. Alonso-Vante, in *Catalysis and Electrocatalysis at Nanoparticle Surfaces*, A. Wieckowski, E. R. Savinova, and C. G. Vayenas Editors, CRC Press (2003).
233. N. Alonso-Vante, in *Electrocatalysis in Fuel Cells*, M. Shao Editor, Springer-Verlag, London (2013).
234. M.-R. Gao, J. Jiang, and S.-H. Yu, *Small*, **8**, 13 (2012).
235. Y. Feng and N. Alonso-Vante, *Electrochim. Acta*, **72**, 129 (2012).
236. W.-J. Yuan, J.-C. Li, P. Chen, Y.-H. Shen, and A.-J. Xie, *J. Nanopart. Res.*, **16**, 2311/1 (2014).
237. A. P. Periasamy, W.-P. Wu, G.-L. Lin, Z.-Y. Shih, Z. Yang, and H.-T. Chang, *J. Mater. Chem. A*, **2**, 11899 (2014).
238. X. Qing, J. Shi, C. Ma, M. Fan, Z. Bai, Z. Chen, J. Qiao, and J. Zhang, *J. Power Sources*, **266**, 88 (2014).

239. L. Xu, G. Pan, X. Shi, C. Zou, Y. Zhou, G. Luo, and G. Chen, *Electrochim. Acta*, Ahead of Print (2015).
240. S. Chao and W. Guo, *Anal Sci*, **29**, 619 (2013).
241. Z. Guo, C. Jiang, C. Teng, G. Ren, Y. Zhu, and L. Jiang, *ACS Appl. Mater. Interfaces*, **6**, 21454 (2014).
242. C. Han, X. Bo, Y. Zhang, M. Li, and L. Guo, *J. Power Sources*, **272**, 267 (2014).
243. J. Qiao, L. Xu, L. Ding, L. Zhang, R. Baker, X. Dai, and J. Zhang, *Appl. Catal., B*, **125**, 197 (2012).
244. J. Wu, S. Dou, A. Shen, X. Wang, Z. Ma, C. Ouyang, and S. Wang, *J. Mater. Chem. A*, **2**, 20990 (2014).
245. Q. Liu, J. Jin, and J. Zhang, *ACS Appl Mater Interfaces*, **5**, 5002 (2013).
246. Y. Hu, O. Jensen Jens, W. Zhang, N. Cleemann Lars, W. Xing, J. Bjerrum Niels, and Q. Li, *Angew Chem Int Ed Engl*, **53**, 3675 (2014).
247. G. Wu, K. L. More, C. M. Johnston, and P. Zelenay, *Science (Washington, DC, U. S.)*, **332**, 443 (2011).
248. M. Lefevre, E. Proietti, F. Jaouen, and J.-P. Dodelet, *Science (Washington, DC, U. S.)*, **324**, 71 (2009).
249. G. Faubert, R. Cote, J. P. Dodelet, M. Lefevre, and P. Bertrand, *Electrochim. Acta*, **44**, 2589 (1999).
250. W. Yang, X. Liu, X. Yue, J. Jia, and S. Guo, *J Am Chem Soc*, **137**, 1436 (2015).
251. X. Zheng, J. Deng, N. Wang, D. Deng, W.-H. Zhang, X. Bao, and C. Li, *Angew. Chem., Int. Ed.*, **53**, 7023 (2014).
252. T. Chung Hoon, H. Won Jong, and P. Zelenay, *Nat Commun*, **4**, 1922 (2013).
253. F. Zhang, X. Pan, Y. Hu, L. Yu, X. Chen, P. Jiang, H. Zhang, S. Deng, J. Zhang, T. B. Bolin, S. Zhang, Y. Huang, and X. Bao, *Proc. Natl. Acad. Sci. U. S. A.*, **110**, 14861 (2013).
254. W. Chen, Z. Fan, X. Pan, and X. Bao, *J. Am. Chem. Soc.*, **130**, 9414 (2008).
255. D. Deng, L. Yu, X. Chen, G. Wang, L. Jin, X. Pan, J. Deng, G. Sun, and X. Bao, *Angew. Chem., Int. Ed.*, **52**, 371 (2013).
256. V. Kiran, K. Srinivasu, and S. Sampath, *Phys Chem Chem Phys*, **15**, 8744 (2013).
257. H. J. Liu, F. Wang, Y. Zhao, and H. Fong, *Nanoscale*, **5**, 3643 (2013).
258. Z. Jin, D. Xiao, and P. Li, *Sci Rep*, **4**, 6712 (2014).
259. Y. C. Kimmel, Synthesis, characterization, and design of precious metal electrocatalysts supported on transition metal carbides, in, UNIVERSITY OF DELAWARE (2014).
260. H. Meng and P. K. Shen, *Chem. Commun. (Cambridge, U. K.)*, 4408 (2005).
261. C. Liang, L. Ding, C. Li, M. Pang, D. Su, W. Li, and Y. Wang, *Energy Environ. Sci.*, **3**, 1121 (2010).
262. H. Meng and P. K. Shen, *Electrochem. Commun.*, **8**, 588 (2006).
263. M. Pang, C. Li, L. Ding, J. Zhang, D. Su, W. Li, and C. Liang, *Ind. Eng. Chem. Res.*, **49**, 4169 (2010).
264. Z. Hu, C. Chen, H. Meng, R. Wang, P. K. Shen, and H. Fu, *Electrochem. Commun.*, **13**, 763 (2011).
265. G. Zhong, H. Wang, H. Yu, and F. Peng, *Fuel Cells (Weinheim, Ger.)*, **13**, 387 (2013).
266. D. J. Ham and J. S. Lee, *Energies (Basel, Switz.)*, **2**, 873 (2009).
267. B. Cao, G. M. Veith, R. E. Diaz, J. Liu, E. A. Stach, R. R. Adzic, and P. G. Khalifah, *Angew. Chem., Int. Ed.*, **52**, 10753 (2013).
268. R. Ohnishi, M. Katayama, D. Cha, K. Takanabe, J. Kubota, and K. Domen, *J. Electrochem. Soc.*, **160**, F501 (2013).
269. H. Wu and W. Chen, *J. Am. Chem. Soc.*, **133**, 15236 (2011).
270. T. Ando, S. Izhar, H. Tominaga, and M. Nagai, *Electrochim. Acta*, **55**, 2614 (2010).
271. J. B. Goodenough, *Rep. Prog. Phys.*, **67**, 1915 (2004).
272. H. Arandiyan, H. Chang, C. Liu, Y. Peng, and J. Li, *J. Mol. Catal. A Chem.*, **378**, 299 (2013).
273. A. Mrakovic, J. Blanusa, D. Primc, M. Perovic, Z. Jaglicic, V. Kusigerski, and V. Spasojevic, *Ceram. Int.*, **39**, 3771 (2013).
274. G. Kerangueven, S. Royer, and E. Savinova, *Electrochem. Commun.*, **50**, 28 (2015).
275. T. Poux, F. S. Napolskiy, T. Dintzer, G. Kerangueven, S. Y. Istomin, G. A. Tsirlina, E. V. Antipov, and E. R. Savinova, *Catal. Today*, **189**, 83 (2012).
276. J. Suntivich and Y. Shao-Horn, *ECS Trans.*, **58**, 715 (2013).
277. H. Yamashige, S. Matsuo, T. Kurisaki, R. C. C. Perera, and H. Wakita, *Anal. Sci.*, **21**, 309 (2005).
278. J. Sunarso, A. A. J. Torriero, W. Zhou, P. C. Howlett, and M. Forsyth, *J. Phys. Chem. C*, **116**, 5827 (2012).
279. D. C. Sorescu, K. D. Jordan, and P. Avouris, *J. Phys. Chem. B*, **105**, 11227 (2001).
280. A. Sarapuu, K. Vaik, D. J. Schiffrin, and K. Tammeveski, *J. Electroanal. Chem.*, **541**, 23 (2003).
281. K. Tammeveski, K. Kontturi, R. J. Nichols, R. J. Potter, and D. J. Schiffrin, *J. Electroanal. Chem.*, **515**, 101 (2001).
282. K. Vaik, A. Sarapuu, K. Tammeveski, F. Mirkhalaf, and D. J. Schiffrin, *J. Electroanal. Chem.*, **564**, 159 (2004).
283. Y. Zhang, J. Ge, L. Wang, D. Wang, F. Ding, X. Tao, and W. Chen, *Sci Rep*, **3**, 2771 (2013).
284. J. Y. Baek, I.-Y. Jeon, and J.-B. Baek, *J. Mater. Chem. A*, **2**, 8690 (2014).
285. S. K. Bikkarolla, P. Cumpson, P. Joseph, and P. Papakonstantinou, *Faraday Discuss.*, **173**, 415 (2014).
286. D.-W. Wang and D. Su, *Energy Environ. Sci.*, **7**, 576 (2014).
287. H. Kiuchi, H. Niwa, M. Kobayashi, Y. Harada, M. Oshima, M. Chokai, Y. Nabae, S. Kuroki, M.-a. Kakimoto, T. Ikeda, K. Terakura, and S. Miyata, *Electrochim. Acta*, **82**, 291 (2012).
288. O. S. Kwon, S. J. Park, J.-Y. Hong, A. R. Han, J. S. Lee, J. S. Lee, J. H. Oh, and J. Jang, *ACS Nano*, **6**, 1486 (2012).
289. Z.-H. Sheng, L. Shao, J.-J. Chen, W.-J. Bao, F.-B. Wang, and X.-H. Xia, *ACS Nano*, **5**, 4350 (2011).
290. Z.-J. Lu, M.-W. Xu, S.-J. Bao, K. Tan, H. Chai, C.-J. Cai, C.-C. Ji, and Q. Zhang, *J. Mater. Sci.*, **48**, 8101 (2013).
291. L. Lai, J. R. Potts, D. Zhan, L. Wang, C. K. Poh, C. Tang, H. Gong, Z. Shen, J. Lin, and R. S. Ruoff, *Energy Environ. Sci.*, **5**, 7936 (2012).
292. Z. Lin, G. H. Waller, Y. Liu, M. Liu, and C.-p. Wong, *Nano Energy*, **2**, 241 (2013).
293. B. Zheng, J. Wang, F.-B. Wang, and X.-H. Xia, *Electrochem. Commun.*, **28**, 24 (2013).
294. Z. Lin, M.-k. Song, Y. Ding, Y. Liu, M. Liu, and C.-p. Wong, *Phys. Chem. Chem. Phys.*, **14**, 3381 (2012).
295. T. Hibino, K. Kobayashi, and P. Heo, *Electrochim. Acta*, **112**, 82 (2013).
296. S. Bag, B. Mondal, A. K. Das, and C. R. Raj, *Electrochim. Acta*, Ahead of Print (2015).
297. V. V. Strelko, V. S. Kuts, and P. A. Thrower, *Carbon*, **38**, 1499 (2000).
298. L. Zhang and Z. Xia, *J. Phys. Chem. C*, **115**, 11170 (2011).
299. D. Yu, Q. Zhang, and L. Dai, *J. Am. Chem. Soc.*, **132**, 15127 (2010).
300. C.-Z. Guo, C.-G. Chen, and Z.-L. Luo, *J. Power Sources*, **245**, 841 (2014).
301. K. Gong, F. Du, Z. Xia, M. Durstock, and L. Dai, *Science (Washington, DC, U. S.)*, **323**, 760 (2009).
302. T. Ikeda, M. Boero, S.-F. Huang, K. Terakura, M. Oshima, and J.-i. Ozaki, *J. Phys. Chem. C*, **112**, 14706 (2008).
303. J. Liang, Y. Jiao, M. Jaroniec, and S. Z. Qiao, *Angew. Chem., Int. Ed.*, **51**, 11496 (2012).
304. G. Fazio, L. Ferrighi, and C. Di Valentin, *J. Catal.*, **318**, 203 (2014).
305. H. Zhang, X. Liu, G. He, X. Zhang, S. Bao, and W. Hu, *J. Power Sources*, **279**, 252 (2015).
306. Y. Li, M. Li, L. Jiang, L. Lin, L. Cui, and X. He, *Phys. Chem. Chem. Phys.*, **16**, 23196 (2014).
307. Y. Su, Y. Zhang, X. Zhuang, S. Li, D. Wu, F. Zhang, and X. Feng, *Carbon*, **62**, 296 (2013).
308. J. Han, J. Y. Cheon, S. H. Joo, and S. Park, *Solid State Sci.*, **33**, 1 (2014).
309. W. Wei, H. Liang, K. Parvez, X. Zhuang, X. Feng, and K. Muellen, *Angew. Chem., Int. Ed.*, **53**, 1570 (2014).
310. Y. Zhang, W.-J. Jiang, X. Zhang, L. Guo, J.-S. Hu, Z. Wei, and L.-J. Wan, *Phys. Chem. Chem. Phys.*, **16**, 13605 (2014).
311. J. Benson, Q. Xu, P. Wang, Y. Shen, L. Sun, T. Wang, M. Li, and P. Papakonstantinou, *ACS Appl. Mater. Interfaces*, **6**, 19726 (2014).
312. J. Wang, H.-S. Wang, K. Wang, F.-B. Wang, and X.-H. Xia, *Sci Rep*, **4**, 6723 (2014).
313. Q. Liu, Y. Duan, Q. Zhao, F. Pan, B. Zhang, and J. Zhang, *Langmuir*, **30**, 8238 (2014).
314. H. Li, X. Cheng, F.-B. Weng, A. Su, and Y.-C. Chiang, *J. Electrochem. Soc.*, **161**, F1140 (2014).
315. M. Yang, D. Yang, H. Chen, Y. Gao, and H. Li, *J. Power Sources*, **279**, 28 (2015).
316. A. Zhao, J. Masa, W. Schuhmann, and W. Xia, *J. Phys. Chem. C*, **117**, 24283 (2013).
317. C. Venkateswara Rao and Y. Ishikawa, *J. Phys. Chem. C*, **116**, 4340 (2012).
318. A. Morozan, P. Jegou, M. Pinault, S. Campidelli, B. Jousselme, and S. Palacin, *ChemSusChem*, **5**, 647 (2012).
319. D. C. Higgins, J. Wu, W. Li, and Z. Chen, *Electrochim. Acta*, **59**, 8 (2012).
320. Z. Ma, C. Guo, Y. Yin, Y. Zhang, H. Wu, and C. Chen, *Electrochim. Acta*, Ahead of Print (2015).
321. Y. Cheng, Y. Tian, X. Fan, J. Liu, and C. Yan, *Electrochim. Acta*, **143**, 291 (2014).
322. W. Li, D. Yang, H. Chen, Y. Gao, and H. Li, *Electrochim. Acta*, Ahead of Print (2015).
323. G. Tuci, C. Zafferoni, A. Rossin, A. Milella, L. Luconi, M. Innocenti, L. Truong Phuoc, C. Duong-Viet, C. Pham-Huu, and G. Giambastiani, *Chem. Mater.*, **26**, 3460 (2014).
324. G. Tuci, C. Zafferoni, P. D'Ambrosio, S. Caporali, M. Ceppatelli, A. Rossin, T. Tsoufis, M. Innocenti, and G. Giambastiani, *ACS Catal.*, **3**, 2108 (2013).
325. A. Dumitru, M. Mamlouk, and K. Scott, *Electrochim. Acta*, **135**, 428 (2014).
326. N. Alexeyeva and K. Tammeveski, *Electrochem. Solid-State Lett.*, **10**, F18 (2007).
327. E. Yeager, *J. Mol. Catal.*, **38**, 5 (1986).
328. M. Zhang, Y. Yan, K. Gong, L. Mao, Z. Guo, and Y. Chen, *Langmuir*, **20**, 8781 (2004).
329. G. Juermann and K. Tammeveski, *J. Electroanal. Chem.*, **597**, 119 (2006).
330. H. Wang and A. Kong, *Mater. Lett.*, **136**, 384 (2014).
331. X. Sun, Y. Zhang, P. Song, J. Pan, L. Zhuang, W. Xu, and W. Xing, *ACS Catal.*, **3**, 1726 (2013).
332. J. Bhattacharjee, *J. Phys. Chem. Lett.*, **6**, 1653 (2015).
333. R. Lv, Q. Li, A. R. Botello-Mendez, T. Hayashi, B. Wang, A. Berkdemir, Q. Hao, A. L. Elias, R. Cruz-Silva, H. R. Gutierrez, Y. A. Kim, H. Muramatsu, J. Zhu, M. Endo, H. Terrones, J. C. Charlier, M. Pan, and M. Terrones, *Sci Rep*, **2**, 586 (2012).
334. Z. Gong, G. Zhang, and S. Wang, *Journal of Chemistry*, **2013**, 1 (2013).
335. Z. Ma, S. Dou, A. Shen, L. Tao, L. Dai, and S. Wang, *Angew Chem Int Ed Engl*, **54**, 1888 (2015).
336. Z.-H. Sheng, H.-L. Gao, W.-J. Bao, F.-B. Wang, and X.-H. Xia, *J. Mater. Chem.*, **22**, 390 (2012).
337. X.-k. Kong, Q.-w. Chen, and Z. Sun, *RSC Advances*, **3**, 4074 (2013).
338. D. Yu, Y. Xue, and L. Dai, *The Journal of Physical Chemistry Letters*, **3**, 2863 (2012).
339. H. Jiang, Y. Zhu, Q. Feng, Y. Su, X. Yang, and C. Li, *Chem. - Eur. J.*, **20**, 3106 (2014).
340. D.-S. Yang, D. Bhattacharjya, S. Inamdar, J. Park, and J.-S. Yu, *J. Am. Chem. Soc.*, **134**, 16127 (2012).
341. A. Shen, Y. Zou, Q. Wang, R. A. W. Dryfe, X. Huang, S. Dou, L. Dai, and S. Wang, *Angew. Chem., Int. Ed.*, **53**, 10804 (2014).

342. B. Winther-Jensen, O. Winther-Jensen, M. Forsyth, and D. R. MacFarlane, *Science (Washington, DC, U. S.)*, **321**, 671 (2008).
343. R. Kerr, C. Pozo-Gonzalo, M. Forsyth, and B. Winther-Jensen, *ECS Electrochem. Lett.*, **2**, F29 (2013).
344. S. Ratso, I. Kruusenberg, M. Vikkisk, U. Joost, E. Shulga, I. Kink, T. Kallio, and K. Tammeveski, *Carbon*, **73**, 361 (2014).
345. J. Sa Young, C. Park, Y. Jeong Hu, S.-H. Park, Z. Lee, T. Kim Kyoung, G.-G. Park, and H. Joo Sang, *Angew Chem Int Ed Engl*, **53**, 4102 (2014).
346. P. Xu, L. Wan, D. Wu, P. Hu, and R. Liu, *J Colloid Interface Sci*, **421**, 160 (2014).
347. P. Chen, L.-K. Wang, G. Wang, M.-R. Gao, J. Ge, W.-J. Yuan, Y.-H. Shen, A.-J. Xie, and S.-H. Yu, *Energy Environ. Sci.*, **7**, 4095 (2014).
348. L. Wei, D. Yu, H. E. Karahan, O. Birer, K. Goh, Y. Yuan, W. Jiang, W. Liang, and Y. Chen, *Catal. Today*, Ahead of Print (2014).
349. M. Y. Song, H. Y. Park, D.-S. Yang, D. Bhattacharjya, and J.-S. Yu, *ChemSusChem*, **7**, 1755 (2014).
350. X. Liu, Y. Zhou, W. Zhou, L. Li, and S. Chen, *Nanoscale*, Ahead of Print (2015).
351. G. Nam, J. Park, T. Kim Sun, D.-b. Shin, N. Park, Y. Kim, J.-S. Lee, and J. Cho, *Nano Lett*, **14**, 1870 (2014).
352. R. Gokhale, S. M. Unni, D. Puthusseri, S. Kurungot, and S. Ogale, *Phys. Chem. Chem. Phys.*, **16**, 4251 (2014).
353. G. Merle, M. Wessling, and K. Nijmeijer, *Journal of Membrane Science*, **377**, 1 (2011).
354. Q. He and X. Ren, *J. Power Sources*, **220**, 373 (2012).
355. J. Ran, L. Wu, B. Wei, Y. Chen, and T. Xu, *Sci Rep*, **4**, 6486 (2014).
356. J. R. Varcoe, P. Atanassov, D. R. Dekel, A. M. Herring, M. A. Hickner, P. A. Kohl, A. R. Kucernak, W. E. Mustain, K. Nijmeijer, K. Scott, T. Xu, and L. Zhuang, *Energy Environ. Sci.*, **7**, 3135 (2014).
357. T. P. Pandey, A. M. Maes, H. N. Sarode, B. D. Peters, S. Lavina, K. Vezzu, Y. Yang, S. D. Poynton, J. R. Varcoe, S. Seifert, M. W. Liberatore, V. Di Noto, and A. M. Herring, *Phys Chem Chem Phys*, **17**, 4367 (2015).
358. R. O'Hayre *Probing Electrochemistry at the Micro Scale: Applications in Fuel Cells, Ionics, and Catalysis* VDM Verlag Dr. Müller (2008).
359. Q.-G. He, A. Kusoglu, I. T. Lucas, K. Clark, A. Z. Weber, and R. Kostecki, *J. Phys. Chem. B*, **115**, 11650 (2011).
360. H. Yanagi and K. Fukuta, *ECS Trans.*, **16**, 257 (2008).
361. D. Yang, H. Yu, G. Li, Y. Zhao, Y. Liu, C. Zhang, W. Song, and Z. Shao, *J. Power Sources*, **267**, 39 (2014).
362. A. J. Lemke, A. W. O'Toole, R. S. Phillips, and E. T. Eisenbraun, *J. Power Sources*, **256**, 319 (2014).
363. P. S. Ruvinskiy, A. Bonnefont, M. Houlle, C. Pham-Huu, and E. R. Savinova, *Electrochim. Acta*, **55**, 3245 (2010).
364. P. S. Ruvinskiy, A. Bonnefont, C. Pham-Huu, and E. R. Savinova, *Langmuir*, **27**, 9018 (2011).
365. A. Schneider, L. Colmenares, Y. E. Seidel, Z. Jusys, B. Wickman, B. Kasemo, and R. J. Behm, *Phys. Chem. Chem. Phys.*, **10**, 1931 (2008).
366. O. Antoine and R. Durand, *J. Appl. Electrochem.*, **30**, 839 (2000).
367. O. Antoine, Y. Bultel, and R. Durand, *J. Electroanal. Chem.*, **499**, 85 (2001).
368. F. Gloaguen, F. Andolfatto, R. Durand, and P. Ozil, *J. Appl. Electrochem.*, **24**, 863 (1994).
369. O. Antoine, Y. Bultel, R. Durand, and P. Ozil, *Electrochim. Acta*, **43**, 3681 (1998).
370. Y. Bultel, L. Genies, O. Antoine, P. Ozil, and R. Durand, *J. Electroanal. Chem.*, **527**, 143 (2002).
371. N. Ramaswamy, Electrocatalysis of oxygen reduction in alkaline media and a study of perfluorinated ionomer membrane degradation, in, Northeastern University (2011).
372. W. Y. Wong, W. R. W. Daud, A. B. Mohamad, A. A. H. Kadhum, K. S. Loh, E. H. Majlan, and K. L. Lim, *Electrochim. Acta*, **129**, 47 (2014).
373. L. Genies, Y. Bultel, R. Faure, and R. Durand, *Electrochim. Acta*, **48**, 3879 (2003).
374. A. Serov, K. Artyushkova, N. I. Andersen, S. Stariha, and P. Atanassov, *Electrochim. Acta*, Ahead of Print (2015).
375. M. Wang, W. Zhang, J. Wang, D. Wexler, D. Poynton Simon, C. T. Slade Robert, H. Liu, B. Winther-Jensen, R. Kerr, D. Shi, and J. Chen, *ACS Appl Mater Interfaces*, **5**, 12708 (2013).
376. O. M. M. Page, S. D. Poynton, S. Murphy, A. L. Ong, D. M. Hillman, C. A. Hancock, M. G. Hale, D. C. Apperley, and J. R. Varcoe, *RSC Adv.*, **3**, 579 (2013).
377. C. G. Arges, J. Parrondo, G. Johnson, A. Nadhan, and V. Ramani, *J. Mater. Chem.*, **22**, 3733 (2012).
378. A. Sarkar, X. Zhu, H. Nakanishi, J. B. Kerr, and E. J. Cairns, *J. Electrochem. Soc.*, **159**, F628 (2012).
379. A. L. Ong, D. K. Whelligan, M. L. Fox, and J. R. Varcoe, *Phys. Chem. Chem. Phys.*, **15**, 18992 (2013).
380. J. C. Meier, C. Galeano, I. Katsounaros, A. A. Topalov, A. Kostka, F. Schueth, and K. J. J. Mayrhofer, *ACS Catal.*, **2**, 832 (2012).
381. A. Zadick, L. Dubau, A. Zalineeva, C. Coutanceau, and M. Chatenet, *Electrochem. Commun.*, **48**, 1 (2014).
382. A. Zadick, L. Dubau, N. Sergent, G. Berthome, and M. Chatenet, *ACS Catal.*, **5**, 4819 (2015).
383. W.-Y. Yan, S.-L. Zheng, W. Jin, Z. Peng, S.-N. Wang, H. Du, and Y. Zhang, *J. Electroanal. Chem.*, Ahead of Print (2015).
384. E. C. M. Tse and A. A. Gewirth, *J. Phys. Chem. A*, Ahead of Print (2015).
385. E. J. Coleman, M. H. Chowdhury, and A. C. Co, *ACS Catal.*, **5**, 1245 (2015).
386. K. A. Kuttiyiel, K. Sasaki, D. Su, L. Wu, Y. Zhu, and R. R. Adzic, *Nat. Commun.*, **5**, 5185 (2014).
387. Q.-L. Zhang, J.-X. Feng, A.-J. Wang, J. Wei, and J.-J. Feng, *RSC Adv.*, **4**, 52640 (2014).
388. A. Cha, J. H. Shim, A. Jo, S. C. Lee, Y. Lee, and C. Lee, *Electroanalysis*, **26**, 723 (2014).
389. G. Fu, Z. Liu, Y. Chen, J. Lin, Y. Tang, and T. Lu, *Nano Res.*, **7**, 1205 (2014).
390. C. Yang, B. Huang, L. Xiao, Z. Ren, Z. Liu, J. Lu, and L. Zhuang, *Chem Commun (Camb)*, **49**, 11023 (2013).
391. J.-J. Lv, S.-S. Li, A.-J. Wang, L.-P. Mei, J.-J. Feng, J.-R. Chen, and Z. Chen, *J. Power Sources*, **269**, 104 (2014).
392. O. Fashedemi Omobosede and I. Ozoemena Kenneth, *Phys Chem Chem Phys*, **15**, 20982 (2013).
393. O. Fashedemi Omobosede, B. Julies, and I. Ozoemena Kenneth, *Chem Commun (Camb)*, **49**, 2034 (2013).
394. H. A. Miller, M. Bevilacqua, J. Filippi, A. Lavacchi, A. Marchionni, M. Marelli, S. Moneti, W. Oberhauser, E. Vesselli, M. Innocenti, and F. Vizza, *J. Mater. Chem. A*, **1**, 13337 (2013).
395. A. Holewinski, S. Linic, and J.-C. Idrobo, *Nat Chem*, **6**, 828 (2014).
396. Y. Lu, N. Zhang, L. An, X. Li, and D. Xia, *J. Power Sources*, **240**, 606 (2013).
397. Y. Wang, Y. Liu, X. Lu, Z. Li, H. Zhang, X. Cui, Y. Zhang, F. Shi, and Y. Deng, *Electrochem. Commun.*, **20**, 171 (2012).
398. A. Slanac Daniel, G. Hardin William, P. Johnston Keith, and J. Stevenson Keith, *J Am Chem Soc*, **134**, 9812 (2012).
399. S. Liu, Q. Zhang, Y. Li, M. Han, L. Gu, C. Nan, J. Bao, and Z. Dai, *J Am Chem Soc*, **137** (2015).
400. H. Yin, S. Liu, C. Zhang, J. Bao, Y. Zheng, M. Han, and Z. Dai, *ACS Appl. Mater. Interfaces*, **6**, 2086 (2014).
401. J. Sanetuntikul and S. Shanmugam, *Electrochim. Acta*, **119**, 92 (2014).
402. S. Liu, C. Deng, L. Yao, H. Zhong, and H. Zhang, *Catal. Commun.*, **58**, 112 (2015).
403. Q. Cui, S. Chao, P. Wang, Z. Bai, H. Yan, K. Wang, and L. Yang, *RSC Adv.*, **4**, 12168 (2014).
404. H.-J. Zhang, H. Li, X. Li, S. Zheng, B. Zhao, and J. Yang, *Appl. Catal., B*, **160–161**, 676 (2014).
405. Y. Xie, C. Tang, Z. Hao, Y. Lv, R. Yang, X. Wei, W. Deng, A. Wang, B. Yi, and Y. Song, *Faraday Discuss.*, Ahead of Print (2014).
406. S. Zhao, H. Yin, L. Du, L. He, K. Zhao, L. Chang, G. Yin, H. Zhao, S. Liu, and Z. Tang, *ACS Nano*, **8**, 12660 (2014).
407. Q. Lin, X. Bu, A. Kong, C. Mao, X. Zhao, F. Bu, and P. Feng, *J Am Chem Soc*, **137**, 2235 (2015).
408. H. Li, W. Kang, L. Wang, Q. Yue, S. Xu, H. Wang, and J. Liu, *Carbon*, **54**, 249 (2013).
409. X. Bo, M. Li, C. Han, Y. Zhang, A. Nsabimana, and L. Guo, *J. Mater. Chem. A*, **3**, 1058 (2015).
410. Q. Dong, X. Zhuang, Z. Li, B. Li, B. Fang, C. Yang, H. Xie, F. Zhang, and X. Feng, *J. Mater. Chem. A*, Ahead of Print (2015).
411. A. Kong, X. Zhu, Z. Han, Y. Yu, Y. Zhang, B. Dong, and Y. Shan, *ACS Catal.*, **4**, 1793 (2014).
412. Q. Liu, Z. Pu, C. Tang, A. M. Asiri, A. H. Qusti, A. O. Al-Youbi, and X. Sun, *Electrochem. Commun.*, **36**, 57 (2013).
413. L. Wang, L. Zhang, L. Bai, L. Han, and S. Dong, *Electrochem. Commun.*, **34**, 68 (2013).
414. Z. Liu, G. Zhang, Z. Lu, X. Jin, Z. Chang, and X. Sun, *Nano Res.*, **6**, 293 (2013).
415. X. Zhou, P. Xu, L. Xu, Z. Bai, Z. Chen, J. Qiao, and J. Zhang, *J. Power Sources*, **260**, 349 (2014).
416. W. Ma, P. Yu, T. Ohsaka, and L. Mao, *Electrochem. Commun.*, **52**, 53 (2015).
417. Y. Yang, J. Liu, Y. Han, H. Huang, N. Liu, Y. Liu, and Z. Kang, *Phys Chem Chem Phys*, **16**, 25350 (2014).
418. Y. Jiang, Y. Lu, X. Wang, Y. Bao, W. Chen, and L. Niu, *Nanoscale*, **6**, 15066 (2014).
419. S. Liu, C. Deng, L. Yao, H. Zhong, and H. Zhang, *Int. J. Hydrogen Energy*, **39**, 12613 (2014).
420. Y.-S. Wang, B.-W. Zhang, Y.-F. Li, D.-J. Liu, X.-Q. He, and Z.-J. Si, *RSC Adv.*, **4**, 62272 (2014).
421. X. Fu, J. Jin, Y. Liu, Q. Liu, K. Niu, J. Zhang, and X. Cao, *Electrochem. Commun.*, **28**, 5 (2013).
422. A. Pacula, K. Ikeda, T. Masuda, and K. Uosaki, *J. Power Sources*, **220**, 20 (2012).
423. J. Shi, P. Xu, M. Zhen, Y. Liu, and J. Qiao, *ECS Trans.*, **58**, 727 (2013).
424. S. Li, D. Wu, H. Liang, J. Wang, X. Zhuang, Y. Mai, Y. Su, and X. Feng, *ChemSusChem*, **7**, 3002 (2014).
425. A. M. El-Sawy, C. K. King'ondu, C.-H. Kuo, D. A. Kriz, C. J. Guild, Y. Meng, S. J. Frueh, S. Dharmarathna, S. N. Ehrlich, and S. L. Suib, *Chem. Mater.*, **26**, 5752 (2014).
426. D. J. Davis, T. N. Lambert, J. A. Vigil, M. A. Rodriguez, M. T. Brumbach, E. N. Coker, and S. J. Limmer, *J. Phys. Chem. C*, **118**, 17342 (2014).
427. S. K. Bikkarolla, F. Yu, W. Zhou, P. Joseph, P. Cumpson, and P. Papakonstantinou, *J. Mater. Chem. A*, **2**, 14493 (2014).
428. S. Bag, K. Roy, S. Gopinath Chinnakonda, and C. R. Raj, *ACS Appl Mater Interfaces*, **6**, 2692 (2014).
429. C. Shi, G.-L. Zang, Z. Zhang, G.-P. Sheng, Y.-X. Huang, G.-X. Zhao, X.-K. Wang, and H.-Q. Yu, *Electrochim. Acta*, **132**, 239 (2014).
430. C. Jiang, Z. Guo, Y. Zhu, H. Liu, M. Wan, and L. Jiang, *ChemSusChem*, **8**, 158 (2015).
431. Y. Ma, H. Wang, J. Key, V. Linkov, S. Ji, X. Mao, Q. Wang, and R. Wang, *Int. J. Hydrogen Energy*, **39**, 14777 (2014).
432. Y. Su, H. Jiang, Y. Zhu, X. Yang, J. Shen, W. Zou, J. Chen, and C. Li, *J. Mater. Chem. A*, **2**, 7281 (2014).

433. D. Zhou, L. Yang, L. Yu, J. Kong, X. Yao, W. Liu, Z. Xu, and X. Lu, *Nanoscale*, **7**, 1501 (2015).
434. Z. Li, G. Li, L. Jiang, J. Li, G. Sun, C. Xia, and F. Li, *Angew Chem Int Ed Engl*, **54**, 1494 (2015).
435. Z.-S. Wu, S. Yang, Y. Sun, K. Parvez, X. Feng, and K. Muellen, *J. Am. Chem. Soc.*, **134**, 9082 (2012).
436. J. Zhang, X. Wang, D. Qin, Z. Xue, and X. Lu, *Appl. Surf. Sci.*, **320**, 73 (2014).
437. J. Wu, D. Zhang, Y. Wang, Y. Wan, and B. Hou, *J. Power Sources*, **198**, 122 (2012).
438. J. Xu, P. Gao, and T. S. Zhao, *Energy Environ. Sci.*, **5**, 5333 (2012).
439. M. Wang, J. Huang, M. Wang, D. Zhang, W. Zhang, W. Li, and J. Chen, *Electrochem. Commun.*, **34**, 299 (2013).
440. J. Xiao, X. Bian, L. Liao, S. Zhang, C. Ji, and B. Liu, *ACS Appl Mater Interfaces*, **6**, 17654 (2014).
441. Z.-Y. Wu, P. Chen, Q.-S. Wu, L.-F. Yang, Z. Pan, and Q. Wang, *Nano Energy*, **8**, 118 (2014).
442. D. Huang, Y. Luo, S. Li, B. Zhang, Y. Shen, and M. Wang, *Nano Res.*, **7**, 1054 (2014).
443. J. Jin, X. Fu, Q. Liu, and J. Zhang, *J. Mater. Chem. A*, **1**, 10538 (2013).
444. Q. Liu and J. Zhang, *Langmuir*, **29**, 3821 (2013).
445. E. Farjami, M. A. Rottmayer, and L. Jay Deiner, *J. Mater. Chem. A*, **1**, 15501 (2013).
446. Q. Li, P. Xu, B. Zhang, H. Tsai, S. Zheng, G. Wu, and H.-L. Wang, *J. Phys. Chem. C*, **117**, 13872 (2013).
447. K. Liu, Y. Song, and S. Chen, *Nanoscale*, **7**, 1224 (2015).
448. Z. Cui, S. Wang, Y. Zhang, and M. Cao, *J. Power Sources*, **272**, 808 (2014).
449. J. Wang, H. L. Xin, J. Zhu, S. Liu, Z. Wu, and D. Wang, *J. Mater. Chem. A*, **3**, 1601 (2015).
450. Z.-Q. Liu, Q.-Z. Xu, J.-Y. Wang, N. Li, S.-H. Guo, Y.-Z. Su, H.-J. Wang, J.-H. Zhang, and S. Chen, *Int. J. Hydrogen Energy*, **38**, 6657 (2013).
451. Y. Xiao, C. Hu, L. Qu, C. Hu, and M. Cao, *Chemistry*, **19**, 14271 (2013).
452. Z. Pu, Q. Liu, C. Tang, A. M. Asiri, A. H. Qusti, A. O. Al-Youbi, and X. Sun, *J. Power Sources*, **257**, 170 (2014).
453. R. Ning, J. Tian, A. M. Asiri, A. H. Qusti, A. O. Al-Youbi, and X. Sun, *Langmuir*, **29**, 13146 (2013).
454. X. Zhai, W. Yang, M. Li, G. Lv, J. Liu, and X. Zhang, *Carbon*, **65**, 277 (2013).
455. W. Menezes Prashanth, A. Indra, R. Sahraie Nastaran, A. Bergmann, P. Strasser, and M. Driess, *ChemSusChem*, **8**, 164 (2015).
456. X. Xu, T. Yuan, Y. Zhou, Y. Li, J. Lu, X. Tian, D. Wang, and J. Wang, *Int. J. Hydrogen Energy*, **39**, 16043 (2014).
457. D. W. Chang, H.-J. Choi, and J.-B. Baek, *J. Mater. Chem. A*, Ahead of Print (2015).
458. K. Parvez, S. Yang, Y. Hernandez, A. Winter, A. Turchanin, X. Feng, and K. Muellen, *ACS Nano*, **6**, 9541 (2012).
459. F. Pan, J. Jin, X. Fu, Q. Liu, and J. Zhang, *ACS Appl Mater Interfaces*, **5**, 11108 (2013).
460. Y. Wang and X. Jiang, *ACS Appl Mater Interfaces*, **5**, 11597 (2013).
461. M. Liu, Y. Song, S. He, W. Tjiu Weng, J. Pan, Y.-Y. Xia, and T. Liu, *ACS Appl Mater Interfaces*, **6**, 4214 (2014).
462. Y. Li, Y. Zhao, H. Cheng, Y. Hu, G. Shi, L. Dai, and L. Qu, *J Am Chem Soc*, **134**, 15 (2012).
463. Z. Zuo, W. Li, and A. Manthiram, *J. Mater. Chem. A*, **1**, 10166 (2013).
464. Z. Yang, Z. Yao, G. Li, G. Fang, H. Nie, Z. Liu, X. Zhou, X. a. Chen, and S. Huang, *ACS Nano*, **6**, 205 (2012).
465. R. K. Shervedani and A. Amini, *Electrochim. Acta*, **142**, 51 (2014).
466. Z. Yao, H. Nie, Z. Yang, X. Zhou, Z. Liu, and S. Huang, *Chem Commun (Camb)*, **48**, 1027 (2012).
467. J. Tai, J. Hu, Z. Chen, and H. Lu, *RSC Adv.*, **4**, 61437 (2014).
468. Y. Zhang, X. Zhuang, Y. Su, F. Zhang, and X. Feng, *J. Mater. Chem. A*, **2**, 7742 (2014).
469. J. Jin, F. Pan, L. Jiang, X. Fu, A. Liang, Z. Wei, J. Zhang, and G. Sun, *ACS Nano*, **8**, 3313 (2014).
470. H. Fei, R. Ye, G. Ye, Y. Gong, Z. Peng, X. Fan, L. G. Samuel Errol, M. Ajayan Pulickel, and M. Tour James, *ACS Nano*, **8**, 10837 (2014).
471. J. Yin, Y. Qiu, J. Yu, X. Zhou, and W. Wu, *RSC Adv.*, **3**, 15655 (2013).
472. D. Liu, X. Zhang, Z. Sun, and T. You, *Nanoscale*, **5**, 9528 (2013).
473. J. Lu, X. Bo, H. Wang, and L. Guo, *Electrochim. Acta*, **108**, 10 (2013).
474. T. C. Nagaiah, A. Bordoloi, M. D. Sanchez, M. Muhler, and W. Schuhmann, *ChemSusChem*, **5**, 637 (2012).
475. X. Bo and L. Guo, *Phys. Chem. Chem. Phys.*, **15**, 2459 (2013).
476. R. Liu, H. Liu, Y. Li, Y. Yi, X. Shang, S. Zhang, X. Yu, S. Zhang, H. Cao, and G. Zhang, *Nanoscale*, **6**, 11336 (2014).
477. S.-A. Wohlgemuth, R. J. White, M.-G. Willinger, M.-M. Titirici, and M. Antonietti, *Green Chem.*, **14**, 1515 (2012).
478. L. Chen, R. Du, J. Zhu, Y. Mao, C. Xue, N. Zhang, Y. Hou, J. Zhang, and T. Yi, *Small* (2014).
479. G. Panomsuwan, S. Chiba, Y. Kaneko, N. Saito, and T. Ishizaki, *J. Mater. Chem. A*, **2**, 18677 (2014).
480. G. Panomsuwan, S. Chiba, N. Saito, and T. Ishizaki, *MRS Online Proc. Libr.*, **1641**, Panomsuwan/1 (2014).
481. Y. Li, T. Li, M. Yao, and S. Liu, *J. Mater. Chem.*, **22**, 10911 (2012).
482. Y.-L. Liu, C.-X. Shi, X.-Y. Xu, P.-C. Sun, and T.-H. Chen, *J. Power Sources*, **283**, 389 (2015).
483. C. You, S. Liao, H. Li, S. Hou, H. Peng, X. Zeng, F. Liu, R. Zheng, Z. Fu, and Y. Li, *Carbon*, **69**, 294 (2014).
484. C. Han, J. Wang, Y. Gong, X. Xu, H. Li, and Y. Wang, *J. Mater. Chem. A*, **2**, 605 (2014).
485. S. Inamdar, H.-S. Choi, P. Wang, M. Y. Song, and J.-S. Yu, *Electrochem. Commun.*, **30**, 9 (2013).
486. S. Zhao, J. Liu, C. Li, W. Ji, M. Yang, H. Huang, Y. Liu, and Z. Kang, *ACS Appl Mater Interfaces*, **6**, 22297 (2014).
487. H.-W. Liang, S. Bruller, K. Mullen, X. Zhuang, and X. Feng, *Nat Commun*, **5**, 4973 (2014).
488. L. Jiang, M. Li, L. Lin, Y. Li, X. He, and L. Cui, *RSC Adv.*, **4**, 26653 (2014).
489. C. You, X. Zen, X. Qiao, F. Liu, T. Shu, L. Du, J. Zeng, and S. Liao, *Nanoscale*, Ahead of Print (2015).
490. C. Deng, H. Zhong, L. Yao, S. Liu, Z. Xu, and H. Zhang, *ChemSusChem*, **7**, 3435 (2014).
491. S. Chao, Z. Bai, Q. Cui, H. Yan, K. Wang, and L. Yang, *Carbon*, **82**, 77 (2015).
492. Y. Ma, R. Wang, H. Wang, J. Key, and S. Ji, *J. Power Sources*, **280**, 526 (2015).

Query

Q1: AU: Please provide a digital object identifier (doi) for Ref(s) 1, 23, 25, 31, 46, 88, 103, 114, 121, 132, 137, 150, 159, 162, 201, 204, 210, 216, 220, 221, 239, 265, 266, 283, 296, 320, 322, 348, 350, 358, 374, 383, 384, 399, 405, 410, 457, 478, and 489. For additional information on doi's please select this link: http://www.doi.org/. If a doi is not available, no other information is needed from you.